THE FORMATION AND EVOLUTION OF MASSIVE CLUSTERS IN EXTRAGALACTIC ENVIRONMENTS

Katherine Elizabeth Hollyhead

Liverpool John Moores University

A thesis submitted in partial fulfilment of the requirements of

Liverpool John Moores University

for the degree of

Doctor of Philosophy.

November 11, 2017

Declaration

The work presented in this thesis was carried out at the Astrophysics Research Institute, Liverpool John Moore's University. Unless otherwise stated, it is the original work of the author.

While registered as a candidate for the degree of Doctor of Philosophy, for which submission is now made, the author has not been registered as a candidate for any other award. This thesis has not been submitted in whole, or in part, for any other degree.

Katherine E. Hollyhead
Astrophysics Research Institute
Liverpool John Moore's University
IC2, Liverpool Science Park
146 Brownlow Hill
Liverpool
L3 5RF
UK

Abstract

There are a host of open questions in the study of massive clusters relating to cluster formation and evolution. Understanding these processes can be useful in studying their host galaxies and how they have evolved. The formation of globular clusters is also a well debated topic, which is yet undecided and requires many more observations to constrain the theories.

Here I present the work carried out during my PhD, with the goal of furthering our understanding of cluster formation and evolution using observations of massive clusters of various ages. Firstly, HST WFC3 data of the well studied face-on spiral galaxy M 83, combined with an existing cluster catalogue, was used to investigate the timescale by which young massive clusters become free of gas. This has implications for globular cluster formation theories, in addition to the survival of clusters at young ages. The presence of Wolf-Rayet stars was also investigated within the clusters and the unreliability of Hα photometry in young cluster age and mass fitting was explored.

Secondly, the cluster population of NGC 1566 was used to investigate the cluster mass function and disruption in the galaxy. Whether the mass function has a truncation in the form of a Schechter function and whether disruption is environmentally and mass dependent are two questions that still persist in this area. For NGC 1566 I find that the mass function does show a truncation and using the observed luminosity function in conjunction with models, that an underlying Schechter mass function fits the observations well. Additionally the galaxy shows evidence for environmentally dependent disruption as the average timescale for the disruption of a 10^4 $M_\odot$ cluster varies with galactocentric radius. A difference in age in radial bins is also indicated in a colour change found with U-B between consecutive bins, that shows more young clusters towards the centre of the galaxy and fewer at the edge.

Finally, low resolution FORS2 spectra of two intermediate age massive clusters in the SMC

(Lindsay 1 and Kron 3, 6-8 Gyr old) were used to look for the signatures of multiple populations (MPs), as observed in ancient GCs. The main driver behind this project was to investigate the possibility that YMCs can be considered young GCs and used to constrain their formation, and also to explore the role cluster age has in determining the presence of MPs. A subpopulation of N-enriched stars was found in each cluster, consistent with the presence of MPs. This indicates that MPs are not limited to ancient GCs and their formation mechanism must be operating until a redshift of at least 0.65, much later than the peak of GC formation at ≈ 3. It hints at a common formation mechanism between massive clusters of varying ages, including GCs, and suggests that YMCs can be used to constrain GC formation.

The publications from these projects have contributed mainly to constraining GC formation theories and provides evidence for commonality in the formation mechanism used to produce GCs and YMCs alike.

Acknowledgements

I would firstly like to acknowledge the significant contributions made to the work in this thesis by others. I shall divide these into the chapters in which the contributions are made, as follows:

- In Chapter 2, after producing a catalogue of clusters for NGC 1566, fitting was required to give estimates of the ages and masses. Angela Adamo helpfully used her SED fitting code to provide these parameters for the project, for which I am grateful, as producing a successful code is difficult and time-consuming. Mark Gieles also provided his model for the behaviour of the luminosity function in different bands, so that we had a theoretical quantity to compare to our observations. In addition to this, a code was provided by Nate Bastian/Mark Gieles to fit the maximum likelihood of the mass function and provide the timescale for cluster disruption and the characteristic turnover mass of the observed Schechter function.

- Contributions to Chapter 3 include the full cluster catalogue for M 83, which was produced and refined over several works, most notably Bastian et al. (2012) and Silva-Villa et al. (2014). Starting with a complete and reliable catalogue was invaluable to making the project quicker. Again, refitting the ages and masses of some clusters with different filter contributions was provided by Angela Adamo.

- I would like to thank Carmela Lardo for help with the work in Chapter 4. Without her knowledge of the methods for calculating abundances from line widths, effective temperatures and other parameters, the chapter and the publication would have been much slower.

Contributions from all the above are discussed in more detail in their respective chapters.

Besides the contributions from all these individuals, I would also like to thank Nate Bastian for being a great supervisor during my PhD and providing such interesting and rewarding projects.

I'd also like to thank all the other PhD students during my time in the department, who helped make the experience a much more fun and lively one, especially Rob and the other D&D and boardgame players! Thanks for introducing us to Dominion and Agricola, amongst other games. I will never forget Sir Brian the Blessed, Clint of the Eastwood or that guy that tried to cut a branch from a tree with a sword and fell out, wherever he ended up.

My parents also deserve thanks, as they have always been so encouraging no matter what I chose to study or do. However, I will subtract some percentage of these thanks to account for the nose that was provided to me.

Finally, I would like to thank Elliott. Without your knack for distracting me with games or naps, I might have just gone and worked too hard, which would have been a real shame.

Publications

The following papers are relevant to this thesis and have been published during the time this work was undertaken:

1. *Age as a Major Factor in the Onset of Multiple Populations in Stellar Clusters*
   Martocchia, S., Cabrera-Ziri, I., Lardo, C., Dalessandro, E., Bastian, N., Kozhurina-Platais, V., Usher, C., Niederhofer, F., Cordero, M., Geisler, D., **Hollyhead, K.**, Kacharov, N., Larsen, S., Li, C., Mackey, D., Hilker, M., Mucciarelli, M., Platais, I., Salaris, M., 2017, arXiv:1710.00831

2. *The search for multiple populations in Magellanic Cloud clusters - II. The detection of multiple populations in three intermediate-age SMC clusters*
   Niederhofer, F., Bastian, N., Kozhurina-Platais, V., Larsen, S., **Hollyhead, K.**, Lardo, C., Cabrera-Ziri, I., Kacharov, N., Platais, I., Salaris, M., Cordero, M., Dalessandro, E., Geisler, D., Hilker, M., Li, C., Mackey, D., Mucciarelli, A, 2017, MNRAS, 465, 4

3. *The Search for Multiple Populations in Magellanic Cloud Clusters III: No evidence for Multiple Populations in the SMC cluster NGC 419*
   Martocchia, S., Bastian, N., Usher, C., Kozhurina-Platais, V., Niederhofer, F., Cabrera-Ziri, I., Dalessandro, E., **Hollyhead, K.**, Kacharov, N., Lardo, C., Larsen, S., Mucciarelli, A., Platais, I., Salaris, M., Cordero, M., Geisler, D., Hilker, M., Li, C., Mackey, D, 2017, MNRAS, 468, 3150

4. *Evidence for multiple populations in the intermediate age cluster Lindsay 1 in the SMC*
   Hollyhead, K., Kacharov, N., Lardo, C., Bastian, N., Hilker, M., Rejkuba, M., Koch, A., Grebel, E. K., Georgiev, I., 2017, MNRAS Letters, 465, 1

5. *The Search for Multiple Populations in Magellanic Cloud Clusters I: Two Stellar Populations in the Small Magellanic Cloud Globular Cluster NGC 121*
   Niederhofer, F., Bastian, N., Kozhurina-Platais, V., Larsen, S., Salaris, M., Dalessandro, E., Mucciarelli, A., Cabrera-Ziri, I., Cordero, M., Geisler, D., Hilker, M., **Hollyhead, K.**., Kacharov, N., Lardo, C., Li, C., Mackey, D., Platais, I., 2017, MNRAS, 464, 1

6. *Properties of the cluster population of NGC 1566 and their implications*
   Hollyhead, K., Adamo, A., Bastian, N., Gieles, M., Ryon, J. E., 2016, MNRAS, 460, 2087

7. *Sizes and shapes of young star cluster light profiles in M83*
   Ryon, J. E., Bastian, N., Adamo, A., Konstantopoulos, I. S., Gallagher, J. S., Larsen, S., **Hollyhead, K.**, Silva-Villa, E., Smith, L. J., 2015, MNRAS, 452, 525

8. *Studying the YMC population of M83: how long clusters remain embedded, their interaction with the ISM and implications for GC formation theories*
   Hollyhead, K., Bastian, N., Adamo, A., Silva-Villa, E., Dale, J., Ryon, J. E., Gazak, Z., 2015, MNRAS, 449, 1106

9. *Constraining globular cluster formation through studies of young massive clusters - V. ALMA observations of clusters in the Antennae*
   Cabrera-Ziri, I., Bastian, N., Longmore, S. N., Brogan, C., **Hollyhead, K.**, Larsen, S. S., Whitmore, B., Johnson, K., Chandar, R., Henshaw, J. D., Davies, B., Hibbard, J. E., 2015, MNRAS, 448, 2224

10. *Constraining globular cluster formation through studies of young massive clusters - IV. Testing the fast rotating massive star scenario*
    Bastian, N., **Hollyhead, K.**, Cabrera-Ziri, I., 2014, MNRAS, 445, 378

11. *The effect of spatial resolution on optical and near-IR studies of stellar clusters: implications for the origin of the red excess*
    Bastian, N., Adamo, A., Schirmer, M., **Hollyhead, K.**, Beletsky, Y., Carraro, G., Davies, B., Gieles, M., Silva-Villa, E., 2014, MNRAS, 444, 38291

The following paper has been submitted for publication:

Further constraining the onset of multiple populations in massive clusters using intermediate age cluster Kron 3 in the SMC

Hollyhead, K., Kacharov, N., Lardo, C., Bastian, N., Hilker, M., Rejkuba, M., Koch, A., Grebel, E. K., Georgiev, I. submitted to MNRAS

”Citizens of Dalaran! Raise your eyes to the skies and observe!”

-Rhonin, archmage and professor of observational astronomy

Contents

List of Tables

List of Figures

Chapter 1

Introduction

The aim of this body of work was to contribute to constraining aspects of cluster formation and evolution using massive clusters in extragalactic environments. This has been achieved in a series of projects focusing on clusters of varying ages, each resulting in a publication.

The first project utilised the population of young massive clusters in the nearby face-on spiral galaxy M 83 to investigate the length of time clusters remain embedded in their natal gas, which also has implications for globular cluster formation scenarios. This work was published in Hollyhead et al. (2015). Secondly the cluster population of NGC 1566, another face-on spiral galaxy at 17 Mpc, was studied with HST WFC3 data to investigate the properties of the cluster population. The relationship between the clusters and their host galaxy and cluster disruption was also studied. This work has been published in Hollyhead et al. (2016). The final project found evidence to support the presence of multiple populations in two intermediate age massive clusters in the SMC. This had significant implications for globular cluster (GC) formation scenarios and lent support to the idea that young massive clusters are analogues to old GCs. The work has been published over two papers in Hollyhead et al. (2017) and Hollyhead et al., 2017, submitted.

These three projects have explored different age ranges of massive clusters observationally, and bring together a variety of aspects of cluster formation and evolution. This section introduces the background behind each project and the justification for the work presented here.

1.1 Clusters in the grand scheme of things

The study of stellar clusters is vital to the understanding of star formation and galaxy evolution, as current theory proposes that the majority of all stars form in groups or clustered environments (e.g. Hopkins, 2013; Kruijssen, 2012). A grouping is defined as any sized collection of stars, independent of whether or not the collection is gravitationally bound. More specifically, a cluster refers to a gravitationally bound grouping while associations are unbound groupings (Blaauw, 1964; Gieles & Portegies Zwart, 2011).

There are a variety of types of clusters, from very low mass open clusters living in the discs of galaxies to the highest mass, dense globular clusters residing in galaxy halos. Many questions remain unresolved in the study of cluster formation and evolution, particularly the early stages after formation. A vigorously debated topic relating to this is the formation of globular clusters and whether they share a common formation mechanism with young massive clusters today.

The lifecycles of clusters have a significant impact on the evolution of their host galaxies, as clusters that are disrupted will go on to feed the field star population. It has also been suggested that globular clusters may contribute to the population of stars in the bulge. This is partly due to stars that have strange chemistry similar to that found seemingly exclusively in secondary enriched populations in GCs (see section 1.3.1) being found in the bulge of the Milky Way (Schiavon et al., 2017). It is therefore important to understand cluster evolution in order to fully understand how the stellar component of galaxies is built. GCs have also been found to have a special relationship with their host galaxy in the number of GCs (or halo mass) associated with a galaxy being correlated with the mass of the central supermassive black hole (Burkert & Tremaine, 2010; Harris & Harris, 2011).

Massive clusters are also likely to be the formation site of the most massive stars, as the stellar IMF can be more fully sampled (e.g. Crowther et al., 2010). Therefore, clusters are excellent laboratories for studying small scale individual star formation up to the large scale compilation of galaxies as we see them today.

Defining a cluster is an important yet difficult aspect of studying clusters, and definitions can vary between studies. Lada & Lada (2003) define clusters as objects that contain 35 or more member stars with densities greater than 1 $M_{\odot}pc^{-3}$. This ensures the clusters are stable against tidal disruption and interstellar clouds and that their evaporation time is greater than 10^8 years.

However, an alternative definition is given in Portegies Zwart et al. (2010), where they impose a lower mass limit of 10^4 $M_\odot$ to ensure that the cluster should survive for at least 1 Gyr, Throughout this thesis I adopt the technique of imposing a mass cut on the data, to attempt to ensure the clusters are bound objects able to survive for a significant time. The adopted mass cut is 5000 $M_\odot$, which should mean that the clusters survive approximately as long as those in Portegies Zwart et al. (2010). Where possible, I also only use clusters above the age of 10 Myr, which should be sufficient time for the cluster to have become virialised (e.g. R136; Hénault-Brunet et al., 2012). This means that the objects above this age are gravitationally bound and will not disrupt rapidly. In addition to this, techniques described in Chapter 2 for creating cluster catalogues means that fewer associations are included as bonafide clusters due to inspection by eye. See § 1.4 for more discussion of identifying bound and unbound objects.

1.2 Cluster formation

Clusters are a natural output of the star formation process due to the effects of turbulence (Elmegreen & Efremov, 1997), which causes a hierarchical formation process of stars, with bound clusters as the smallest, densest structures formed (Elmegreen, 2011; Hopkins, 2013). Both the progenitor gas clouds and the resulting clusters follow the same density distributions due to the scale-free nature of turbulence (Bressert et al., 2010). Clusters of a wide range of masses appear have a common formation mechanism, which can be ascertained from the cluster mass function. In many cases this can be approximated by a power law with a slope of -2 (e.g. Bastian et al., 2012), though the current GC mass function is a log-normal distribution (the initial GC mass function is still an open question). This means that by studying massive clusters, information about lower mass clusters can potentially be inferred from the results.

There are still many open questions regarding the formation of clusters, though many observations have been made to provide constraints to the current models. There are several different theories for the formation of clusters, the two basic ideas being: star formation within a cloud of gas that is already at an appropriate density for the resulting cluster ("in situ" model), or star formation occurring at lower surface densities and merging together to form the cluster ("conveyor-belt model", Longmore et al., 2014). In agreement with the "conveyor-belt" model, the initial gas clouds that form the stars have been observed to be highly substructured (e.g. Carpenter & Hodapp, 2008; Henshaw et al., 2016) with filaments and complex struc-

tures. Very young clusters also show evidence for substructure (Allen et al., 2007), though this quickly disappears as the cluster becomes mass segregated (e.g. Cartwright & Whitworth, 2004; Allison et al., 2009; Parker et al., 2014). Clusters are also observed to form in a subvirial state (Kirk et al., 2007), which is a requirement for rapid removal of substructure (Goodwin & Whitworth, 2004). Also in agreement with a conveyor-belt model, YMCs have been found to have higher densities than the molecular clouds from which they form (Walker et al., 2015, 2016), suggesting that they have not expanded since formation, but rather evolved to a denser state.

A traditional idea of early cluster evolution involves all stars forming in clusters and any remaining gas being expelled by feedback over fairly short timescales (e.g. R136 in 30 Doradus is observed to be gas free at an age of ≈ 3 Myr). Due to a low or average star formation efficiency, as the gas (which makes up the majority of the cluster's mass) is expelled, the cluster expands and is potentially dissolved, feeding the field star population and leaving $\sim 10\%$ of stars in clusters (e.g. Lada & Lada, 2003; Boily & Kroupa, 2003; Baumgardt & Kroupa, 2007).

However, more recently gas exhaustion has been suggested as the primary reason why clusters survive and associations are destroyed, and why clusters are free of gas on such short timescales (e.g. Kruijssen, 2012). Observational evidence also suggests that many well-studied young massive clusters are virialised and not expanding, and therefore gas expulsion is not playing a major role in their evolution (e.g. R136, Arches clusters; Hénault-Brunet et al., 2012; Clarkson et al., 2012).

Kruijssen (2012) suggests that bound clusters form in denser environments where the free-fall time is shorter than the feedback timescale and so star formation efficiency (SFE) is above average (Ginsburg et al., 2016). This leaves less gas to be removed from the cluster in order to evolve to a gas-free state, as observed during the work described in Chapter 3. Associations that will dissolve quickly form with a lower SFE and so the loss of a larger amount of gas leads to their dissolution. The relationship between ISM density and cluster formation has also been observed in the increase between the star formation rate surface density (also molecular gas density) and cluster formation efficiency (Kruijssen, 2012; Adamo et al., 2015; Johnson et al., 2016).

One of the open questions in cluster formation is still the efficiency of the removal of gas after cluster formation. Further constraining the age at which clusters are free of gas may have

implications for globular cluster formation theories in particular. Also, determining which source (e.g. gas exhaustion, stellar winds or radiation pressure) is the prevalent contributor to the removal of gas could be of interest. Chapter 3 tackles this question, investigating the timescales for removal of gas in YMCs in M 83 and contributing a significant number of clusters observed to be gas free to a fairly small existing sample.

1.2.1 Do all clusters disrupt?

As discussed in § 1.2, bound clusters form in denser environments with a higher star formation efficiency, while unbound associations and smaller stellar aggregates form in lower efficiency environments (Kruijssen, 2012). The 'classical' idea of early cluster destruction labelled 'infant mortality' suggested that rapid gas expulsion after formation followed by mass independent violent relaxation of the system was responsible for destroying many young clusters (e.g. Bastian & Goodwin, 2006). Now with evidence of very young massive clusters ($\sim$ 2 Myr) being already virialised and not expanding, this idea has fallen from favour. The products of a lower star formation efficiency, such as associations (which are known to be short-lived), can still be destroyed in this way, as more gas will be left over from a lower SFE. Whether the remnants of more efficient star formation are also destroyed as associations are is still a question.

There is a decrease in the number of clusters at ages less than 10 Myr. The gas rich birth environment of clusters has been suggested to actually cause many of the young clusters to disrupt before they can migrate to areas that are more gas poor (e.g. Elmegreen & Hunter, 2010b; Kruijssen et al., 2011), in which case the local environment would play a strong role in the determination of the survival fraction of young clusters. Alternatively, this could highlight the difficulty in determination between clusters and associations at ages less than 10 Myr.

Any clusters lucky enough to survive their more turbulent young years do not survive indefinitely, and will continue to dissolve through a combination of internal and external processes. This can be seen as a decrease in the number of clusters with increasing age (e.g. Elmegreen & Hunter, 2010b). Clusters can disrupt by a process of evaporation where stars are lost due to interactions between the stars and external influences on the cluster's dynamics. This can include the tidal field that the cluster lies in, which can make the stars escape more easily (e.g. Baumgardt, 2001). Tidal forces can also cause heating, which gives the stars more kinetic energy, leading to them escaping the cluster; an example of which is the passage of a globular

cluster through the galaxy disk (Ostriker et al., 1972; Gnedin & Ostriker, 1997). Tidal shocks are also induced by the passage of giant molecular clouds nearby to the cluster, as well as moving through the arm of a spiral galaxy (Gieles et al., 2006c, 2007b). GMCs have been found to be the most prevalent cause for the disruption of clusters (e.g. Gieles et al., 2006c; Lamers & Gieles, 2006).

1.3 Massive clusters

Massive clusters exist across all ages, from today's young massive clusters (YMCs) to globular clusters (GCs), some of the most ancient objects in the universe. The three flavours of massive cluster that are studied are YMCs, intermediate age massive clusters (IMCs) and GCs. The ages spanned are continuous, though generally clusters can be divided into one of these three groups based on certain observations. Each group has particular differences that seem to define them, though with recent studies these divisions are becoming more blurred. Massive clusters present excellent opportunities to study cluster formation and evolution at distances greater than the Milky Way as they are more easily resolved, particularly with Hubble Space Telescope (HST) data. Additionally, as there appears to potentially be a common formation mechanism across cluster mass scales due to the hierarchical process of star formation (e.g. Adamo & Bastian, 2015), the formation and evolution of clusters of all masses may be inferred from the massive variety. This may also include GCs.

GCs are extremely massive ($\sim 10^{4-7}$ $M_{\odot}$), old (> 9 Gyr) and dense systems that are usually found in the halos of galaxies. All of the globular clusters we see today formed in the early universe, so studying their formation and evolution is not an easy task. YMCs are often used as analogues to GCs (e.g. Schweizer & Seitzer, 1998; Kruijssen, 2015) to study how these massive clusters could have formed, though whether it is correct to compare the two is still debated. This assumption has so far been vital in constraining GC formation as it otherwise would not be possible to observe GCs' early evolution with the same detail. GCs were once believed to be the ultimate single stellar population (consisting of stars of the same age and chemistry), however with increasing accuracy of spectroscopy and photometry, this has been shown to be untrue. The most intriguing and problematic discovery has been that of multiple populations (star-to-star variations in certain elemental abundances) and the consequences they have for not only GC formation but also evolution of the YMCs observed today.

IMCs are the younger brethren of GCs, at 2-9 Gyr old. They can be around the same mass as GCs ($\approx 10^5$ $M_\odot$, e.g. Lindsay 1; Glatt et al., 2008) but have not formed in the very early universe. Only recently, the discovery of multiple populations (as discussed later in § 1.3.1) in IMCs linked their formation mechanism to that of GCs. A wealth of clusters of this age exist within distances where it is possible to resolve individual stars. They can be found in the SMC (Lindsay 1, Kron 3, NGC 416, NGC 339), though there is a lack of them in the LMC. The Milky Way hosts some clusters, though these are difficult to study within the disc.

YMCs bridge the gap between the lower mass clusters found in discs of galaxies and old massive GCs, as they primarily reside in the disc. At ages < 2 Gyr and masses $\gtrsim 10^{4-5}$ $M_\odot$ (though this can reach 10^8 $M_\odot$) they are often considered analogues to GCs and show that massive cluster formation is not limited to the early universe but is still ongoing today. They are found in a variety of galaxies, from within the Milky Way (e.g. Westerlund 1, Arches) to galaxies at fairly significant distances from us ($\sim$ 100 Mpc), possible due to their high luminosity (e.g. Haro 11, Adamo et al., 2010b). Galaxies with a high star formation rate typically host 10s of the most massive clusters (up to 10^7 $M_\odot$, e.g. Whitmore et al., 1999), with large numbers also found in quiescent spirals (e.g. Larsen, 2004a, but not usually sampled to such high masses). Within the local universe, the Magellanic clouds are particularly well populated with such clusters (Hunter et al., 2003; de Grijs & Anders, 2006). The evolution of YMCs is generally studied in different phases; the cloud/proto-star phase (which can be studied in great detail in the centre of the Milky Way, e.g. the Brick Longmore et al., 2013), the very youngest clusters where star formation is still ongoing, when the cluster is free of gas and still losing stars (clusters as young as 2 Myr, e.g. R136; Schneider et al., 2014, see also Chapter 3), and when the cluster is bound and dynamically evolving due to only the stellar component (Portegies Zwart et al., 2010). YMCs provide the ideal environment to study such early stages of cluster evolution due to their higher luminosity and greater sampling of the stellar IMF.

A key difference separating massive clusters is multiple populations (MPs), which will be discussed in detail in the following section. GCs universally show evidence for MPs while this is not the case for all younger clusters; IMCs have now been found to contain MPs, however YMCs have not. Another disparity between massive clusters is that of the observed mass functions (MFs). YMCs have been observed to have a MF best fit with either a -2 power law or a Schechter function with a characteristic truncation mass dependent on environment (see § 1.4.1 for detail, e.g. Bik et al., 2003; Johnson et al., 2017). GCs however, show a log-normal

MF, which could suggest that they do not share a common formation mechanism. Work on the initial GC MF has yielded results that suggest an initial power law MF that rapidly evolved into today's GC MF (e.g. Elmegreen, 2010a) while others maintain the MF was also initially log-normal (e.g. Schaerer & Charbonnel, 2011). Most recently, Johnson et al. (2017) found a correlation between the characteristic Schechter truncation mass of GCs with the surface density of star formation ($\Sigma_{\rm SFR}$) of the host galaxy, the same as discovered for disc clusters. This supports a common formation mechanism.

Possibly the most important open question here is whether YMCs can truly be considered precursors to GCs and can be used to constrain their formation. In order to determine whether this is the case, the formation mechanisms of each need to be understood. Initial mass functions are extremely hard to decipher, though they would be invaluable in solving this problem. Observationally, however, there is already evidence to suggest YMCs can be considered young GCs. The work on intermediate age clusters Lindsay 1 and Kron 3 in Chapter 4 shows MPs are now found in younger clusters, alluding to a common formation mechanism between massive clusters and potentially removing one of the major doubts concerning the use of YMCs to constrain GCs.

1.3.1 Multiple populations

GCs have been found to host multiple populations (MPs) of stars, an indication that they are not the simple stellar systems they were once thought to be. These MPs are characterised by abundance variations between stars that can be seen in both photometry (from splits and spreads in the Main Sequence (MS) or Red Giant Branch (RGB) in appropriate filters, for example (e.g. Piotto et al., 2015) and spectroscopy (from chemical abundance variations (e.g. Gratton et al., 2012a).

In all cases, GCs contain some percentage of stars with abundances similar to low metallicity field stars, which are labelled as the 'first population' and one or more 'secondary populations' with various levels of chemical enrichment. Measuring the ratio between these populations provides a key constraint to potential formation mechanisms. Precise ratios can be difficult to measure, as spectroscopic and photometric studies generally have their own biases as to the sampling of stars in the cluster. However, so far the majority of stars in GCs belong to the second population, which appears to scale with the mass of the cluster (more massive clusters

have more second population stars, e.g. Milone et al., 2017a).

In addition to measuring the ratio of enriched stars to non-enriched, the spatial distribution of the second population stars within the cluster has been investigated and found to show a concentration towards the centre of clusters in most cases (e.g. Lardo et al., 2011). This provides difficulties for the study of MPs with spectroscopy, as the central regions of the cluster are often too crowded for individual stars to be observed. Studies using high resolution spectroscopy can be severely affected, as they are usually based on just a few stars and largely only sample the outer regions of clusters. Chapter 4 discusses this difficulty for the study of Lindsay 1 and Kron 3. High precision photometric studies with HST can probe the central regions, however with limited spatial coverage can miss the outermost regions, and potentially underestimate the number of first population stars. There are few clusters with full coverage with HST (e.g. Dalessandro et al., 2014).

Until very recently, this phenomenon was thought to be limited to ancient GCs, however new evidence from both photometry and spectra indicate that these peculiarities can be observed in younger massive clusters and may be present in clusters still forming in the present day.

Abundance variations

The first chemical anomalies discovered in ancient GCs were anti-correlations in the CN and CH band strengths (and therefore the underlying [C/Fe] and [N/Fe] abundances) of RGB stars of similar luminosities (e.g. Bell & Dickens, 1980; Norris et al., 1981). This discovery was possible due to the fact that CN and CH band strengths can be measured in low resolution spectra, as described in Chapter 4, and can be observed in all ancient GCs, as well as some intermediate age massive clusters, which will be discussed later.

The availability of high resolution spectra for previously studied clusters allowed the measurement of more element abundances, which also showed evidence for a secondary population with different enrichment. An enrichment of sodium was found to correlate with the nitrogen enrichment and anti-correlate with both carbon and oxygen (e.g. Sneden et al., 1992). In some clusters a similar anti-correlation between aluminium and magnesium has been found, however this is not ubiquitous as with C/N and O/Na patterns (e.g. Gratton et al., 2004, 2012b; Mészáros et al., 2015). The strength of a Mg-Al anti-correlation appears to depend on cluster mass and metallicity, with higher mass lower metallicity clusters tending to exhibit stronger

anti-correlations (Pancino & the GES collaboration, 2017).

Helium variations have also been observed in GCs spectroscopically, with enhanced He correlated with Na (Mucciarelli et al., 2014b; Villanova et al., 2009). Additionally, helium spreads have been shown to exist from photometry (Bellini et al., 2013), as optical colours are strongly affected by changes in helium. Isochrone fitting to spreads in optical colours of main sequences can be used to estimate the spread in helium abundance (Cassisi et al., 2017). Iron has been found to be largely homogeneous within clusters, (e.g. Carretta et al., 2009), though there are several anomalous GCs that do show strong evidence for an intrinsic iron spread (e.g. ω Centauri and Terzan 5; Sollima et al., 2005; Marino et al., 2011; Ferraro et al., 2009; Origlia et al., 2013). α elements, such as calcium are also generally not found to vary within GCs, except for a few anomalies (e.g. Carretta et al., 2010).

Multiple populations, while a common feature of old massive clusters, have not been found in lower mass open clusters, regardless of their age (e.g. Berkeley 39; Bragaglia et al., 2012). Additionally, stars with these abundances (i.e. 2nd population stars) are very rarely found in field star populations, and any that are likely originated in a GC (Martell et al., 2011).

Abundance variations (N enrichment) have been observed with spectroscopy in intermediate age massive clusters (Lindsay 1 and Kron 3; Hollyhead et al., 2017, Hollyhead et al., 2017, submitted) down to an age of ≈ 6.5 Gyr. YMCs below 2 Gyr do not show evidence for any chemical anomalies, though the mass of stars observed on the RGB is not comparable to stellar masses in GCs or IMCs. This could indicate the stellar mass of observed stars plays a role in the formation of chemical enrichment (see the upcoming review on multiple populations by Bastian & Lardo). However, no evidence of aluminium enrichment have been observed in massive stars in YMCs in integrated spectra (Cabrera-Ziri et al., 2016; Lardo et al., 2017).

Colour magnitude diagrams of massive clusters

MPs can also be detected using photometric data in the colour magnitude diagrams (CMDs) of massive clusters. This is characterised in multiple branches of a variety of phases of the CMD. Ultimately, the cause of these variations is the underlying chemistry, the specific elements responsible depend on the range of filters used and the section of the CMD where the split or spread is observed.

In optical colours, a significant helium spread is required to produce a splitting of the main sequence (MS) and turn-off (TO), with little variation in the red giant branch (RGB) (Salaris et al., 2006). Individual light element abundance anti-correlations do not strongly influence the colours in optical bands, however a change in the sum of C, N and O can produce a split in the sub-giant branch (SGB, e.g. Piotto et al., 2012). The requirement of a large change in helium to produce a spread on the MS is why original optical CMDs of GCs did not display clear evidence for MPs, along with a lower precision on measurements. Variations in C, N and O (even with a constant sum) produce splits and spreads on the RGB, visible particularly below the bump in the luminosity function (an overdensity of stars on the RGB caused by a discontinuity in H within the star and a drop in surface brightness and the corresponding luminosity function, e.g. Riello et al., 2003).

While there are few strong atomic lines of C and N in the optical region of the spectrum, cool stars (e.g. RGB stars) can have strong molecular features associated with these elements, namely CN and CH. The primary wavelengths for measuring CN and CH (tracing N and C respectively) lie at 3839 and 4300 Å, and therefore the wide variation seen in these elements in GCs is shown well in filters that span these wavelengths. Exotic combinations of near-UV filters creating specific colours show extreme sensitivity to changes in these abundances. The now widely used "CUBI" filter combination ((U-B)-(V-I) vs V, in the Cousins-Johnson filter system and in approximately equal HST filters) has been found to display clear splits in the RGB, with each branch containing stars of a specific population (i.e. 1st or 2nd population if bi-modal; clusters with continuous abundance changes show spreads; Monelli et al., 2013; Niederhofer et al., 2017a,b). These filters have also been used to identify MPs in intermediate age clusters Lindsay 1, NGC 339 and NGC 416 (Niederhofer et al., 2017a,b).

Unexpected features have also been observed in the CMDs of YMCs. These anomalies appear as extended main sequence turn-offs (eMSTOs), which were originally identified in massive clusters 1-2 Gyr in age (e.g. Bertelli et al., 2003; Mackey et al., 2008; Piatti et al., 2014). This peculiarity was interpreted as being due to the presence of multiple stellar populations characterised by an age spread of $\sim$ 200-700 Myr (e.g. Goudfrooij et al., 2014). However, the extent of the proposed age spreads were found to be proportional to the age of the cluster, and therefore unlikely to be real (Niederhofer et al., 2015a). Additionally, these eMSTOs were also found in younger clusters (80-300 Myr), where the age spread - cluster age relation persists (Milone et al., 2015; Bastian et al., 2016). This indicates that the cause of eMSTOs is very

unlikely to be MPs, but is now thought to be due to stellar rotation (Bastian & de Mink, 2009; Niederhofer et al., 2015a).

CMDs of YMCs in UV filters also show a split in the main sequence (Milone et al., 2015), which cannot be accounted for in any models involving abundance spreads, such as those seen in GCs. Instead, this seems to be further evidence for rotation at work, as found by D'Antona et al. (2015) using models including rotation. The fraction of rapidly rotating stars dominates the slower rotators (Milone et al., 2017b), which was confirmed for NGC 1850 and NGC 1856, where a large number of Be stars were observed (Bastian et al., 2017).

Cluster age and mass

Cluster mass was considered the first primary indicator of whether MPs should be present in GCs or not. This was due to MPs being absent from lower mass open clusters (e.g. Berkeley 39; Bragaglia et al., 2012). Currently, the lowest mass GC that hosts MPs is NGC 6535 at $10^{3.3}$ $M_{\odot}$(Milone et al., 2017a; Bragaglia et al., 2017), however some GCs with similar masses do not show evidence for MPs (e.g. Cluster E3 at 1.4×10^4 $M_{\odot}$ Salinas & Strader, 2015). This could indicate that there is a cut-off for MP formation in clusters that have initial masses that are likely to result in these present day masses (though significant mass loss is not expected for GCs, Bastian & Lardo, 2015). Additionally, cluster mass has an affect on the properties of the populations, as previously discussed in § 1.3.1.

Despite this, mass is unlikely to be the only parameter determining the presence of MPs; age is also a key factor. Until recently, MPs were thought to be constrained to ancient GCs of reasonable mass, particularly as YMCs did not show any evidence for them. However, results in both spectroscopy and photometry have recently revealed MPs existing in intermediate age clusters (2-9 Gyr). The first of these clusters was Lindsay 1 (discussed in Chapter 4, Hollyhead et al., 2017; Niederhofer et al., 2017b) at $\sim$ 8 Gyr. Now this has been extended to clusters around 6 Gyr (Kron 3 (see Chapter 4), NGC 416 and NGC 339; Hollyhead et al,. 2017, submitted; Niederhofer et al., 2017a). This indicated that the mechanism responsible for MPs must have operated more recently than the peak of GC formation at z $\approx$ 3, and so any formation mechanism should still be able to operate today. Indeed, this age has now been reduced further to $\approx$ 2 Gyr with NGC 1978 (Martocchia et al., submitted). NGC 419 in the SMC at an age of $\approx$ 1.7 Gyr has been found to not show MPs (Martocchia et al., 2017), which has narrowed

down the age for the onset of MPs to a small range around 2 Gyr. This has provided strong constraints to any MP formation mechanisms.

Formation mechanisms of MPs

The cause of chemical inhomogeneities in GCs was first thought to be simply due to evolutionary mixing as dredge-ups can change the surface compositions of more evolved stars. However, with observations made of the same anomalous chemistry in non-evolved stars on the main sequence or at the turn-off, this was determined to not be the case (e.g. Harbeck et al., 2003; Briley et al., 2004). Additionally, as more evolved stars observed show similar magnitudes of variation in abundances to lesser evolved ones, MPs cannot be explained by accretion of material onto stars that have formed, as a dilution of the chemical patterns observed would be changed through successive evolutionary phases (i.e. the surface is mixed Gratton et al., 2004, 2012c).

The long-lived low mass stars that are observed in GCs today would be unable to produce the enhancement in elements such as sodium or potentially aluminium and magnesium as their core temperatures are too low for the necessary fusion reactions (Prantzos et al., 2007). This indicates that the material used to form today's 2nd population GC stars is likely produced by more massive stars, though the mechanism for its incorporation in lower mass stars is yet uncertain as it is believed the enriched stars would need to form from this material. Though there are many disagreements over the fine details of these processes, it is generally accepted that supernovae cannot be responsible, due to the variation in iron that should be observed between GC stars, and which is not.

There are several leading theories for the polluter responsible for chemical spreads, and the mechanism by which this material is incorporated into the enriched population of stars. Many scenarios describing the origin of MPs invoke multiple generations of stars in order to explain said features in the CMDs of clusters and chemical variations. The AGB (e.g. D'Ercole et al., 2008), FRMS (Fast Rotating Massive Star; e.g. Decressin et al., 2007) and interacting massive binaries (e.g. de Mink et al., 2009) scenarios use the ejecta of either evolved stars or massive main sequence stars to pollute a second generation forming later than the first. In these scenarios age spreads of up to $\sim$ 300 Myr would be expected to be observed between the successive generations. The early disc accretion scenario alternatively uses the ejecta of stars

of the same generation to pollute pre-MS stars (Bastian et al., 2013b).

However, these scenarios cannot reproduce all light element abundance variations (Bastian et al., 2015) without succumbing to significant issues, such as the mass budget problem (e.g. Larsen et al., 2012; Bastian & Lardo, 2015; Kruijssen, 2015), where a significant amount of first population stars would need to be lost to reproduce the observed ratios and the clusters would have had to be much larger at the time of formation. Additionally, sufficient gas reservoirs have not been found in YMCs at the ages required for formation of a second generation with the proposed age spreads (Cabrera-Ziri et al., 2015; Longmore, 2015). In conflict with the FRMS scenario in particular, clusters have been found to be gas free by 2-3 Myr (e.g. Bastian et al., 2014b; Hollyhead et al., 2015), and so enough pristine gas cannot be accreted within 25 Myr to form the second generation.

Another difficult aspect of MPs to incorporate into a working theory is their variation from cluster to cluster. The strength of each anti-correlation is not constant across all clusters with this signature of strange chemistry, and the wide variation in magnesium and aluminium, requires a theory to allow for these differences (e.g. Bastian et al., 2015).

Open questions in GCs mostly revolve around further constraints on GC formation theories and the onset of MPs. Until 2016, it was thought that MPs were limited to ancient GCs, implying their cause was linked with the early universe. In Chapter 4, I describe the study using low resolution spectra of intermediate age massive clusters (ages 6-8 Gyr) in the SMC to test this assumption. These clusters formed well after the peak of GC formation ($z \approx 0.65$*) so are well placed to test the suggested cosmological origin of MPs (e.g. D'Ercole et al., 2016).*

1.4 Cluster populations

While single clusters can provide excellent snapshots into aspects of cluster evolution at a range of ages, studying a galaxy's entire cluster population allows the study of the full range of cluster behaviour over all ages. They also provide statistically significant numbers of clusters across all age bins able to probe distances up to $\sim$ 100 Mpc (Adamo et al., 2010b; Fedotov et al., 2011). They also allow for statistics of cluster property distributions, such as age and mass, to be calculated and any relationships between them identified. In addition to this, they allow the relationship between the clusters and their host galaxy to be explored using quantities

such as the cluster formation efficiency. This can be achieved with great success using HST data, which provides excellent quality data for such work with integrated cluster photometry (Adamo et al., 2015).

Cluster population studies can suffer from contamination of samples at young ages (< 10 Myr) from short-lived associations. It is difficult to define a cluster at such a young age, as without detailed kinematical information of all group members (and potentially the gas in the region as well) it is not possible to determine if the grouping is bound. At young ages there exists a continuous distribution of structures, whereas at ages greater than 10 Myr, a bimodal distribution arises with bound (compact) and unbound (expanding associations) groups (Portegies Zwart et al., 2010). Hence, an object can only definitely be defined and classified as a cluster once it is dynamically evolved. This is in agreement with hierarchical star formation models, which indicate that clusters are not well defined and unique objects at young ages (Bastian et al., 2011). This can strongly alter cluster population distributions, in particular the age distribution, where associations can create the illusion of a rapidly decreasing number of clusters as the associations disperse, up to ~ 10 Myr.

The problem with defining and determining a cluster from an unbound grouping also lies in the limited spatial resolution of the telescope (e.g. Bastian et al., 2012). One simplistic way is to use the size of the grouping. As shown in the SMC, groupings with an effective radius above 6 pc rapidly decline in number as a function of age (t^{-1}), i.e., 90% of groups get disrupted every dex, but for groups with sizes below 6 pc, there is a flat distribution suggesting little disruption (Portegies Zwart et al., 2010). By limiting cluster population studies to systems containing dense, centrally concentrated groups with ages > 10 Myr, issues with identifying bound structures can be resolved. Unfortunately, this technique can miss information about cluster evolution below 10 Myr, which is a crucial to understanding cluster formation.

There are a variety of cluster population properties that can be studied to yield insights into cluster formation, evolution and death by disruption. The populations of clusters in fairly nearby galaxies such as M 31 (e.g. Narbutis et al., 2008; Caldwell et al., 2009; Peacock et al., 2010) have previously been studied and can give more accurate and expansive results due to their position outside of the Milky Way, where extinction effects are at a minimum.

1.4.1 Population properties

The luminosity function (LF) of a cluster population provides insight into the mass function of the clusters. It is found to behave as $\mathrm{dN/dL} \propto \mathrm{L}^{-\alpha}$, although some deviations from a pure single valued power-law have been reported (Gieles et al., 2006a), including a steepening at the bright end. An example is the bend observed in the LF in the Antennae galaxies by Whitmore et al. (1999), which can be fit with a double power law. When the power law section of the distribution is fit, α is usually found to be ≈ 2, with small variations (e.g. de Grijs et al., 2003; Larsen, 2002). This indicates that the most luminous cluster in the distribution will scale linearly with the number of clusters and no special processes have to be introduced in order to form higher luminosity clusters (Portegies Zwart et al., 2010). A similar relation has been found between the maximum luminosity and the star formation rate (Weidner et al., 2004; Bastian, 2008).

The luminosity function can be considered a proxy for the mass function of clusters using a directly observable quantity. A direct comparison may not be made, however, as clusters of the same mass but varying ages will have different luminosities due to fading over time. A down-turn in the LF can result from a truncation at the high mass end of the cluster initial mass function (CIMF, e.g. Gieles, 2010). However, this truncation in the CIMF may be difficult to discern due to low numbers of massive clusters, though if a truncation is observed it can indicate that the mass function has been well sampled and points to the existence of a maximum cluster mass (Gieles et al., 2006b). Fully understanding the CIMF would be invaluable for cluster formation studies, as well as work on cluster disruption, though its estimation is extremely difficult.

The shape of the mass distribution has been questioned in a variety of studies, with some concluding that it is best fit with a pure power law (e.g. Bik et al., 2003; Whitmore et al., 2010; Chandar et al., 2010a, 2011) where $\mathrm{dN/dM} \propto \mathrm{M}^{-\beta}$ with $\beta \approx 2$ (e.g. Zhang & Fall, 1999; Bastian et al., 2012). Others report a truncation at the high mass end, best fit by a Schechter function (e.g. Larsen, 2009; Gieles et al., 2006b; Maschberger & Kroupa, 2009). In the latter case, the fit is characterised by a power law at low masses with an exponential truncation at the high mass end as $\mathrm{N\ dM} \propto \mathrm{M}^{-\beta}\exp(-\mathrm{M/M_C})\ \mathrm{dM}$, where $\mathrm{M_C}$ is the characteristic truncation mass. M_C is found to be $\sim 2 \times 10^5$ $\mathrm{M_\odot}$ in spiral galaxies (e.g. Gieles et al., 2006b) and $\gtrsim 10^6$ $\mathrm{M_\odot}$ for interacting galaxies, such as the Antennae (Bastian, 2008), indicating that this value

is dependent on galactic environment. Johnson et al. (2017) report a truncated MF for M 31, with currently the lowest characteristic turnover mass, which they find scales with the surface density of star formation.

Another property of clusters that has been measured across populations is that of cluster sizes. Studies of clusters in a variety of galaxies, including the Milky Way (e.g. Portegies Zwart et al., 2010) and others nearby (e.g. Mackey & Gilmore, 2003; Larsen, 2004b) show a fairly uniform peak value in the size distribution of effective or half-light radii of 2-3 pc. Cluster half-light radius also does not seem to be strongly correlated with age (e.g. Larsen, 2004b) and may increase with increasing galactocentic radius (e.g. Jordán et al., 2005). Most interestingly, despite a correlation between mass and radius in GMCs, which are cluster progenitors (e.g. Scheepmaker et al., 2007), there is no observed similar correlation in cluster mass and radius (Zepf et al., 1999; Larsen, 2004b). While the half-light radii do not seem to correlate with age, cluster core radii have a strong relationship with age, where older clusters have larger core radii (Mackey & Gilmore, 2003; Glatt et al., 2009).

Confirming a truncation in the mass function is a key aspect of cluster population studies that has yet to be resolved. Chapter 2 explores this question for NGC 1566, confirming the presence of a truncation for this galaxy.

1.4.2 Cluster disruption and property distributions

Theoretically, disruption should depend on the cluster's initial mass and its environment, with clusters in weaker tidal fields or higher masses surviving longer (e.g. Baumgardt & Makino, 2003; Gieles et al., 2006c). However, empirical studies have resulted in two separate theories for the disruption process: MID (Mass Independent Disruption) and MDD (Mass Dependent Disruption).

Understanding and interpreting age and mass distributions of clusters strongly depends on how disruption is modelled during the cluster lifetime. MDD has been evidenced and displayed via empirical studies (Boutloukos & Lamers, 2003; Lamers et al., 2005) and N-body simulations (Baumgardt, 2001; Gieles et al., 2004) where disruption is found to depend on the initial mass of the cluster and the environment within the galaxy. The timescale for disruption has been found to depend on the cluster mass as M^{γ}, where γ varies slightly between different galaxies, with a mean value of $\gamma = 0.62$ (Boutloukos & Lamers, 2003). Simply, this indicates that higher

mass clusters live longer. In this scenario, disruption is also dependent on environment due to tidal effects and the ambient density within the galaxy (Lamers et al., 2005; Lamers & Gieles, 2006).

The opposing idea to MDD has been proposed, claiming that disruption, up to an age of $\sim$ 1 Gyr, is independent of mass and galaxy environment (Whitmore et al., 2007). MID is based on studies of the Antennae (Fall et al., 2005), Large Magellanic Cloud (Chandar et al., 2010a) and the central regions of M 83 (Chandar et al., 2010b). According to these studies, independence of disruption from mass and environment results in a quasi-universal age and mass distribution with the number of clusters declining as a function of age as t^{-1} (Whitmore et al., 2007). However, the cause of this rapid disruption has not been suggested, i.e. what process within clusters could be independent of mass and environment and destroy clusters at such high rates.

Potential models combining these two ideas have been explored and can be found to fit observed data for fast or slow disruption and disruption from internal mechanisms or outside influence (such as nearby clouds) with certain assumptions within reasonable limits (Elmegreen & Hunter, 2010b). Additionally, if tidal shocks are sufficiently strong, disruption may be mass independent (with an age distribution as t^{-1}; Kruijssen et al., 2011), however there will still be a strong environmental influence. This indicates that fully constraining disruption mechanisms can be a difficult process.

Age distributions have been widely studied for different galaxies and can provide insight into the process of disruption in a galaxy. The general shape of the distribution is a power law section with a steepening at high ages. The shape of the distribution is determined by the star formation history of the galaxy and the amount of disruption present. If approximated as a single power-law, $\log(dN/dt) \propto t^{\zeta}$, where studies to date have found ζ to vary between 0 and -1 (e.g. Fall et al., 2005; Gieles et al., 2007a; Chandar et al., 2010b; Silva-Villa & Larsen, 2011; Bastian et al., 2012; Ryon et al., 2014). Lamers (2009) suggested that within an MDD framework the age distribution could adopt a three-part shape with a decrease over the first $\sim$ 10 Myr, a flat period up to $\sim$ 100 Myr and a further decrease at large ages.

Studies of M83 show environmental dependence in the age distribution, ranging from nearly flat ($dN/dt \sim t^{0}$) to relatively steep ($dN/dt \sim t^{-0.7}$; Silva-Villa et al., 2014) at different galactocentric distances and so consistent with a strong environmental influence. This was also

found by Chandar et al. (2014) (radially dependent index of the age distribution) who needed to invoke radially dependent differences in the cluster formation history in order to bring the age distributions in the inner and outer regions of the galaxy into agreement.

Bastian et al. (2012) found that both the MID and MDD scenarios could provide good fits to the observed age distributions of clusters in M83, however, disruption needed to be strongly dependent on environment. Additionally, these authors found that the mass function for the clusters was truncated, and the truncation value depended on environment. The truncation in the mass function was necessary to include in disruption analysis in order to explain the age distribution in the MDD framework.

An open question in cluster disruption is still the confirmation that disruption is environmentally and mass dependent. This is explored for NGC 1566 in Chapter 2.

1.4.3 Tracing host galaxy properties

More recently, other cluster properties have been used to investigate the relationship between the clusters and their host galaxy. One such property is the magnitude of the brightest cluster in the V-band of a population, $M_V^{brightest}$ (Larsen, 2002; Whitmore, 2003). There is an observed relation between this quantity and the star formation rate (SFR) of the galaxy which is interpreted to be due (mainly) to a size-of-sample effect (see Adamo & Bastian, 2015, for a recent review).

Γ, or the cluster formation efficiency (CFE), is the fraction of stars that form within clusters in a given environment/galaxy (see Bastian, 2008). Kruijssen (2012) presented a model that relates the CFE to the formation process of clusters, so when local density distributions are taken into account, the CFE should scale with the gas surface density of the galaxy leading to a decrease with distance from the centre of any individual (spiral) galaxy. The cluster formation efficiency should also then scale with the surface density of star formation (Σ_{SFR}) in the galaxy via the Schmidt-Kennicutt law (Kennicutt, 1998; Kennicutt & Evans, 2012), which has been observed in many galaxies to date (e.g. Goddard et al., 2010; Ryon et al., 2014; Adamo et al., 2015). This indicates that Γ can be used to probe the effect of galactic environment on cluster population properties. Additionally, a variation in CFE with distance from the galactic centre has been found for M 83 (Silva-Villa et al., 2013; Adamo et al., 2015) and a variation with environment in M 31 (Johnson et al., 2016). Johnson et al. (2016) also report that gas

depletion time must be taken into account to reduce the scatter in the CFE - $\Sigma_{\rm SFR}$ relation, as low intensity star formation. Measurements of CFE over different timescales can also provide insight into cluster disruption. A minor difference between successive time bins (such as for M 31; Johnson et al., 2016) indicates a low level of disruption in the galaxy, at least on the timescales measured.

One of the problems with using the CFE as a statistic is that it can be highly dependent on the definition of a cluster used for the calculation. The value can vary if associations are also considered clusters. Additionally, it is dependent on techniques such as SED fitting for cluster ages, which do introduce their own errors and dependencies (e.g. Pacifici et al., 2015).

Chandar et al. (2015) recently presented a new statistic mean to test the CFE; a relation involving the cluster mass function normalised by the star formation rate of the galaxy (CMF/SFR). They report only a weak correlation between the CMF/SFR and the SFR of the host galaxy, and no correlation with $\Sigma_{\rm SFR}$ for the young ($<$10 Myr) cluster population in their sample. When using an older population (100-300 Myr), they did find similar trends as expected based on previous works using Γ (e.g. Adamo et al., 2015). CMF/SFR is not subject to all of the same uncertainties as Γ, though ages, masses and extinctions do still need to be modelled. New findings by Johnson et al. (2017) support a relationship between the cluster mass function and $\Sigma_{\rm SFR}$, as they find a correlation between this and the characteristic truncation mass of the CMF, also without the uncertainties surrounding CFE determination. Kruijssen & Bastian (2016) showed that the discrepancy, at least in part is due to a lack of distinction of bound and unbound aggregates at young ages in Chandar et al. (2015), as well as the need to account for cluster disruption at later ages. It is worth noting, however, that some of the galaxies presented in Adamo et al. (2015) also do not make the distinction between bound and unbound aggregates, though several make age cuts to remove young clusters that likely cause contamination of unbound sources. This lack of uniformity is addressed by the LEGUS survey (Calzetti et al., 2015).

Another correlation between cluster population properties and their host galaxy has been investigated by Larsen & Richtler (2000), where they showed that the percentage of total U band luminosity of a galaxy contained within young massive clusters (YMCs) ($\rm T_L(U)$) shows a relationship with several host qualities including $\Sigma_{\rm SFR}$ and the density of HI emission. $\rm T_L(U)$ can also provide insight into the environmental dependence of cluster populations in the galaxy

(Larsen, 2002). As U band luminosity traces young stellar populations, $\mathrm{T_L(U)}$ can be related to star formation and used as a proxy for CFE with directly observable quantities. The relationship between $\mathrm{T_L(U)}$ and Σ_{SFR} of the galaxy indicates that the amount of star formation occurring in clusters increases with Σ_{SFR}, and so CFE should also increase, though the exact relation between the CFE and $\mathrm{T_L(U)}$ has not yet been quantified. $\mathrm{T_L(U)}$ is found to range from $\approx$ 0.1 - 15 in galaxies with a small cluster population to merging systems, respectively (Larsen & Richtler, 2000).

Fully understanding the relationship between clusters and their host galaxy is still an open question and measuring properties such as Γ *and* $\mathrm{T_L(U)}$ *for more galaxies will help to constrain how the host galaxy environment affects cluster formation and evolution, and how cluster populations affect galaxy properties and evolution. Information about star formation can also be inferred from this, most intriguingly in the high redshift universe using the relationship between* $\mathrm{M_*}$ *and* Σ_{SFR} *for GCs by Johnson et al. (2017). Chapter 2 explores* Γ *and* $\mathrm{T_L(U)}$ *for NGC 1566.*

1.5 Age and mass fitting of clusters using SEDs

Throughout this thesis, the age, mass and reddening estimates for cluster populations have been provided by Angela Adamo, using the process of SED fitting, which has been used extensively in cluster population studies previously (e.g. Bastian et al., 2012; Ryon et al., 2014). The principle of SED fitting is simple in concept, but rather more complicated to put into practise. In terms of clusters, the process requires the synthesis of simple, or single stellar populations (SSPs) emulating the combined light emitted from a collection of stars. The emission is affected by a range of factors that need to be taken into account in order to produce a successful SSP model, including age, stellar spectral type and the metallicity. For clusters however, the assumption of the cluster as an SSP is an acceptable one, as generally they are believed to form in one episode of star formation (e.g. Massey & Hunter, 1998).

Once SEDs are produced from SSP modelling, they are compared to the data of the clusters and the best fit mass is given. Furthermore, age and extinction of the object is provided by comparing the colour of the cluster to a model track in colour space and finding the nearest point on the model track that changes with age. The nearest point on the model along the extinction

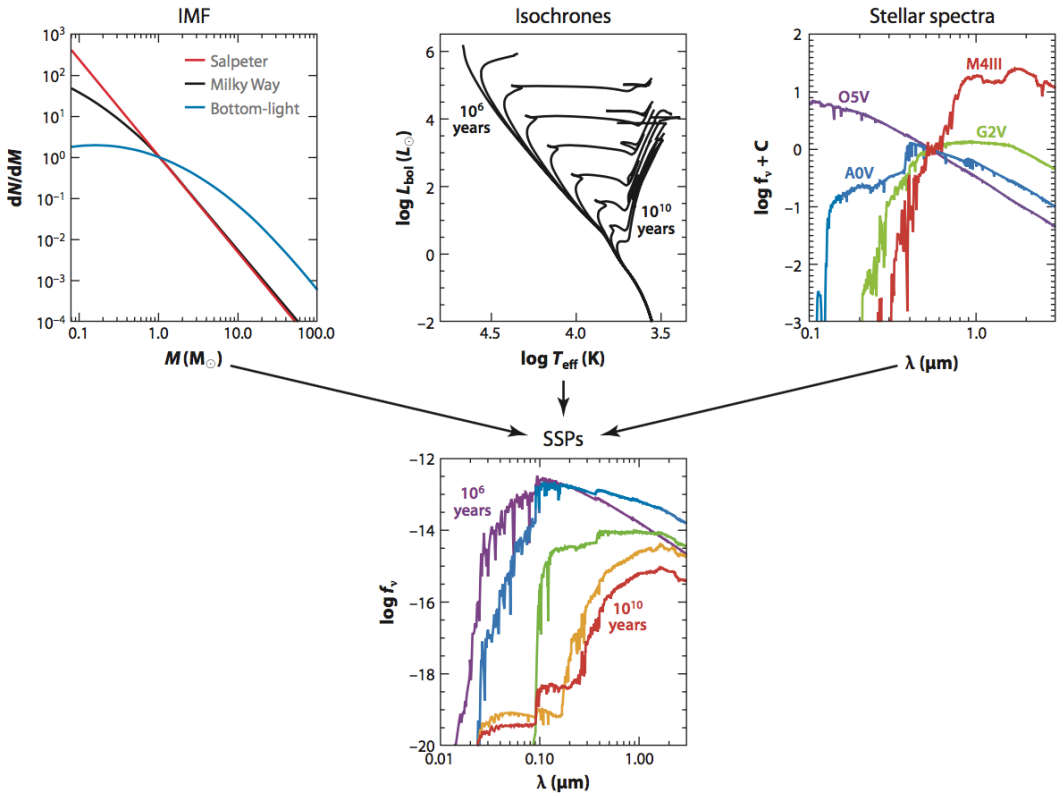

Figure 1.1: Figure illustrating the formation of an SSP model, which was edited and taken from Conroy (2013).

vector (found by considering the levels of extinction in each band used for the colours) provides the cluster age and extinction (Adamo et al., 2010a,b). This process, as well as the process of creating the SEDs and model tracks is subject to many limitations, sources of error and degeneracies.

1.5.1 Limitations and difficulties

Generating SSP models requires the combination of a stellar IMF, isochrones modelling the stars' evolution and known spectra of stars to provide estimates of the stars' chemical composition. This is summarised in Fig. 1.1, which has been taken and edited from Conroy (2013). There are many uncertainties associated with all of these contributions to an SSP model, one of the most fiercely debated being the correct IMF, and whether this is universal or not (e.g. Bastian et al., 2010), though observationally a universal IMF appears to be the case (e.g. Selman & Melnick, 2008). Besides this however, there is also the question of which IMF is correct. A Kroupa (Kroupa & Boily, 2002) or Salpeter (Salpeter, 1955) IMF is most commonly used, with the only significant difference being in the treatment of low mass stars. This is only important

for cluster mass estimation from SSPs, however, as their light is dominated by massive stars and low mass stars contribute a negligible amount of luminosity (Portegies Zwart et al., 2010).

Isochrones also introduce error into the SSP models, as aspects of stellar evolution are not well understood, particularly the later stages. There are also several different libraries of isochrones to choose from, each with slightly different treatment of the stages of stellar evolution. The most common options are the Padova (Girardi et al., 2002) or Geneva (Lejeune & Schaerer, 2001) tracks that offer different modelling of the red giant branch in particular. These differences are not important when studying young clusters, though the Geneva tracks have been found to describe young populations better due to their handling of young RSGs (Bastian et al., 2006).

The process of fitting the resulting SEDs from the SSPs is also affected by a number of degeneracies between the different quantities, most notably the age-metallicity degeneracy. This effect is not significant again for young clusters, as they are assumed to have the same metallicity as the ISM (e.g. Patrick et al., 2016). There are also degeneracies in fitting age and extinction to young clusters using only U, B, V and I colours, however also using Hα or better yet UV (as it is a better tracer of young populations) can break this degeneracy and greatly improves the estimates at young ages (de Meulenaer et al., 2014). A choice of extinction law must also be made when fitting the data. Adamo et al. (2010b) compared the results for ages and masses when using different extinction laws; the Calzetti extinction law (Calzetti et al., 2000) and an extinction law used for the LMC (Fitzpatrick, 1986; Misselt et al., 1999). They found no significant difference in ages and masses with the two laws, only differences in the value for extinction given.

The majority of the sources of error discussed have less of an effect when simulating a young cluster population as the differences and errors in models arise in the low mass regime (which negligibly affects clusters that are dominated by massive stars' flux), or at more advanced ages (after RGB). Additionally, age-dating young clusters can be greatly improved with the inclusion of UV photometry, which is a good tracer of young populations.

1.5.2 Fitting in this work

Throughout this thesis, the age and mass estimates have been obtained using the method in Adamo et al. (2010a,b). This particular fitting process utilises the Yggdrasil SSP models (Za-

ckrisson et al., 2011), which use a Kroupa IMF (Kroupa, 2001) with Padova-AGB isochrones and Starburst99 model spectra (Vázquez & Leitherer, 2005) with Z = 0.02 (Bresolin & Kennicutt, 2002).

The Yggdrasil model has several advantages over other options, such as the modelling of SEDs for both stars and ionised gas, which can have a significant impact on the results for young populations (Anders & Fritze-v. Alvensleben, 2003; Zackrisson et al., 2008). Including nebular and continuum emission allows for the use of Hα to break the age-extinction degeneracy at young ages. Synthetic stellar atmospheres for the model are from Lejeune et al. (1998) and include pre-main sequence evolution. Emission and continuum lines for the gas are estimated using CLOUDY (Ferland et al., 1998), a photoionisation code, and the resulting spectra are redshifted to the target's location.

1.6 Structure of this work

This thesis consists of work undertaken involving contributions to the previously discussed areas of cluster formation and evolution. Chapter 2 investigates the cluster population of the face-on spiral galaxy NGC 1566, including age and mass distributions, while Chapter 3 explores early cluster evolution using a subsample of YMCs from a catalogue for M 83. Chapter 4 searches for multiple populations in two intermediate age massive clusters in the SMC. Finally, Chapter 5 presents a brief overview of the conclusions of each project and ties them together while Chapter 6 discusses the future work required in this field to advance our understanding of cluster formation and evolution.

Chapter 2

The cluster population of NGC 1566

Summary

In this chapter, I present the results of a photometric study into the cluster population of NGC 1566, a nearby grand design spiral galaxy, sampled out to a galactocentric radius of $\approx$ 5.5 kpc. Using HST WFC3 data, age and mass distributions are formed, as well as the luminosity function. Changes in these properties of the cluster population are also studied with increasing galactocentric distance, in order to investigate the effect of galaxy environment on cluster evolution. Additionally, the cluster formation efficiency (Γ) and the specific U-band luminosity of clusters ($\mathrm{T_L(U)}$) are calculated. All of these quantities help to reveal the relationship between a cluster population and its host galaxy, which can provide invaluable information for galactic evolutionary studies as well as cluster formation and evolution. The work presented in this chapter has been published in Hollyhead et al. (2016).

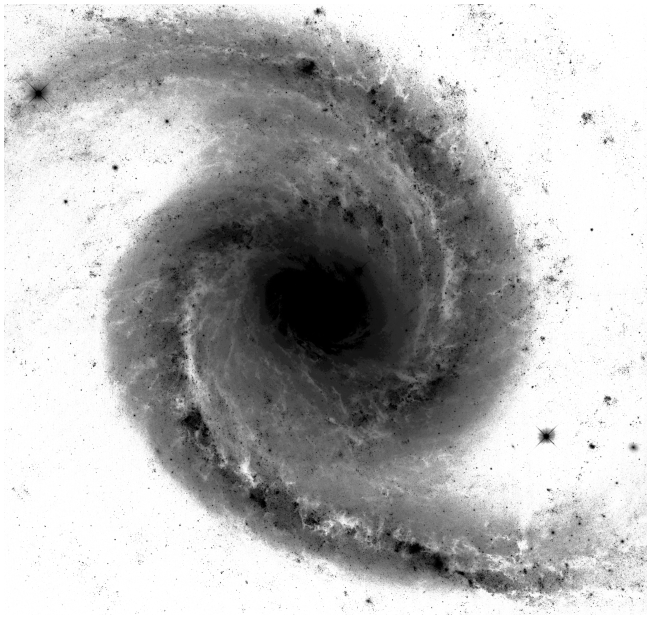

Figure 2.1: Image of NGC 1566 using HST WFC3. The image was produced by equalizing and combining fits images of the galaxy in the B, V and I bands. The resulting image was then edited in the GNU GIMP image processing utility to change the image to black and white and invert the colours.

2.1 Introduction

The study of cluster populations, as opposed to individual clusters, can provide a wealth of information not only about the formation and evolution of clusters, but also their host galaxies. There are many benefits to studying an entire population, as information about cluster formation and evolution can be statistically significant due to the large numbers of clusters.

Much work has been done on cluster populations in several nearby galaxies, most notably on M 83 (e.g. Chandar et al., 2010b; Bastian et al., 2012; Adamo et al., 2015), the Small (e.g. Rafelski & Zaritsky, 2005; de Grijs & Goodwin, 2008) and Large Magellanic Clouds (Baumgardt et al., 2013) and the Antennae (e.g. Fall et al., 2005). By studying the distributions of different cluster properties across the galaxy you can infer how the clusters formed and determine how they evolve over time.

Age and mass distributions as well as luminosity functions have been widely studied for different galaxies. These three tools, as described in more detail in Chapter 1, form the basis of cluster population studies and can reveal information about the history of cluster formation in the galaxy as well as their disruption. More recently, other galactic properties have been used to study cluster populations, such as the magnitude of the brightest cluster in the V-band of a population, $M_V^{brightest}$ (Larsen, 2002; Whitmore, 2003), which has a relationship with the star

formation rate (SFR) of the galaxy. Γ, or the cluster formation efficiency (CFE), which is the fraction of stars that form within clusters in a given environment/galaxy (see Bastian, 2008) is also used. A final property is the percentage of total U band luminosity of a galaxy contained within young massive clusters (YMCs) ($\mathrm{T_L(U)}$), which shows a relationship with several host qualities including Σ_{SFR} and the density of HI emission (Larsen & Richtler, 2000).

This chapter describes a study of the properties of the cluster population of NGC 1566, as shown in Fig. 2.1, the brightest member in the Dorado group of galaxies. It is a face-on spiral Seyfert galaxy (de Vaucouleurs, 1973) at a distance of $\sim$ 17 Mpc (Karachentsev & Makarov, 1996), at which individual clusters can still be resolved using HST data, providing integrated photometry for each cluster. Extensive HST data are already available for NGC 1566 on the Hubble Legacy Archive, covering the inner $\sim$ 5 kpc in many bands from the UV to the optical. This galaxy has also been studied in HI, Hα, CO, X-ray and radio continuum (Kilborn et al., 2005; Korchagin et al., 2000).

Here I construct a catalogue of clusters with photometry in a variety of bands using HST data and simple stellar population models are fitted to the photometry to obtain ages, masses and extinctions. I then inspect the age and mass distributions of clusters in different areas of the disc. Throughout this work I use three separate radial bins to investigate changes in properties with environment. These bins were chosen so that they contained the same number of clusters, and this number was large enough to provide a significant result in each bin. They are arranged from 0-3.3 kpc, 3.3-4.7 kpc and 4.7 kpc to the edge of the image for radial bins 1, 2 and 3 respectively. Fits for the mass and age distributions are then compared to studies of other galaxies.

In § 2.2 I discuss the observations and techniques used to analyse the HST images of the galaxy. § 2.3, § 2.4, § 2.5 discuss results for the observations from NGC 1566, while § 2.6 and § 2.7 discuss comparisons of the data with models. § 2.8 provides an overview of the results.

2.2 Observations and Techniques

2.2.1 Data and photometry

The images used in this study were taken from the Hubble Legacy Archive (HLA), having previously been fully reduced and drizzled with exposures covering the inner regions of NGC 1566 (out to ≈ 5.5 kpc) over a range of wavelengths, assuming a distance modulus of $\mathrm{m} - \mathrm{M} \approx 31.2$. The galaxy is part of the Legacy ExtraGalactic UV Survey (LEGUS; Calzetti et al., 2015, HST project number GO-13364) and as such has complete and homogeneous imaging coverage in the UV (F275W), U (F336W), B (F438W), V (F555W) and I (F814W) bands with WFC3. No conversion was made to the Cousins-Johnson filter system, but the central wavelengths of these bands are approximately equal to the WFC3 bands, so we use this nomenclature for simplicity.

No prior catalogue was available for this galaxy at the time, so I carried out photometry on the images, using SOURCE EXTRACTOR (Bertin & Arnouts, 1996) within the GAIA package (Draper et al., 2014) included in the Starlink software to locate potential clusters throughout the galaxy using the V band image (the band where most clusters should be visible). No limiting parameters were applied to the source extraction procedure to minimise the number of clusters unintentionally omitted from the detection. Additionally, the catalogue would undergo extensive refinement at a later stage, so any unreliable sources or false detections would later be removed. ~ 20000 sources were identified. The resulting coordinates were then used to carry out aperture photometry in the DAOPHOT package in IRAF. Magnitudes for each source were obtained using apertures of 1, 3 and 5 pixels (corresponding to 0.04, 0.12 and 0.2 arcseconds respectively, or 3.3, 9.9 and 16.5 pc), with sky background annuli between 15 and 17 pixels (0.60 and 0.68 arcseconds or 49.5 and 56.0 pc respectively) for the UV, U, B, V, and I bands.

2.2.2 Catalogue refinement

The source catalogue included many false detections and unwanted objects such as stars or possibly background galaxies. The first cut made to the objects to reduce the number of false detections involved removing any objects that were not sufficiently detected in the U, B, V and I bands. Any objects without photometric magnitudes in all of these bands were removed.

Similar to the work done by Chandar et al. (2010b) and again by Bastian et al. (2012) and Silva-Villa et al. (2014) for M 83, I used concentration indices (CIs) to refine the sample further. A CI is a measurement of how centrally concentrated emission is for a source using a calculation such as that shown in Equation (2.1), where Mag_1 pix denotes the magnitude measured for the cluster using a 1 pixel aperture, and likewise $\mathrm{Mag}_{3\mathrm{pix}}$ for a 3 pixel aperture. This value helps distinguish between field stars and clusters; stars should be highly centrally concentrated as point sources, whereas clusters have extended profiles.

$$\mathrm{CI}_{1-3} = \mathrm{Mag}_{1\mathrm{pix}} - \mathrm{Mag}_{3\mathrm{pix}} \tag{2.1}$$

The CIs were calculated by subtracting the magnitudes in the 3 pixel aperture from the 1 pixel aperture and a magnitude cut of $\mathrm{m_V} = 26$ (corresponding to $\mathrm{M_V} =$) -5.2 was applied to remove any sources with poor photometry. This value was selected by minimising the loss of sources and the average error of the remaining sources simultaneously, as shown in Fig. 2.2. A magnitude of 26 also corresponds to a chosen error cut of 0.2 (as also shown in Fig. 2.2), which is applied after CI selection to ensure all sources have good S/N. Additionally, cutting sources below this magnitude is an initial step in reducing the number of stars. The overlapping of the two different populations indicates that there may still be some stellar contamination in the remaining cluster population. A fairly severe cut was chosen to ensure that the catalogue more reliably consisted of extended sources, meaning that some compact clusters may be missed.

The estimated number of clusters lost due to the CI cut is $\approx 34\%$ or ≈ 750 cluster candidates. This value was obtained from Monte Carlo simulations of a Gaussian with the same parameters as the peak of clusters in the plot. Using 1000 random distributions generated, the mean of the number of clusters below a CI of 1.3 was calculated and converted to a percentage of total clusters, which was then applied to the number of cluster candidates obtained from the data.

The plot of the CIs shown in Fig. 2.3 demonstrates three peaks: the first at ~ 0.5 likely consists of cosmic rays, dead pixels or other incorrect object detections such as bright areas near the image borders, the second contains singular stars and the final peak with a smooth tail is the cluster population. Removing all sources with CIs not in the final peak leaves the cluster candidates.

Aperture corrections were calculated in each of the bands to account for flux missed by using

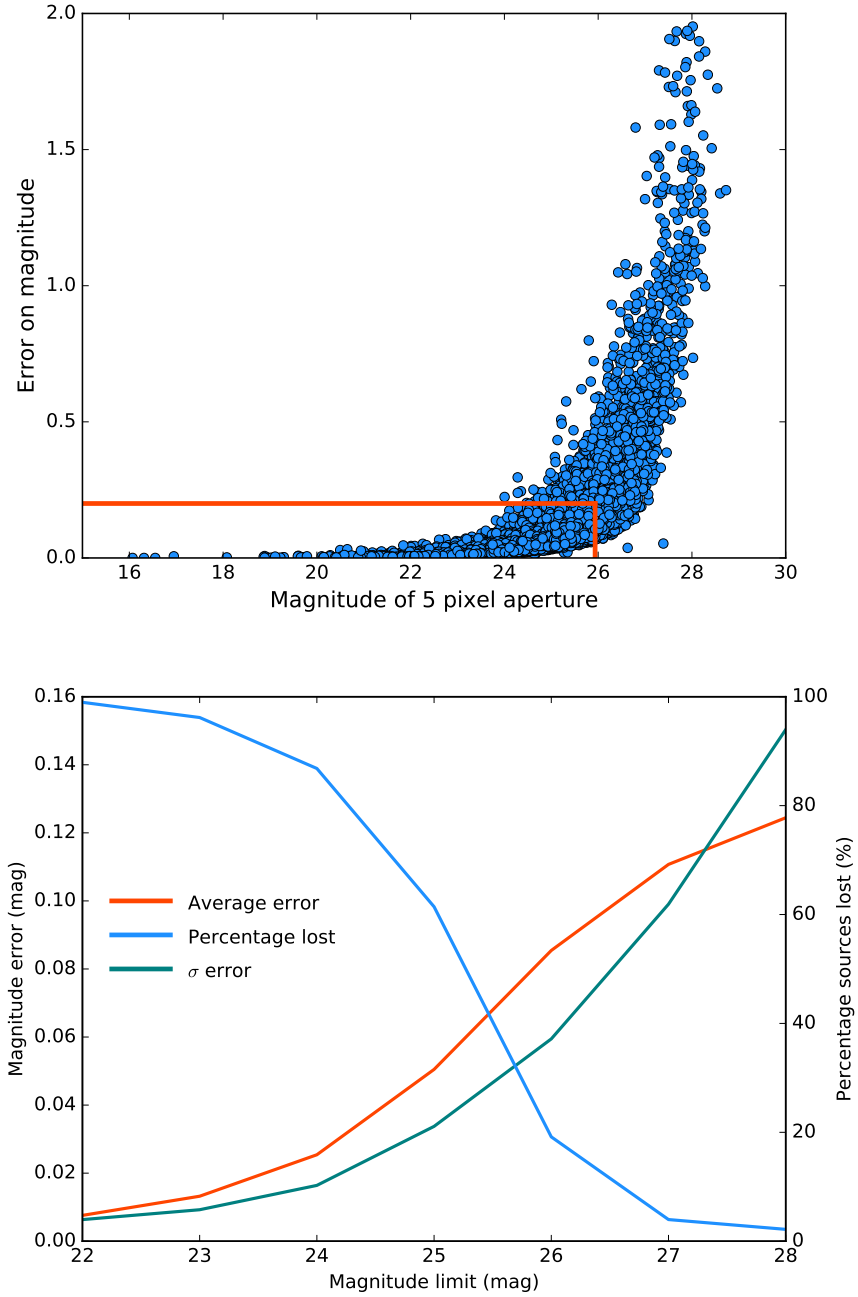

Figure 2.2: Criteria used to determine the magnitude cut applied to the data prior to further refinement. The top plot shows the magnitude measured in the V band in a 5 pixel aperture against the error. An error cut of 0.2 is indicated, which corresponds to a magnitude cut of 25.9. On the bottom plot, the left y axis shows the error on magnitudes, while the right y axis shows the percentage of clusters lost when different magnitude cuts are applied. The x axis shows the various magnitude cuts applied between 22 and 28 using V band data. The red line plots the change with average error, the blue the percentage of clusters lost and the teal shows the standard deviation on the error for different cuts.

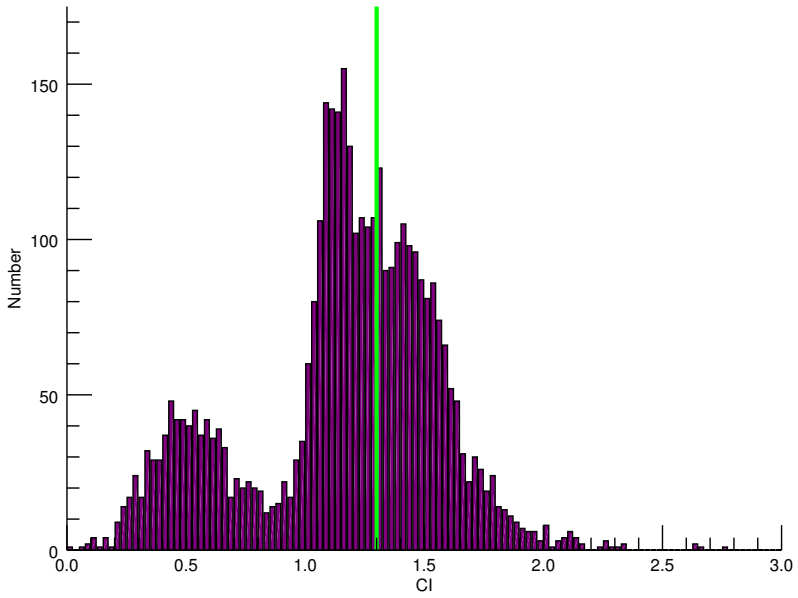

Figure 2.3: Histogram of the concentration indices calculated by subtracting the 3 pixel magnitude from 1 pixel magnitudes for each of the cluster candidates. The main distribution clearly displays two peaks: the first sharper peak consists of stars with a low concentration index, the second with a longer tail is the cluster population. The left-most sub-population at CI = 0.5 is likely due to cosmic rays. The green line indicates the value of the CI that we used to cut the detections into point sources and clusters.

a small aperture. This process involved visually selecting $\sim$ 30 extended sources that were isolated in a variety of locations in the galaxy and using IRAF to obtain photometry with apertures from 1-15 pixels at 1 pixel intervals. A radial profile for each cluster was created using these magnitudes for each filter. Ideally the profiles would rise rapidly from the centre for the first few pixels then begin to flatten asymptotically to the magnitude equivalent to using an infinite aperture. In practice this is not always the case, so each radial profile was inspected visually to remove any sources that would pollute the final aperture corrections. This included sources with dips in the profiles, and those that had not flattened sufficiently, but were still rising at 15 pixels (likely due to the sampling of nearby sources).

The aperture corrections were calculated by averaging the difference between the 5 pixel and 15 pixel apertures in each band: 0.40, 0.34, 0.34, 0.32 and 0.36 magnitudes for the UV, U, B, V and I bands respectively. These corrections were subtracted from the magnitudes of each cluster.

The previous magnitude cut of 26 mag was applied across all bands to ensure high quality photometry in addition to the current cut in the V band. This ensured all final sources were reliably detected across these key wavelengths for the purposes of age and mass fitting. Detection in the UV band was useful if possible but not essential. An error cut of 0.2 was then applied. At this point, automated computer-based methods are poor at refining the catalogue and reducing the number of contaminants, so source inspection by eye was carried out on the remaining 3802 objects, as per Bastian et al. (2012); Silva-Villa et al. (2014) and Adamo et al. (2015).

Each source was labelled according to the degree of likelihood of being a true cluster by utilising the IMEXAM tool in IRAF with DS9. With this software it is possible to view the radial profile and density map of the cluster's emission and ensure each cluster was a single extended source and not multiple stars within the same aperture, or an association. Unresolved single stars could also be identified this way using the magnitude and sharpness of the peak in the profile. With these tools I assigned a label to each cluster based on the following descriptions: 'Class 1' was assigned to sources that were clusters, i.e. they were symmetrical and extended without an extremely sharp peak, 'class 2' was assigned to sources that could potentially be clusters but were more likely to be associations i.e. multiple peaks in the density profile and 'class 3' was assigned to objects that were not clusters, such as unresolved point sources or possibly background galaxies.

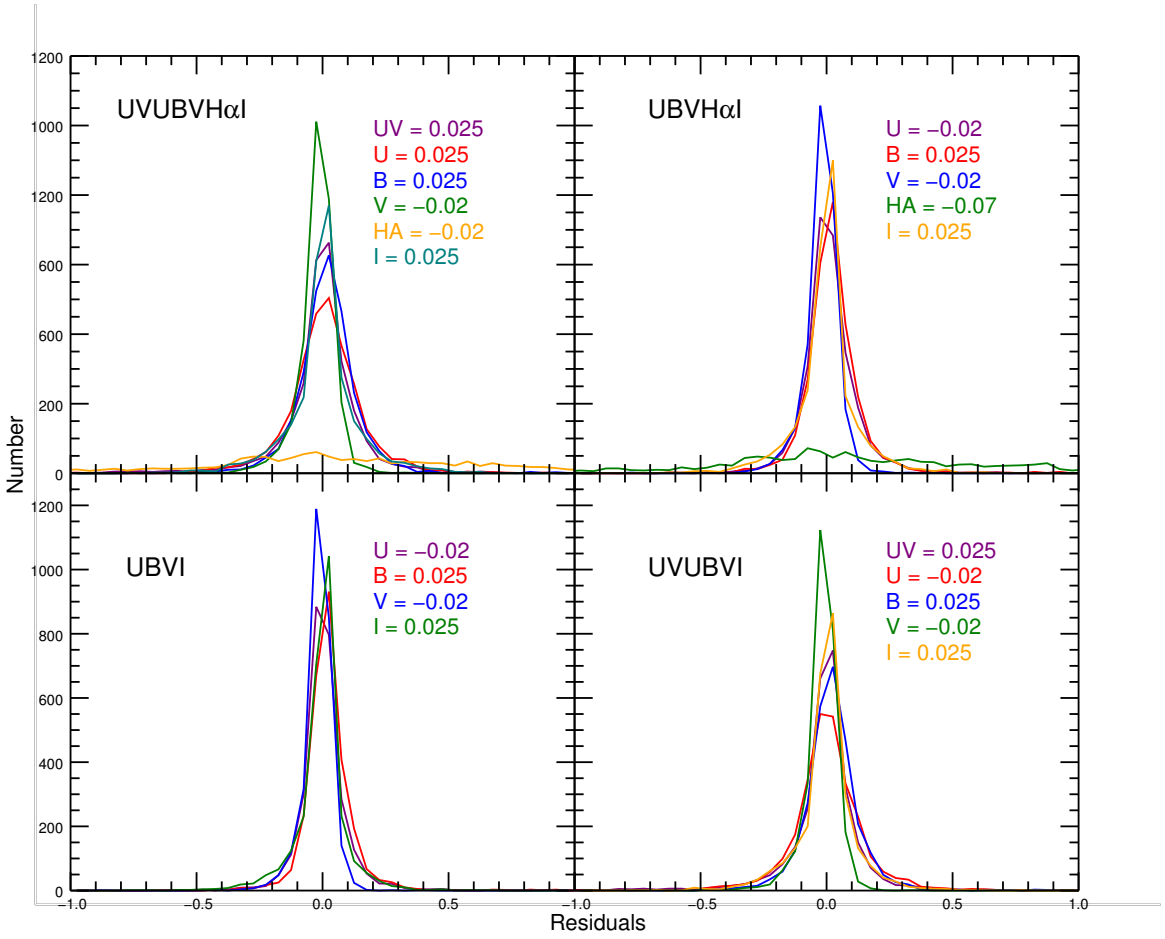

Figure 2.4: Plots of the residuals for each potential fit. The value of the peaks for each band are displayed beside each plot. Most bands peak very close to zero for all fits.

2.2.3 Age and mass fitting

The magnitudes for each cluster obtained from photometry were used to fit ages and masses for each of the clusters. The fitting procedure was done as per Adamo et al. (2010a,b), by comparing each cluster's SED with simple stellar population Yggdrasil models (Zackrisson et al., 2011) using a Kroupa IMF (Kroupa, 2001). The models incorporate super solar metallicity and account for nebular and continuum emission.

Traditionally, Hα magnitudes (magnitude measurements obtained from photometry of images taken with the F657N filter that traces Hα, as used in Bastian et al., 2012) are used to break the degeneracy between age and extinction at young ages (e.g. Whitmore et al., 2010) in order to give more accurate estimates of cluster ages. However, the Hα image for NGC 1566 is only available in WFPC2 data, with smaller coverage of the galaxy, therefore these procedures were repeated for a number of different combinations of bands used to create the cluster's

SED. For example, ages and masses were fitted for the combinations of UV, U, B, V, Hα and I (UVUBVHαI), U, B, V, and I (UBVI) and the most widely used combination: U, B, V, Hα and I (UBVHαI). These fits could all potentially have issues in accurately age-dating the clusters as not all sources have Hα or UV band magnitudes.

Each of these fits were compared using the residuals (difference in magnitude between the measured value and the value corresponding to the best fit age and mass) in each band. The fit with the majority of the bands peaking closest to zero would indicate the best fit, as the model magnitudes are closest to the actual data. Plots of the residuals for each fit are shown in Fig. 2.4. Most of the bands for every fit peak around very similar values, apart from Hα in the UBVHαI fit, which peaks at -0.07 instead of the -0.02-0.025 for all other bands. The plot also clearly displays the large difference in numbers of clusters with UV, U, B, V and I photometry compared to those with Hα.

SSP models assume that contributions to the flux from ionised gas emission are present in young clusters, however it has been shown that clusters as young as 2-4 Myr have expelled their remaining gas (Bastian et al., 2014b; Hollyhead et al., 2015), as discussed in detail in Chapter 3. The early removal of gas means that the Hα emission is lower than model predictions, which likely gives an older age for the cluster than its actual age. Additionally, the distributed nature of Hα means that it can be difficult to identify whether emission is actually associated with the cluster itself or due to nearby (unrelated) objects.

Due to these factors, UV was a better choice for disentangling degeneracies in the fitting procedure than Hα. Furthermore, UV emission is associated with massive stars within clusters, and so is more reliably representative of the cluster. The potential for using UV to disentangle degeneracies in age dating of clusters is a key aspect of the LEGUS survey (Calzetti et al., 2015).

2.3 Colour-colour plots

An interesting result of previous studies of cluster populations has been that clusters closer to the central regions of the galaxy display different properties than those further towards the edge of the galaxy, showing variations in quantities such as age and mass. Outer cluster populations would be expected to contain more old clusters due to lower levels of disruption.

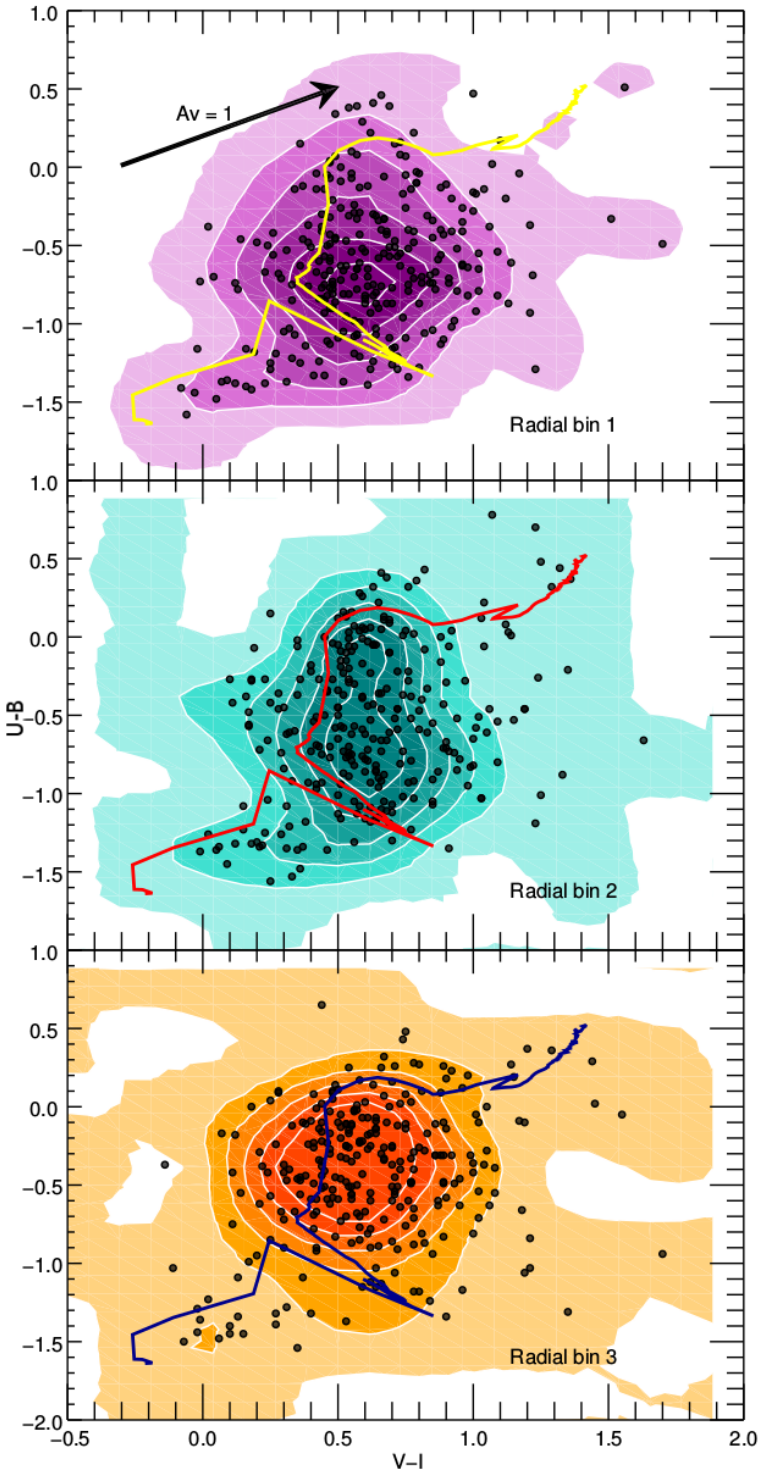

Figure 2.5: Colour-colour plots for clusters in NGC 1566. The clusters have been split into equal numbers in radial bins of 0-3.3 kpc, 3.3-4.7 kpc and 4.7 kpc outwards. The plots show the traditional U-B vs V-I colours. They are overplotted with models showing the evolutionary tracks of clusters and contours are plotted to show the concentration of the clusters in colour space. The extinction vector showing the movement of clusters on the plot due to extinction effects is in the top left corner.

	Median U-B	Median V-I
Bin 1	-0.90/ **-0.64**/-0.33	0.46/ **0.60**/0.78
Bin 2	-0.92/ **-0.57**/-0.18	0.46/ **0.60**/0.77
Bin 3	-0.68/ **-0.38**/-0.11	0.44/ **0.59**/0.78

	Mean U-B	Mean V-I
Bin 1	-0.62±0.03	0.62±0.02
Bin 2	-0.55±0.03	0.63±0.02
Bin 3	-0.43±0.03	0.62±0.02

Table 2.1: The difference in colour properties for cluster populations at different galacto-centric distances. The three bins are those used throughout the analysis. The top table shows median U-B and V-I colours (shown in bold) that were calculated over the entire populations and then compared to see if there were major differences in the colour properties of the clusters at further distances from the centre. Values to the left of the median are the lower quartiles and to the right are the upper quartiles. There is little difference in the values for V-I, but U-B shows more variation. The second bin with two maxima on the contour diagram has the largest inter-quartile range, which would be expected of a more spread distribution. The bottom table shows the mean values of each bin, which show a similar change in U-B values compared to no change in V-I as seen in the medians. The changes in U-B are greater than the standard error on the mean, as stated, whereas they are within errors for V-1.

A study of NGC 4041 found a marked difference in the position of clusters in colour space, with clusters closer to the centre of the galaxy in a bluer space than those in the outer regions (Konstantopoulos et al., 2013). Additionally, M 83 also displays a variation in colour for clusters in outer and inner regions of the galaxy (Bastian et al., 2011). In contrast to this finding, Ryon et al. (2014) report no difference in colour space for the cluster population of NGC 2997, though this study compared clusters specifically in the circumnuclear region to the rest of the disk, which could be considered slightly different to other studies.

Fig. 2.5 shows our U-B vs V-I colour-colour plots for NGC 1566. These plots include a mass cut of 5000 $M_{\odot}$ applied to the catalogue to account for stochastic sampling of the IMF and inaccuracies experienced in fitting low mass clusters, and includes only class 1 sources. The catalogue has been split into the three populations at different radial distances from the centre of the galaxy as described in § 2.1, with each bin containing $\approx$ 270 clusters. The evolutionary models for the clusters have been plotted over the points. The clusters that lie to the left of the model track are sources with larger uncertainties.

To investigate the distributions, I found the median U-B and V-I value for each population and found that they were all located in approximately the centre of the distribution, as shown in Table 2.1. The observed trend is very similar to that found for M 83 (Bastian et al., 2011). There is no variation in V-I colour, however there is some difference in the U-B colours, with the middle population displaying 2 peaks in the density of points in the centre, with each

corresponding approximately to the values of the single peaks of the other bins. This indicates that the median U-B colour is continuously changing between bins. Clusters further towards the centre of the galaxy are slightly bluer, in agreement with the results for NGC 4041. The difference indicates that there could be small variations in the ages of the clusters radially from the centre, as age would be the primary contributor to a change in colour. If this is the case, V-I colour would not be expected to change, as it is largely independent of age in the range sampled here (10 - 300 Myr). Therefore, only a vertical shift should be observed, which agrees with the results.

2.4 The luminosity function

Many previous cluster population studies have explored the luminosity function (LF) of clusters in other galaxies. As luminosity is proportional to mass (modulo age), this can provide insight into the behaviour of the cluster mass function using an observed quantity, rather than a modelled one. While this section explores the observed luminosity functions, § 2.6.2 models the LF using information about the clusters from the mass function and presents a comparison with the actual data.

Fig. 2.6 shows the luminosity functions for the three radial bins, showing how the luminosity function for each band varies with distance from the galactic centre. The plots show separate luminosity functions for each of the UV, U, B, V and I bands using the log of the cumulative fraction for the clusters plotted against their magnitude.

The cluster luminosity function is believed to behave largely as $\mathrm{NdL} \sim \mathrm{L}^{-\alpha}\mathrm{dL}$, though the shape is not usually a pure power law, but one that is truncated at the brighter end and can sometimes be better approximated with a double power law function (e.g. Gieles et al., 2006a). Fig. 2.6 shows a levelling at the faintest end, likely due to a combination of reaching the reliable detection limit and potentially the disruption process, which primarily affects lower mass clusters if a mass dependent disruption regime is considered. The truncation at the brighter end is caused by a similar truncation in the cluster mass function at high masses, though this is not always in a one-to-one ratio as differential fading across wavelengths alters the position of clusters of the same mass in the luminosity function. The gradient of the power law section (α) of the curve is measured using the CURVE_FIT utility in PYTHON, which performs a

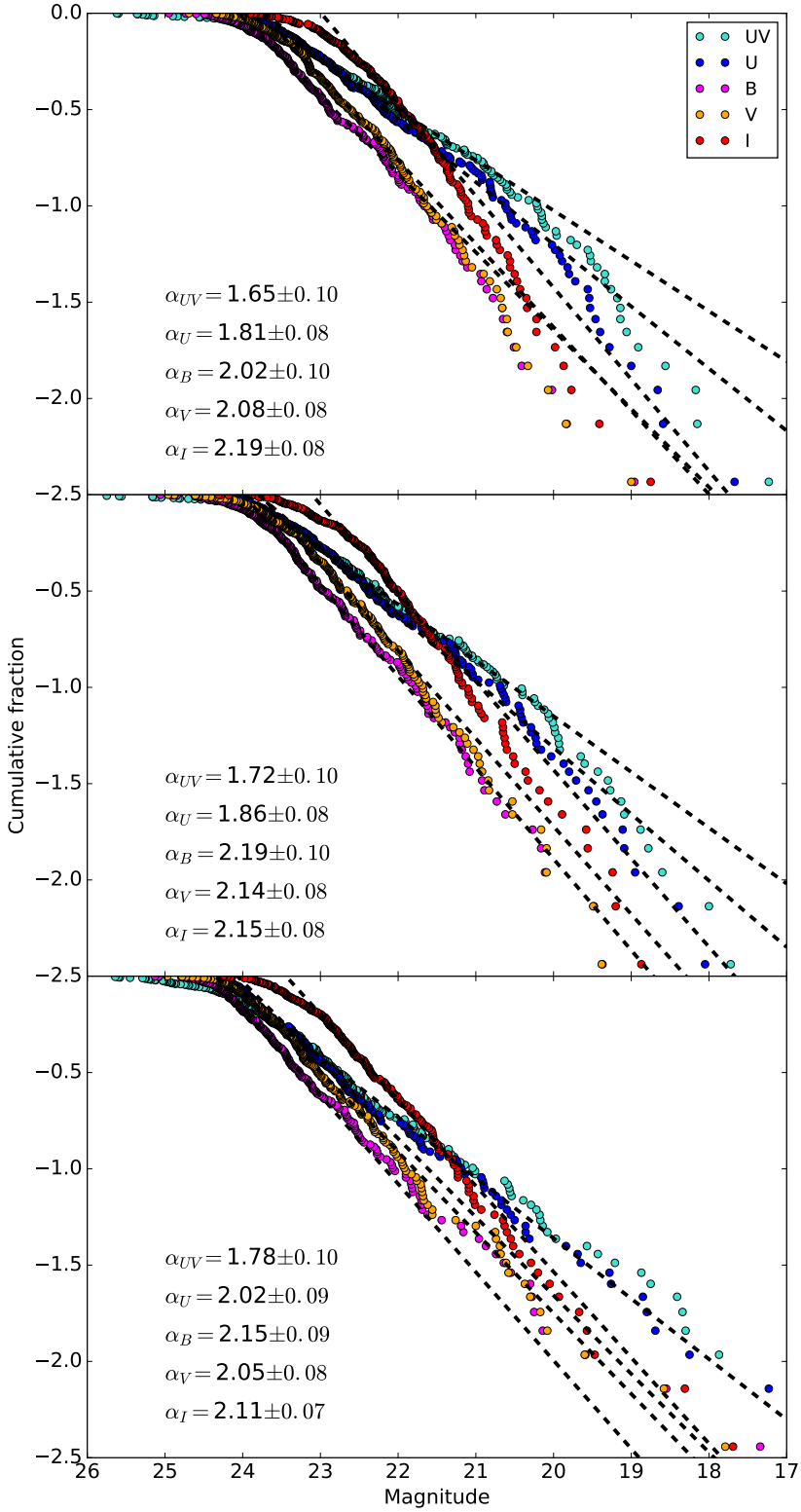

Figure 2.6: Luminosity functions of the three binned regions of the galaxy as a log plot of the cumulative fraction, shown for each band. The shape of the function can be approximated by a power law and the values displayed on the plots are the gradient of fitting the power law section of the function, using the CURVE FIT utility in PYTHON with errors found from fitting synthetic populations created by Monte Carlo techniques.

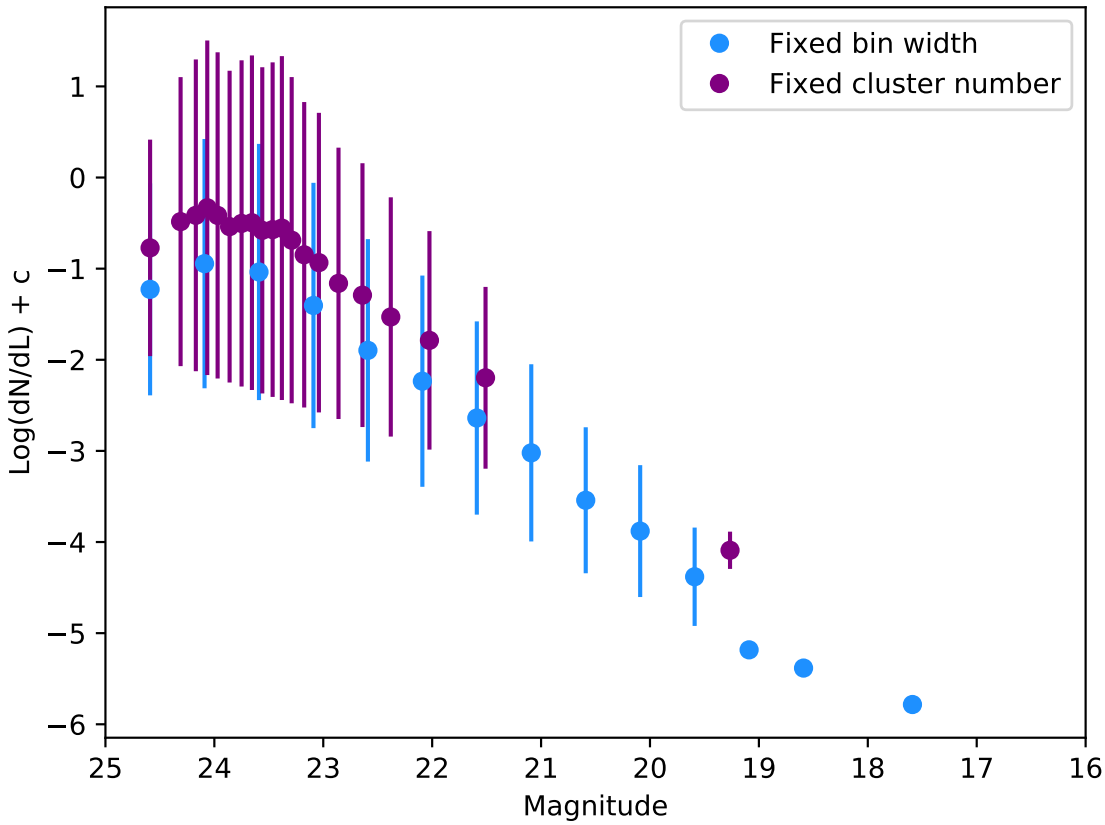

Figure 2.7: The luminosity functions for the whole cluster population above 5000 $M_{\odot}$ for class 1 sources in the B band created by binning the clusters, rather than using a cumulative function. The purple points show a binned function using variable bin width with equal numbers of clusters in each bin and he blue points represent a function with fixed bin width and variable numbers of clusters. The turnover at low luminosity is due to incompleteness and occurs at approximately the same values as for our cumulative function. Far less of a truncation at the bright end is seen in the binned functions, which can easily be dismissed as being within Poisson noise, when in fact this could be a physical effect. Poisson errors are shown for each bin.

Band	Min fit	Max fit
UV	23.5	21
U	23	21.5
B	23.5	22
V	23.5	22
I	22.5	21.5

Table 2.2: The maximum and minimum magnitudes used for the fit of each of the lines in the first radial bin. Other bins were fitted with approximately the same values.

least-squares fit.

The range of luminosities selected for the fits varied slightly between each band, as the position of the power law section changed. The flat end of the distribution at faint luminosities was never included in the fit as the cause of the shape is most likely dominated by our detection limits and magnitude cuts. Additionally, the brighter end of the distributions were also not included due to the low number of clusters and therefore poor statistical significance. The ranges of fits chosen by selecting the magnitude ranges outside of the flat or low cluster number regimes that contained the majority of clusters, so were a good representation of the cluster population. Table 2.2 shows the exact fit ranges for the first bin, with other bins being approximately the same values. The fits are plotted over the curves for each band, and the values of α for each fit are displayed on the plot.

Other similar studies may use a binned luminosity function, as shown in Fig. 2.7 for the B band. All class 1 clusters above a mass cut of 5000 $M_{\odot}$ are used and the plot includes results for variable bin width (purple) and fixed bin width (blue). The turnover at the faint end is due to incompleteness and occurs at approximately the same magnitude as the equivalent turnover in Fig. 2.6. There is less evidence of a truncation at the bright end as seen in the cumulative fraction plots, however the dramatic increase in bin size (for variable bin width) in the bright bins containing the same number of clusters indicates that there are far fewer bright clusters and that there could potentially be a truncation, which is not clearly evident from a binned function. The slight dip in the fixed bin width distribution could be easily dismissed as Poisson noise, when in fact the effect could be physical. Using the cumulative fraction is more sensitive to changes at the bright end, though with the caveat of low cluster numbers and therefore poorer statistics.

Previous studies have found that the value of α is usually ≈ 2, with small variations (de Grijs et al., 2003). Studies of M 83 show that the value is slightly higher for clusters in the outer regions

of the galaxy, indicating a decrease in the number of bright clusters (Bastian et al., 2012). The inner areas of galaxies (just outside of the bulge) would be expected to experience higher levels of star formation than further out into the arms due to a higher density of molecular gas. Ryon et al. (2014) find slightly different results for NGC 2997. The circumnuclear regions were found to be slightly shallower than the disk in the U and B bands but steeper in the V and I bands.

The results agree with the other cluster population studies; $\alpha \approx 2$ with small variations. There are only very small variations in the slopes for clusters between radial bins, with the most prominent differences seen in the UV and U bands. These variations are within the errors on the fit and therefore no definite trend can be determined from these values.

A variation has also been seen in the index of the power law slope between bands of different wavelength. The bluer UV and U bands consistently have shallower slopes than the redder bands in several galaxies (Ryon et al., 2014; Bastian et al., 2014a; Grosbøl & Dottori, 2012). The reason for this trend is likely differential fading of clusters across the different filters. Bluer bands fade more quickly than redder bands so clusters of the same mass will contribute across a wider luminosity range in the UV, for example, while occupying a smaller range in the I band. This spreading out of clusters in the UV and U bands creates a shallower slope (e.g. Gieles et al., 2006a). This is also observed in NGC 1566 with bluer bands generally having shallower slopes. This difference varies from 0.16 to 0.72, when comparing UV and I bands across all bins including their errors. The average difference is 0.43 with $\sigma = 0.18$. All differences are larger than the fit errors shown of ≈ 0.1.

The luminosity function has been observed to be consistent with indices of 2 for associations in addition to tightly bound clusters (Bastian et al., 2007). To investigate this effect within NGC 1566 the same luminosity functions were plotted but only for class 2 sources (i.e. associations and groups). The fits were generally steeper than for class 1 sources, with all between 2 and 3. The slight difference could potentially be explained by the quality of the sources. Unlike class 1 sources, the objects defined as class 2s are more likely to be incorrectly identified as associations, and the sample is more likely to be contaminated with stars (Whitmore et al., 2014). The sample could potentially be polluted with many unreliable sources with poor photometry. Despite this, the value is not drastically different and, in agreement with other studies, points to a process of star formation independent of the scale of the ISM due to the similarity between

the cluster luminosity function and the association luminosity function (Elmegreen, 2002).

2.5 Age and mass distributions

The mass and age distributions of a population of clusters are highly useful for studying the star formation history of the galaxy and the effects of the disruption process. Cluster population studies generally impose a mass cut on the population. This accounts for inaccuracies in age and mass fitting and stochastic sampling of the stellar IMF (Silva-Villa & Larsen, 2011; Fouesneau & Lançon, 2010). Additionally, a mass-limited sample prevents bias in the age distribution caused by young clusters. Fig. 2.8 is the age-mass diagram for class 1 sources in the catalogue for NGC 1566. There appears to be very little difference between the three populations of clusters in varying distances from the galactic centre. The blue line indicates the mass cut applied to the catalogue at 5000 $M_{\odot}$. A large percentage of clusters are lost after applying the cut, ($\sim$50%), however this step is necessary for the reasons mentioned previously.

The limit that appears above the data is due to the mass function - clusters cannot form to an infinitely large mass - the maximum cluster mass and likelihood of forming a cluster of such a mass is determined by the mass function. Additionally, the cut off of data on the lower right hand side of the plot is due to the detection limit of the data. A magnitude limit is imposed by our detectors, which creates the sharp cut off of visible clusters, and which is used to determine the age and mass at which populations are incomplete - our sample appears to be incomplete after $\approx$ 100-200 Myr, when lower mass clusters become too faint to observe.

The age-mass diagram also displays some less populated areas, such as the gap around 10-30 Myr. This is a well-known artefact from the mass and age fitting process and has been previously identified in other galaxies such as M51 (Bik et al., 2003; Bastian et al., 2005) and M83 (Chandar et al., 2010b).

2.5.1 Number of clusters per age bin

Age distributions of clusters across the galaxy can provide information on the formation history of the clusters and the scale or strength of the effect of disruption. By studying different areas of the galaxy you can also determine whether the disruption process is environmen-

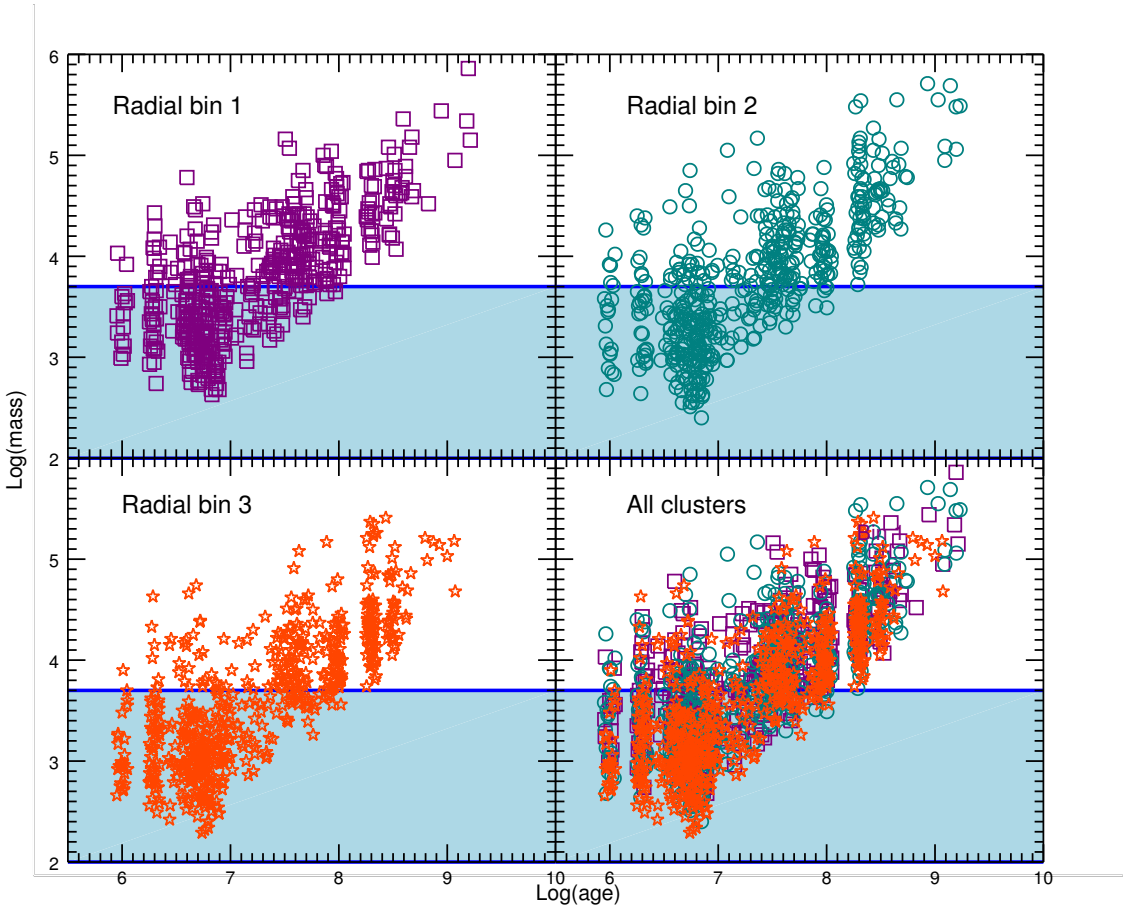

Figure 2.8: Age vs mass for all class 1 sources in the catalogue. Each bin is displayed separately, with the combined population in the final plot. The blue line indicates the age cut applied to the catalogue. The lower limit line on the right side of the plots represent the detection limits in the catalogue, as well as the magnitude cut imposed during the catalogue creation. The apparent ceiling to the data is due to the mass function.

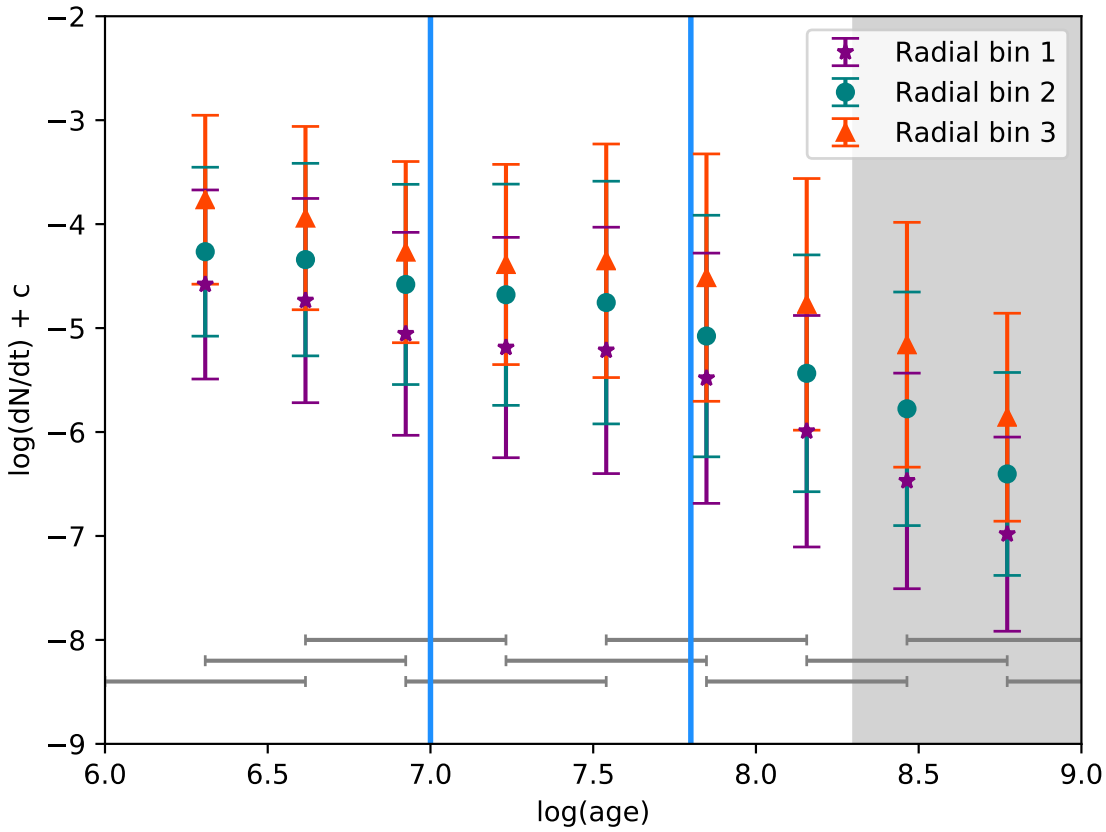

Figure 2.9: The age distributions for different sections of the galaxy. Only class 1 sources above 5000 $M_{\odot}$ have been included. Overlapping bins have been used to remove unphysical variations caused by the binning procedure, with the coverage of each bin shown by the bars at the bottom of the plot. As shown, there is little difference between the shapes of the distributions. A factor has been added to each of the lines to separate the points and make the shape of the distribution easier to see. The two blue vertical lines indicate the separate regimes within the age distribution for the model by Lamers (2009), as described in the text. The plot is shaded after 200 Myr to indicate incompleteness. Poisson errors are shown for each bin.

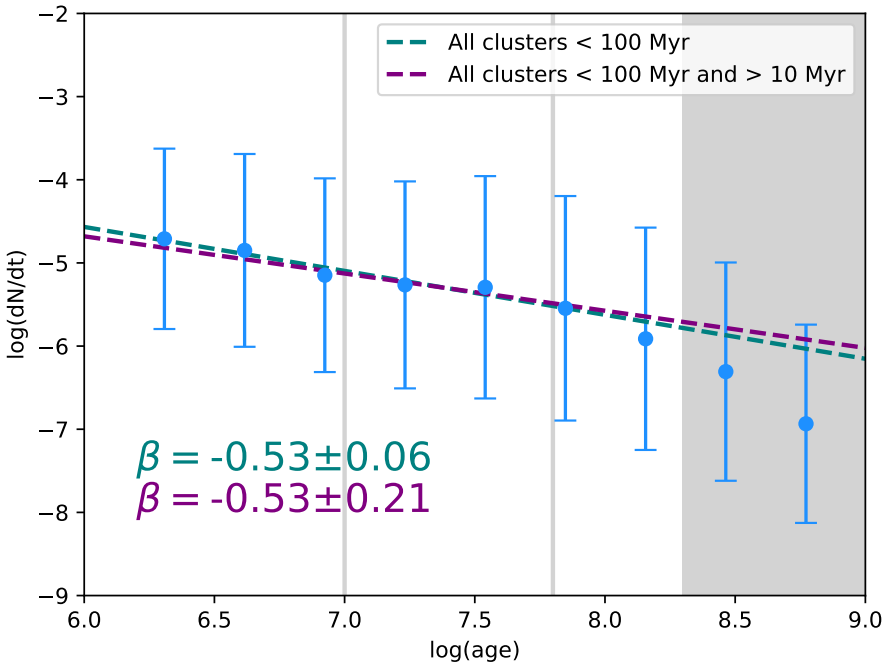

Figure 2.10: The binned age distribution for all clusters $> 5000 M_{\odot}$ and class 1. Poisson error bars are shown on the plot, as well as fits to the data over different age ranges. The teal line shows fits for all clusters younger than 100 Myr, while the purple line shows the fit for clusters older than 10 Myr and younger than 100 Myr. The fits are the same, though the error is larger on the purple fit due to less points being included. The three-component piecewise function could not be fit to the data.

tally dependent (see Chapter 1 for an overview of the differences between mass-dependent and mass-independent disruption). It can be assumed that the shape of the age distribution is only dependent on cluster formation and disruption as the sample is mass-limited. This means that a minimum detection luminosity should not be shaping the distribution until after 100 Myr (e.g. Gieles et al., 2007a), as can be seen in the age-mass diagram.

Fig. 2.9 shows the age distributions of clusters in the three radial subsections of the galaxy, separated by distances of 0.5 in log space to clearly show their shape. The purple, teal and red points show the consecutive radial bins and overlapping bins are used to minimise the effects of the stochastic nature of bin fitting, with the bin sizes shown at the bottom of the plot. Poisson error bars are plotted on each bin and the grey shaded area indicates the regime in which we are incomplete, as is evident from the age-mass diagram in Fig. 2.8.

The shape of an age distribution can usually be roughly approximated by a single power law with steepening at high ages due to incompleteness. When the plot is observed without the Poisson errors, a potential three-component shape could be visible, which is predicted for a regime of mass-dependent disruption, as summarised by Lamers (2009). The blue vertical

lines on the plot indicate the ages at which the three components would separate: 10 Myr within which the decline is caused by the dissolution of young clusters, particularly lower mass systems. However, at least part of this drop is likely due to the inclusion of unbound associations in our cluster sample (Bastian et al., 2012). Another reason for the steepening of the age distribution at young ages could be observational biases. NGC 1566 is a fairly distant galaxy at $\approx$ 17 Mpc, and therefore the densest clusters in the galaxy may appear as point sources, which would be removed by the concentration index cut or visual inspection phases. The full impact of the loss of more compact sources is difficult to estimate, as their properties and contributions to the age distribution are unknown, particularly as there is no observed trend between cluster effective radii and mass, or age, (e.g. Larsen, 2004b).

The next section of a three-component function would go up to 100 Myr and would be flat, indicating little disruption. The final section after this drops due to incompleteness and disruption (Boutloukos & Lamers, 2003). The large error bars on each bin, however, indicate that there is unlikely to be a distinct three-part shape evident in the data.

In order to test whether the plot was indicative of the Lamers (2009) model, the data were fitted with both a normal power law and a three-component piecewise function. The fit was carried out on the entire cluster population with the same mass and class cut as for the radial populations, as shown in Fig. 2.10 using CURVE_FIT in PYTHON. The figure also shows Poisson errors on the bins and grey background indicates incompleteness, while the two vertical grey lines indicate the same sections as in Fig. 2.9. Two fits were carried out: the first is the teal line, which fit a power law to all clusters younger than 100 Myr, as per Silva-Villa et al. (2014). The second, purple line shows the fit for clusters between 10 and 100 Myr, as per Chandar et al. (2014). There is little difference between the fits, apart from the smaller error on the teal line due to the inclusion of more points. A piecewise function was also fitted, however the covariance could not be constrained, as there was no clear fit for such a function with the error bars taken into account, so no fit could be calculated. Therefore, there is no evidence for a three-component shape that may be initially visible by eye.

The age distribution can be susceptible to changes in the binning procedure used to represent the data, though binning is important to overcome small variations caused by artefacts in age fitting. Fig. 2.11 shows how shifting bins can alter the age distribution. Poisson errors of similar magnitude to those displayed in previous figures are present, though not plotted, as it

would be more difficult to see the fits to each function. The top plot fits from 10-100 Myr, while the bottom plot includes all clusters below 100 Myr. As the fit range is so small in the top plot, the fit varies between -0.55 and 0.077, though the bottom plot indicates that there is little difference in the shape of the age distribution between consecutive bins.

Studies have shown that the age distribution is strongly related to the star formation history (SFH) in the galaxy (e.g. Bastian et al., 2009). The distribution can be considered to be independent of cluster formation history if the galaxy is known to have a quiescent history with a constant star formation rate. It is unknown if this is the case for NGC 1566, though the current fairly high rate of star formation (4.3 $M_{\odot}yr^{-1}$; Thilker et al., 2007, amended, discussed later in § 2.7) is likely not a new development as there does not appear to be an over-abundance of very young clusters, as shown in the age distribution. This could suggest a star formation history with a fairly high constant rate of formation. Additionally, while most studies can assume a constant star formation history due to little activity in the galaxy, NGC 1566 is a Seyfert galaxy and is a member of a galaxy group, potentially affecting its recent star forming activity.

A theory of disruption independent of environment (mass-independent disruption, MID, see Chapter 1) would be expected to have the same shape of the age function in all areas of the galaxy as clusters should disrupt uniformly, unaffected by their environment. In this scenario, a single power-law age distribution is expected, with an index of $\sim$ -0.8 to -1 (e.g. Whitmore et al., 2007). More recently, Chandar et al. (2014) have claimed that variations in fit between fields in M 83 is due to differences in the SFH between fields, rather than varying levels of disruption. NGC 1566 does not show any strong evidence for variations in consecutive radial bins, though the fit to the age distribution is shallower than expected for MID.

2.5.2 Observed cluster mass function

The mass distribution of clusters can be approximated by a power law function of the form $\mathrm{Ndm} \sim \mathrm{M}^{-\beta}\mathrm{dm}$ with a possible downturn at the high mass end that could be fit with a Schechter function. Fig. 2.12 shows the mass distributions for the three radial bins for clusters older than 10 Myr and younger than 100 Myr. This age range was selected as incompleteness will affect the shape after 100 Myr (as shown by the age-mass diagram in Fig. 2.8) and below 10 Myr, contamination from associations can affect the results (e.g. Bastian et al., 2012). Additionally age and mass fitting is less accurate below 10 Myr. Only class 1 sources and

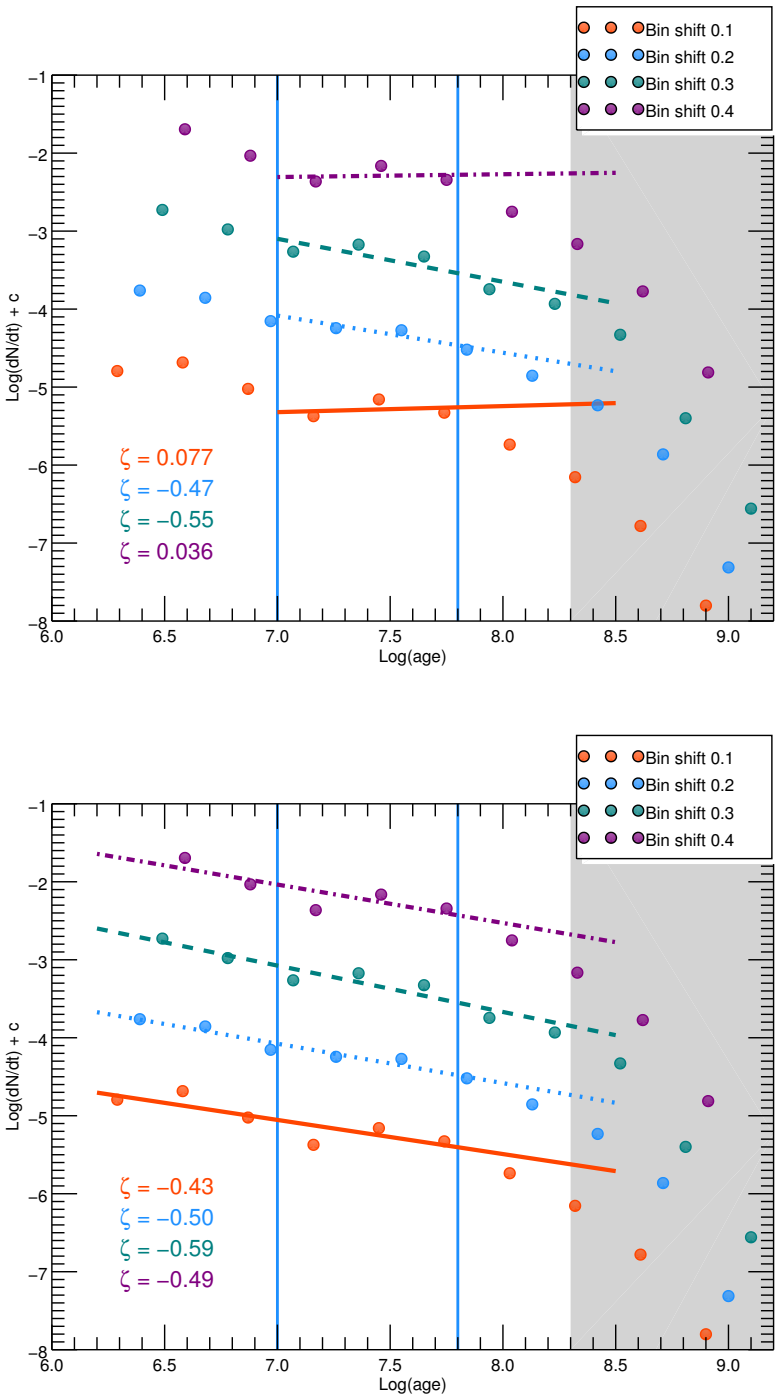

Figure 2.11: The effect of shifting bins in the age distribution for all clusters more massive than 5000 $M_\odot$ and only class 1 sources. This plot uses the same binning procedure as the previous age distribution. The top plot is fitted from 10-100 Myr, not including clusters $<$ 10 Myr, as per Chandar et al. (2014) and the bottom plot includes all clusters below 100 Myr, as per Silva-Villa et al. (2014). The bottom plot, which fits of more points and is more likely to be reliable, shows that there is little difference between the functions for shifted bins, and that binning shouldn't strongly affect the results in the age range where the data is not incomplete.

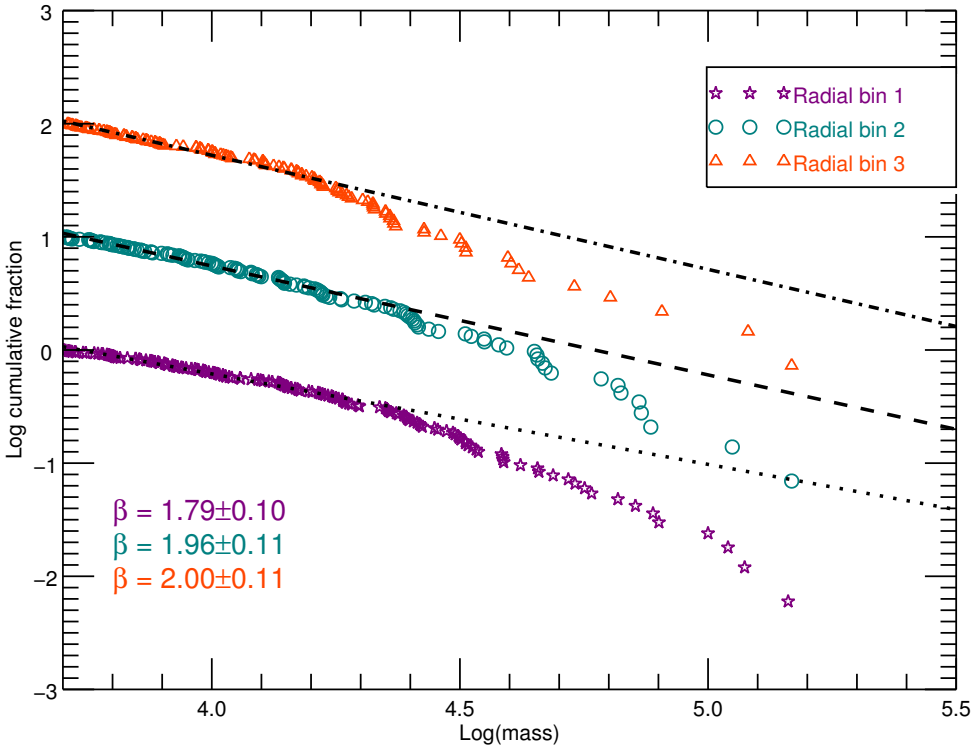

Figure 2.12: The mass distribution for clusters in bins of distance from the centre of the galaxy. The fit to distribution is highly dependent on the range over which the line is fitted. Clusters older than $\approx$ 100 Myr were removed due to incompleteness at high ages. Clusters younger than 10 Myr have also been removed due to possible incompleteness and difficulty in age and mass fitting in this age regime.

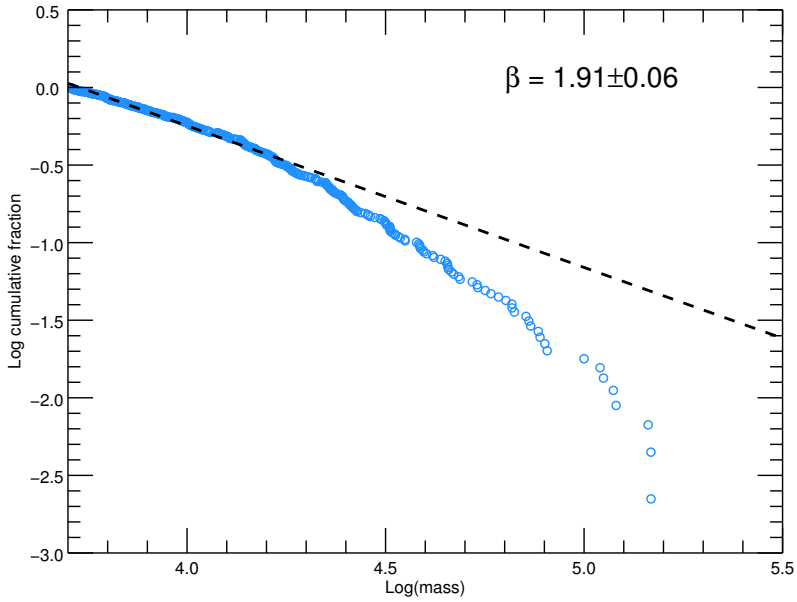

Figure 2.13: The mass distribution for all class 1 sources in the catalogue, with a mass cut of 5000 $M_{\odot}$. The best fit to the power law section is shown in the top right.

those more massive than 5000 $M_{\odot}$ are included. The distributions were fitted by minimising χ^2 from $\approx$ 5000-30000 $M_{\odot}$.There is a variation seen in the best fit for the power law section with respect to galactic radius, with a steeper slope the further out the bin. This could indicate the presence of more lower mass clusters than in the inner regions, which would agree with an environmentally dependent process of disruption. However, the differences are within the estimated errors on the fits and therefore no definite trend can be determined.

Fig. 2.13 shows the distribution for all clusters younger than 100 Myr and older than 10 Myr. The high mass end of the distribution displays evidence of a non-discrete truncation as it deviates from the power law fit line (shown as black dashed line). This effect is unlikely to be due to disruption in a MDD regime, as more massive clusters are affected less by disruption but it could play a part if MID is considered. The errors on the fits are found through Monte Carlo simulations of mass distributions.

2.6 Comparison of NGC 1566 with modelled quantities

While observed quantities such as age, mass or luminosity can provide a wealth of information, the underlying processes producing their distributions are not always evident solely from observations. The modelling of physical processes underpinning the evolution of clusters is important in relating observables to the physics behind them. In this section data are fit to obtain information about the cluster population and model functions are formed, to which the data are compared.

2.6.1 Cluster disruption in NGC 1566

Throughout this analysis, property distributions and functions have been fit with power laws in order to make comparisons between studies of other galaxies, however as previously stated, the mass function shows evidence of a turnover, indicative of a Schechter function, which is not unexpected. In this section, the aim is to quantify the parameters that can be ascertained from fitting a Schechter function to the data with the assumption of underlying mass-dependent disruption, namely the timescale of disruption for a cluster and the characteristic turnover mass. In order to do this, the mass-age distribution is used to fit an evolved Schechter function using a maximum likelihood fitting method, The evolved Schechter function, as formulated in equation 26 in Gieles (2009), takes a Schechter Cluster Initial Mass Function (CIMF) and evolves it over time to include mass dependent disruption due to GMCs etc, and the effects of mass loss due to cluster evolution. The evolved Schechter function is shown in equation (2.2) where N is counts, M is cluster mass, A is the constant that scales with cluster formation rate, γ is the index relating cluster mass to cluster disruption timescale, M_* is the characteristic turnover mass of the function and $\Delta_\gamma = \gamma t/t_0$ where t is time and t_0 is the average disruption timescale of a 1 $M_\odot$ "cluster".

$$\frac{dN}{dM} = \frac{AM^{\gamma-1}}{[M^\gamma + \Delta_\gamma]^{(\gamma+1)/\gamma}} exp(-\frac{[M^\gamma + \Delta_\gamma]^{1/\gamma}}{M_*}) \tag{2.2}$$

The method of likelihood fitting used, as presented in Gieles (2009) involves creating models with parameters M_*, t_4 (the average disruption timescale of a 10^4 $M_\odot$ cluster) and simultaneously maximising the likelihood of each of these quantities to give the best fit solution. The fit

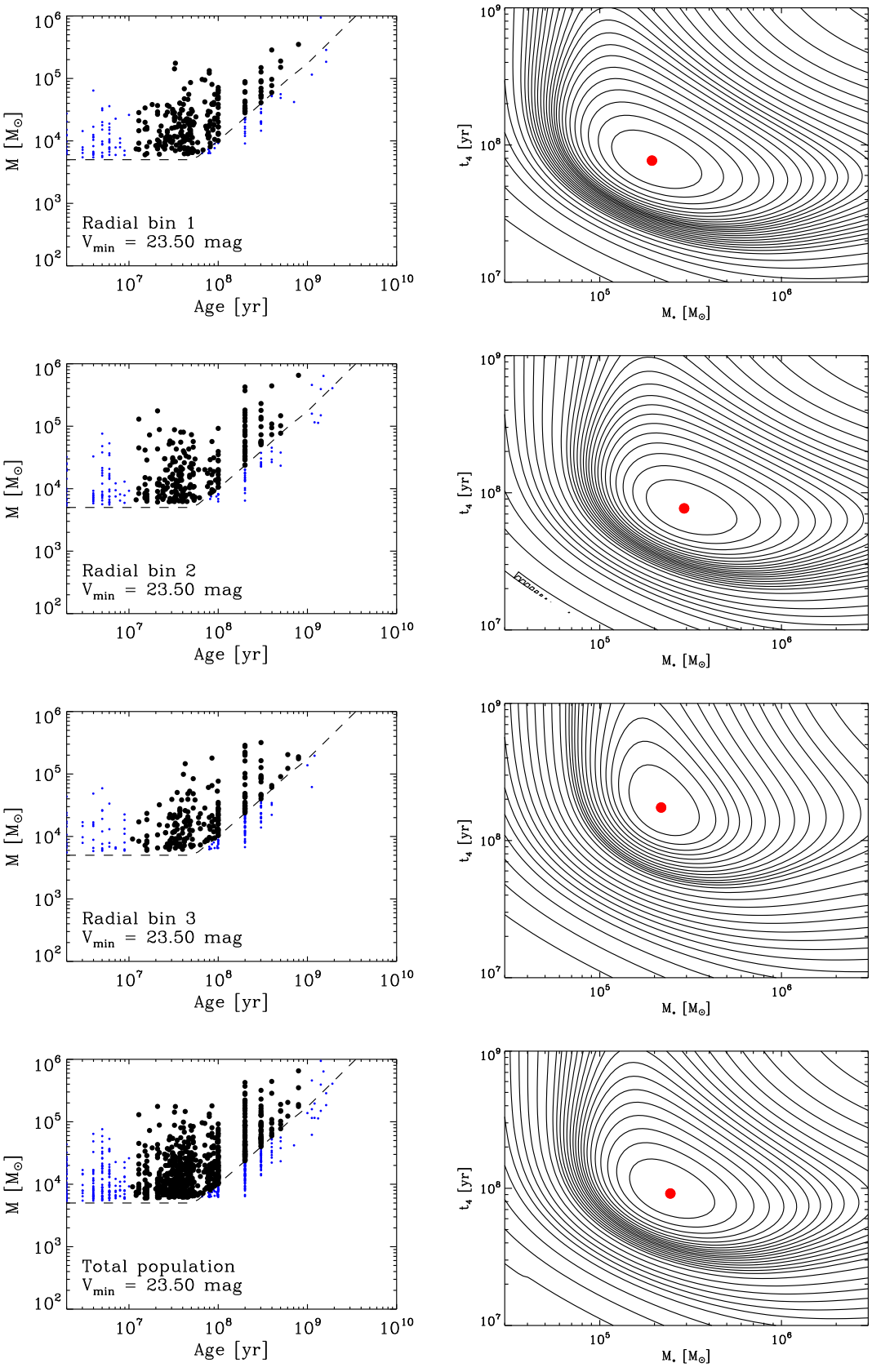

Figure 2.14: Maximum likelihood fits of the age-mass distributions for each bin and the total population. The left hand plots show the age-mass distributions for each radial bin (labelled) and the total population. The black line indicates the population model used to cut the sources, while the black points are those used in the maximum likelihood fit, with magnitude and age cuts of > 10 Myr and $M_V < 23.5$ applied. The right hand column of plots show the maximum likelihood fit for the mass function truncation value (M_*) and the timescale for disruption of a 10^4 $M_\odot$ cluster. The red point is the best fit while the contours show the distribution of the likelihood in equally spaced bins. Lines that are closer together indicate a higher rate of change in likelihood.

uses $\gamma = 0.62$ from the model of MDD by Boutloukos & Lamers (2003) and only uses clusters older than 10 Myr with a minimum V band magnitude of 23.5 mag in each bin to ensure completeness.

Fig. 2.14 shows eight panels describing the fits to the data, which has been divided into the three radial bins with the final panels showing the results for the entire cluster population. The plots on the left side are the age-mass plots indicating the cuts used for the fits; black points are the clusters included. The plots on the right show the maximum likelihood fits to each of the sets of data. The red point indicates the best fit for t_4 and M_* while the contours show the distribution of the likelihood arranged in equally spaced bins; areas with contours that are closer together indicate a larger difference in likelihood. The fit estimates $M_* \approx 2.5 \times 10^5$ $M_\odot$ and t_4 as $\approx$ 100 Myr, using the full, un-binned cluster population.

There is little difference in M_* for each successive radial bin. This suggests the truncation value in the mass function for each section should occur at the same mass. The truncation value in Fig. 2.12 is difficult to determine accurately for the three populations due to dwindling cluster numbers at high masses. t_4 is very similar for the inner two radial bins, however is around a factor of 2 larger in the outermost bin. This result may not be significant but indicates that outer clusters are possibly disrupted more slowly than inner clusters.

The values for M_* and t_4 were used to model the contributions from different aged stellar populations to the luminosity function for NGC 1566, as discussed in the next section. The model requires t_4 to be scaled to t_0 (the average disruption timescale of a 1 $M_\odot$ "cluster", as given in equation (2.2)). t_4 was found to be 100-200 Myr, for which we took the average of the two values.

2.6.2 Luminosity function modelling

The shape of the luminosity function depends on the cluster formation history, the mass function of the clusters, their mass evolution and extinction. Clusters fade as they age and there are, therefore, clusters with different ages and masses contributing to the number of clusters at a given luminosity. To get a better understanding of how the LF depends on the various implied properties of the cluster population in NGC 1566, the LF is modelled based on the underlying mass functions and cluster disruption timescale derived earlier, using a model provided by Mark Gieles (Gieles, 2010).

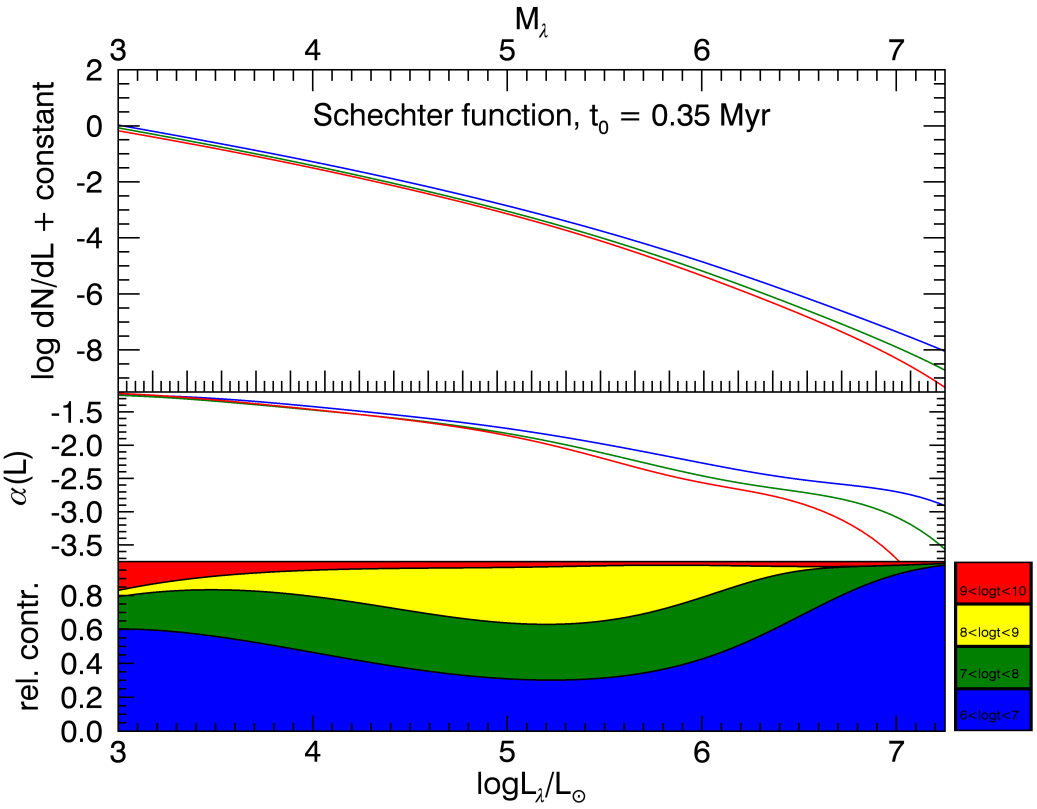

Figure 2.15: Modelled relative contributions of varying cluster ages made to the luminosity function for a Schechter mass function. The three panels are as follows: the shape of the luminosity function in the B, V and I bands, the value of α for the function at each point and the contributions of clusters in four different age bands. The blue band is clusters aged $10^6 - 10^7$ years, the green is $10^7 - 10^8$ years, the yellow $10^8 - 10^9$ years and the red $10^9 - 10^{10}$ years. t_0 is the average disruption timescale of a 1 $M_\odot$ cluster.

A constant cluster formation rate for 10^{10} yr is assumed and a Schechter function for the cluster initial mass function (CIMF) is used, with an index of α = -2 at the low-mass end and a truncation mass of $M_* = 2.5 \times 10^5$ $M_\odot$ as obtained from the maximum likelihood fitting method in § 2.6.1. A disruption timescale of $t_0 = 0.35$ Myr is used, also as found in § 2.6.1. The mass evolution of individual clusters changes the shape of the cluster mass function. For the mass-dependent cluster disruption model the expression for the 'evolved Schechter' mass function given in equation (26) of Gieles (2009) can be used. With this, the number density of points in age-mass bins are computed, and the contribution of each mass to the LF in the B, V and I filters is found from the age-dependent mass-to-light ratios of the single stellar population models of Bruzual & Charlot (2003). The logarithmic slope (α) is derived from the LF using the symmetric difference quotient. Similar procedures to model the LF are presented in Fall (2006); Larsen (2009); Gieles (2010).

Fig. 2.15 shows the resulting LF model. The top panel shows the LF in the three filters, the

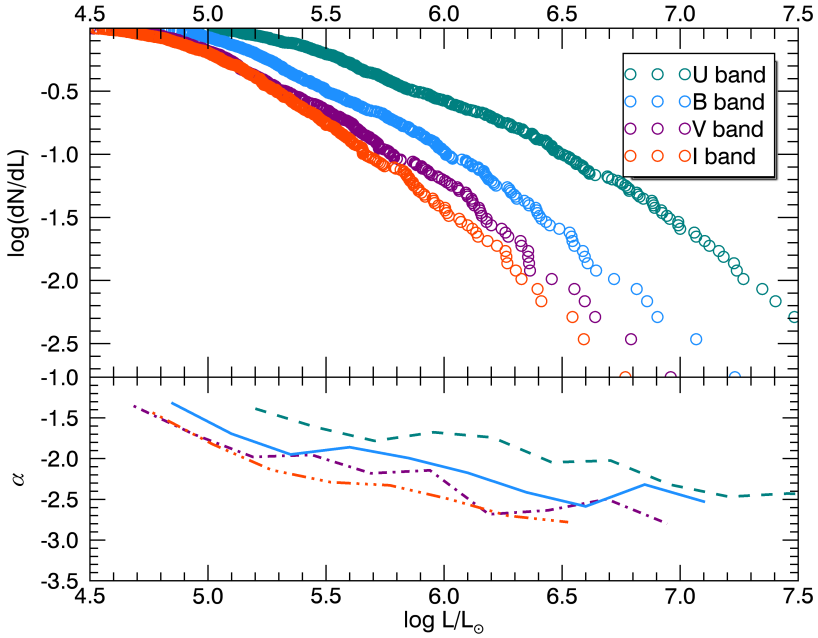

Figure 2.16: The luminosity functions in the U, B, V and I bands with magnitudes converted to luminosities. The top panel on the plot shows the shape of the functions for all class 1 clusters above 5000 $M_{\odot}$ and younger than our incompleteness limit of $\sim$ 100 Myr, while the bottom panel shows the fits for the distributions in each band (α) along the curves. α is found by fitting the functions above by minimising χ^2, with overlapping bins of 0.5 dex.

middle panel shows the luminosity dependent α and the bottom panel displays the relative contributions of different age bins. Young clusters dominate at the bright-end as the result of the truncation in the CIMF and evolutionary fading (i.e. old M_* clusters are fainter than young M_* clusters). At low luminosities the majority of the clusters are also young, which is due to disruption.

Fig. 2.16 shows the LF (top panel) and α (bottom panel) for the clusters in NGC 1566. α is calculated using the LINFIT procedure in IDL. Overlapping bins of 0.5 dex are used to ensure that no anomalous peaks in the luminosity function dominate the fit for α.

The general behaviour of the LF and α in different filters is similar to that of the model in Fig. 2.15. The LF is steeper at higher luminosity, which in the model is the result of the exponential truncation (at high luminosity) and mass dependent disruption (at low luminosity). The LF is steeper in redder filters, which in our model is due to the truncation of the mass function and more rapid fading in bluer filters. This cannot be due to a luminosity dependent extinction, as the opposite would be expected: a steeper LF in the bluer filters. The average and median value for α for the data corresponds very well to the average and median for the

Mean values for α

Band	Observed	Model
B	-2.08	-2.02
V	-2.19	-2.16
I	-2.25	-2.27

Median values for α

Band	Observed	Model
B	-1.99	-1.97
V	-2.14	-2.11
I	-2.29	-2.18

Table 2.3: Average and median values for α for the observed luminosity function and model function. The values are very similar across all bands, indicating that the results are comparable.

model values of α, as shown in Table 2.3. This modelling exercise further supports the finding of a truncation or steepening in the underlying mass function.

2.7 Galactic parameters and cluster populations

Clusters and associations are the building blocks of galaxies, and therefore are vital to understanding star formation processes. Adamo et al. (2015) recently showed how tracing the properties of clusters across M 83 provides information on how the galactic environment has influenced the cluster formation process, and consequently gives insight into star formation throughout the galaxy. Here I discuss several galactic parameters that provide insight into cluster populations and their histories, including $\mathrm{M_V^{brightest}}$, Γ and $\mathrm{T_L(U)}$.

2.7.1 Brightest absolute V band cluster

Fig. 2.17 shows the absolute V band magnitude of the brightest cluster in the NGC 1566 catalogue plotted against the log star formation rate of the galaxy. The SFR was found by reducing the value for the SFR of NGC 1566 provided in Thilker et al. (2007) to account for the area of the galaxy covered by the HST WFC3 images, which is smaller. Thilker et al. (2007) use the same distance for NGC 1566 as this study, which makes this calculation trivial.

A Hα SINGS survey image of NGC 1566 was obtained from the archive. The ratio of the flux within an aperture covering the entire galaxy, as used in the original calculation of the SFR in Thilker et al. (2007) and the flux in the smaller aperture that is covered by HST (out to $\approx$ 5.5

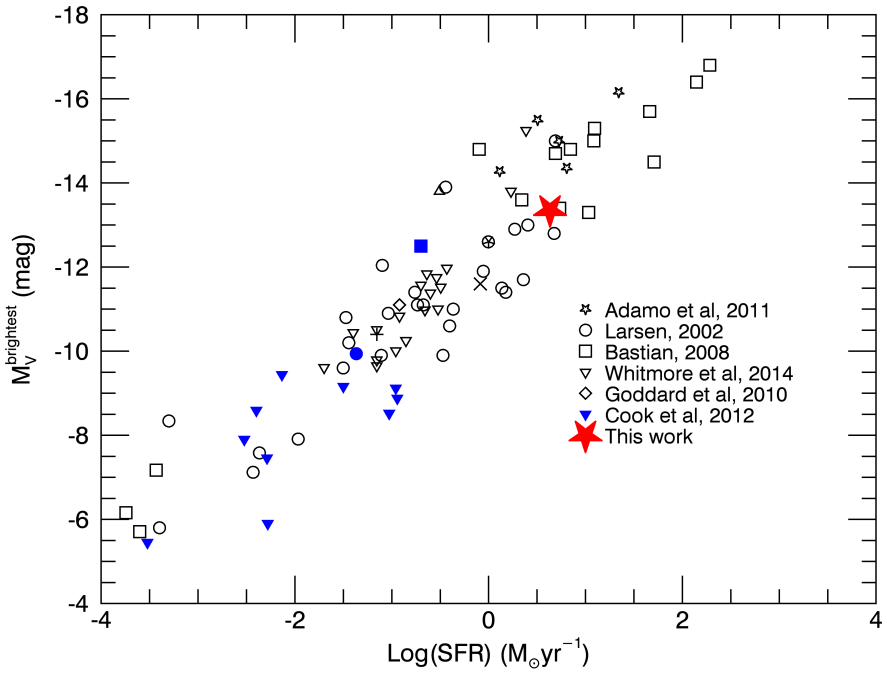

Figure 2.17: A collection of clusters in nearby galaxies' with the brightest V band magnitude in their respective populations plotted against the galaxies' total star formation rates. There is a clear relationship between these two quantities, displaying the stochastic element of the cluster formation process. The value for NGC 1566 is shown as a red star. Major contributors to the number of sources on the plot are listed to the right, please see Table B1 of Adamo et al. (2015) for the literature containing this information.

kpc) was calculated. This ratio was then used to reduce the SFR to one representative of the area covered by HST, giving a value of 4.3 $M_\odot yr^{-1}$.

NGC 1566 is displayed as the red star. The other data points for other galaxies were taken from Adamo et al. (2015) (please see Table B1 of that paper for the full list of objects included). The clear correlation between these two parameters is the result of the stochasticity of the cluster formation process and size of sample effect, where higher SFR galaxies are able to sample the initial mass and luminosity functions to brighter and higher mass clusters (Larsen, 2002; Bastian, 2008). NGC 1566 is no exception to this effect, lying comfortably at the end with the higher rate of star formation.

2.7.2 Cluster formation efficiency

As discussed in § 2.1 and in the general introduction, the CFE, or Γ, is the amount of star formation contained within clusters compared to the total star formation in a defined area.

Previous studies have found that values of Γ for different galaxies vary according to the surface density of star formation of the galaxy ($\Sigma_{\rm SFR}$; Goddard et al., 2010; Ryon et al., 2014). Γ is also found to decrease within the same galaxy further from the galactic centre (Silva-Villa et al., 2013; Adamo et al., 2015). Γ can provide information on how galactic environment can affect cluster population properties.

Calculation method

Γ is calculated for two different age ranges of clusters: 0-10 Myr and 10-50 Myr. The division at 10 Myr is due to the difficulty in fitting ages and masses to clusters younger than this age, which introduces inaccuracy in the calculation of Γ for 0-10 Myr. The mass cut of 5000 $M_\odot$ applied to the rest of this work was again applied here to attempt to account for stochastic IMF sampling by using a mass-limited sample. Additionally, only class 1 sources were included to avoid contamination of a 'true cluster' population.

Γ is found by dividing the cluster formation rate (CFR) by the total star formation rate of the galaxy. The CFR can be estimated using the total mass of clusters formed divided by the time over which they form. The first step in calculating a CFR is the integration of a chosen cluster mass function (CMF) over 2 sets of limits. The first set corresponds to finding a theoretical total cluster mass ($M_{\rm c,tot}$), with a lower limit of 100 $M_\odot$ and an upper limit of 1.5×10^6 $M_\odot$ the observed highest mass cluster. The second set provides an estimate of a theoretical observed cluster mass ($M_{\rm c,obs}$), and uses a lower limit of 5000 $M_\odot$ and the same upper limit as the previous integration. Using the ratio of the resulting integrated functions, the CFR can be estimated in the two selected age ranges and therefore calculate Γ.

The CMF used is a simple power law ($dN \propto m^{-\beta} dm$), as observed to fit many cluster populations' mass distributions fairly well, including NGC 1566. The validity of using a power law function is discussed in the next section. The value of β used was 2, the average value found for most galaxies. The ratio of the two integrations provides the factor for calculating a total cluster mass in NGC 1566 based on data, rather than theoretical. For example, if the theoretical ratio of observed to total cluster mass is 0.5, then an estimate of a total cluster mass based on data would be double the summation of all observed clusters in the catalogue. This value is then carried forward to find a CFR by dividing the total mass by 10 for $\rm CFR_{0-10Myr}$ and 40 for $\rm CFR_{10-50Myr}$ and Γ is then CFR/SFR $\times$ 100 for each age range.

Results and limitations

Fig. 2.18 shows the trend between Γ and log of $\Sigma_{\rm SFR}$ (surface density of star formation) observed for a variety of objects taken from the literature by Adamo et al. (2015) (again, please see Table B1 in this paper for the full details of the points and their sources), with values calculated for NGC 1566 shown by the red and teal stars. The value of log $\Sigma_{\rm SFR}$ is found by dividing the SFR by the area covered in kpc, and is found to be ≈ 0.033 $\mathrm{M_{\odot}yr^{-1}kpc^{-2}}$. For NGC 1566, $\Gamma \approx 8.8 \pm 1.1$ for clusters in the 0-10 Myr age range and $\Gamma \approx 5.4 \pm 0.7$ for the 10-50 Myr range. The fiducial model by Kruijssen (2012) is also plotted over the data points. This model is a theoretical framework that describes the formation of clusters and predicts that bound stellar clusters form at the peaks of density within the ISM. It predicts that there should be a higher star formation efficiency in these areas due to the short free-fall time and bound clusters survive, while unbound associations form in lower density regions. This model is in agreement, therefore, with the data points on the plot, showing that cluster formation efficiency is closely tied with the surface density of star formation, or gas.

NGC 1566 fits into the correlation with the other points in support of the idea that the amount of star formation occurring in clusters, and therefore the number of clusters is dependent on the surface density of star formation in the galaxy. However, conversely to the idea that a higher SFR can be linked to a higher $\Sigma_{\rm SFR}$ and therefore a higher Γ is that NGC 1566 has a fairly high star formation rate (when compared to similar galaxies) and yet has a lower cluster formation efficiency and $\Sigma_{\rm SFR}$. This indicates that the galaxy is primarily forming stars outside of bound clustered environments possibly because of insufficient gas density. It is likely, therefore that Γ is not strongly related to the star formation rate in the galaxy, and instead depends mainly on the $\Sigma_{\rm SFR}$, which itself is a direct function of the surface density of gas.

There are many limitations to this calculation of Γ, as discussed in detail for NGC 3625 by Goddard et al. (2010). In their work they used synthetic cluster populations to examine the accuracy and effectiveness of their calculations. They identified many potential sources of error, which can also be applied to NGC 1566.

Firstly, using the total observed cluster mass during the conversion from total cluster masses found through integration to estimates based on the data assumes that all clusters have been detected in the galaxy. Some clusters are inevitably missed during the detection and catalogue refinement phase, especially the youngest clusters that may be obscured by dust. The catalogue

likely misses few of these clusters, however as Whitmore & Zhang (2002) found that when comparing the detection of the youngest clusters in radio bands and optical bands, there is $\sim$ 85% overlap. Hollyhead et al. (2015) found a similar result for M 83, where detections in the H band confirmed few clusters would be missed.

Ages and masses of clusters are obtained by fitting photometric data to SSP models. The parameters of the SSP model, for example the metallicity used, can affect the resulting cluster properties by altering the numbers of clusters at different ages or masses (Bastian et al., 2005). Goddard et al. (2010), however, report a difference of 5-10% for differing SSP models, so the effect is likely negligible.

The assumed mass function also plays an important role in the calculation. A power law with an index of -2 and an upper limit of two times the observed maximum mass was used, which fits the majority of the mass function, however, many studies find a Schechter function that incorporates a truncation at the high mass end is a more accurate fit. The calculation will therefore have overestimated the contribution of high mass clusters to the total amount. An overestimate of the total mass would give a lower value for the CFR and CFE. Goddard et al. (2010) show that the difference between a power law and Schechter function makes little difference in the calculation of the total mass for a truncation value of 10^6 $M_\odot$ or higher. The estimate of the truncation value for NGC 1566, however, is $\approx$ $10^{5.4}$ $M_\odot$, which is shown to have a larger difference. The difference in integrated mass between a power law and a Schechter function with turnover mass equal to that of NGC 1566 is ≈ 0.75. This means that the total mass could be ≈ 1.3 times lower than calculated, giving a value for Γ that is also 1.3 times lower, or ≈ 6.8 for 0-10 Myr and ≈ 4.2 for 10-50 Myr.

2.7.3 $T_L(U)$

Another quantity that is related to Γ and gives an indication of the effect that environment plays on cluster populations is the percentage of U band light from a galaxy emitted by clusters, or $\mathrm{T_L(U)}$. U band light primarily traces the young clusters in the population, as they are usually brighter in bluer bands (older clusters have faded and emit more strongly in redder bands), and therefore should be linked to star formation. Unlike Γ however, $\mathrm{T_L(U)}$ is a purely observational quantity, therefore free of the biases and errors introduced by selecting an approximate mass function and using quantities derived from SSP models. $\mathrm{T_L(U)}$ is also not strongly affected by

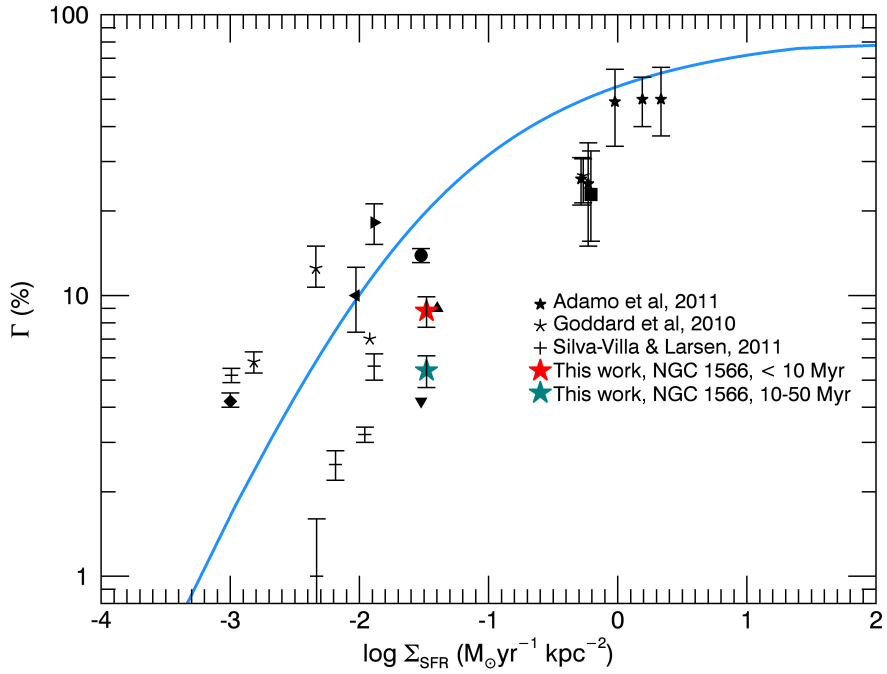

Figure 2.18: Cluster formation efficiency against the surface density of star formation for a variety of objects, including NGC 1566. The correlation indicates that clusters form in denser areas of cold gas. NGC 1566 is shown by the red and teal stars, which display a fairly low CFE and surface density in comparison to the SFR. Major contributors to the data points are listed on the right, the other sources can be found in Table B1 of Adamo et al. (2015). The blue line represents the model to the data from Kruijssen (2012).

Band	m_{gal}	T_L^1	T_L^{1+2}
U	11.59	10.1	12.7
B	11.81	4.8	5.9
V	10.94	2.3	2.8
I	9.76	1.3	1.5

Table 2.4: Percentage of total galaxy luminosity emitted from clusters in the U, B, V and I bands. $\mathrm{m_{gal}}$ is the magnitude of the whole galaxy in each band (only measured within the field of view of the HST image), $\mathrm{T_L^1}$ is the percentage given for only class 1 sources and $\mathrm{T_L^{1+2}}$ is for class 1 and 2 sources.

extinction as the clusters and the host galaxy will be affected approximately equally.

$\mathrm{T_L(U)}$ was calculated by summing the U band luminosities of all clusters in the catalogue, dividing by the total measured U band luminosity for the entire galaxy obtained by aperture photometry and multiplying by 100. The usual mass cut of $5000\ \mathrm{M_\odot}$ was applied and split the catalogue into class 1 and class 2 sources. It was found that $\mathrm{T_L(U)} \approx 10.1\%$ for class 1 sources and $\mathrm{T_L(U)} \approx 12.7\%$ for class 1 and 2 sources.

Fig. 2.19 shows the relationship between Σ_{SFR} and $\mathrm{T_L(U)}$. The purple, teal and black points are those taken from Larsen & Richtler (2000), where purple points are starburst galaxies and mergers, while the black and teal points are other galaxies. The blue points are BCGs taken from Adamo et al. (2011) and the red star is for NGC 1566. The plot demonstrates that the galaxy fits well onto the current relationship and is also in the section of the plot populated by starburst galaxies and merging systems. This would be expected of a galaxy with a high star formation rate, though $\mathrm{T_L(U)}$ correlates less strongly with SFR than Σ_{SFR} (Larsen & Richtler, 2000; Larsen, 2002).

In addition to $\mathrm{T_L(U)}$, Larsen & Richtler (2000) provided values for $\mathrm{T_L(V)}$ for all of the galaxies. Fig. 2.20 shows the relationship of $\mathrm{T_L(V)}$ with Σ_{SFR}. Little difference is seen between the plots for the two different bands. NGC 1566 however, shows a fairly large difference between the U and V bands. If the star formation rate has been increasing, this could be due to the galaxy having many young clusters, so they contribute more strongly to $\mathrm{T_L(U)}$ than $\mathrm{T_L(V)}$. The effect on the percentage of the total luminosity emitted from clusters in the U, B, V and I bands was investigated further.

Table 2.4 shows the data for the different bands, giving the total magnitude of the galaxy and the percentages for only class 1 sources and class 1 and 2 sources. There appears to be a general trend, as expected, in the values of $\mathrm{T_L}$. Less luminosity in redder bands is emitted by clusters and by calculating $\mathrm{T_L(I)}$ the light from clusters is being compared to the large field stellar

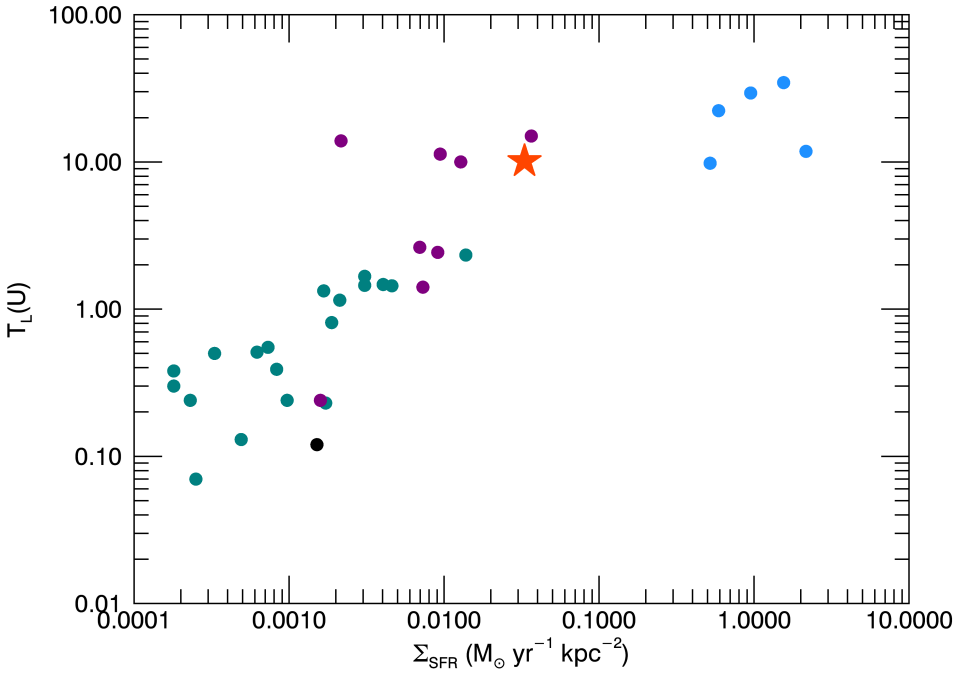

Figure 2.19: $T_L(U)$ for galaxies taken from Larsen & Richtler (2000) and Adamo et al. (2011) and now including the data for NGC 1566. The teal points indicate galaxies that were taken from Larsen & Richtler (1999), the purple points are starburst and merger galaxies introduced in Larsen & Richtler (2000), the black points are other galaxies from Larsen & Richtler (2000) and the blue are BCG galaxies from Adamo et al. (2011). The red star is NGC 1566. Both axes are log units.

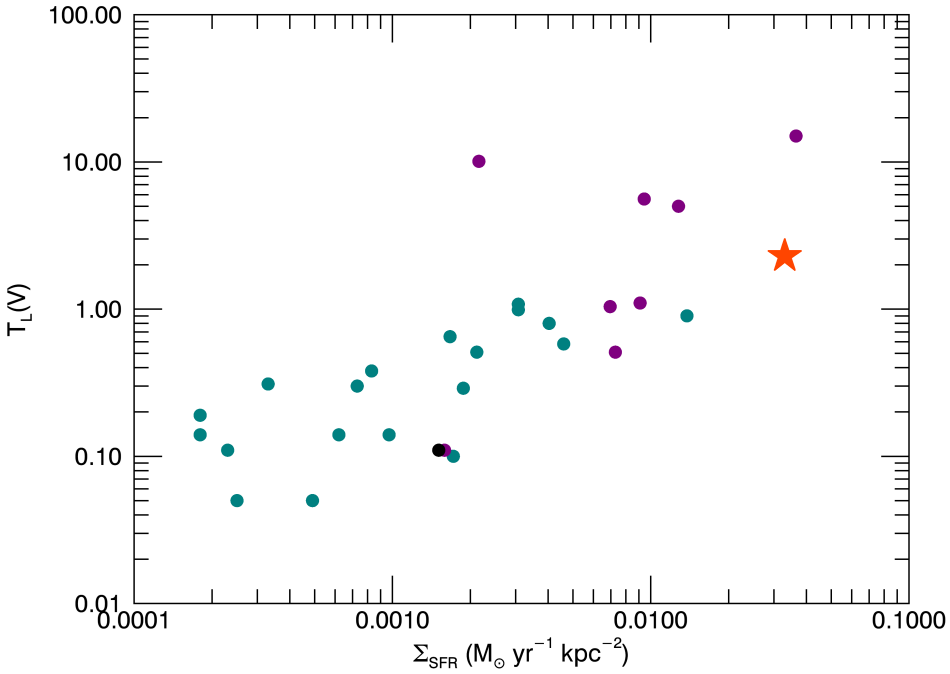

Figure 2.20: $T_L(V)$ for galaxies taken from Larsen & Richtler (2000) and now including the data for NGC 1566. The colours indicate the same classifications of galaxies as described in the previous figure.

population throughout the galaxy, consisting of older stars, which will contribute much more strongly at longer wavelengths. This could be an effect of disruption, where more stars exist in clusters at young ages (which are brighter in blue bands) than at older ages where the majority are in the field (and are brighter in red bands), due to the destruction of clusters over time.

2.8 Conclusions

2.8.1 A radial variation in cluster properties?

NGC 1566 displays negligible variations in several cluster properties at different galactocentric distances within the $\sim$ 5.5 kpc covered by the WFC3 observations. A summary of the values calculated for various properties for each bin is shown in Table 2.5. The conclusions that can be taken from these results are as follows:

- There is a significant variation in U-B and a negligible change in V-I in colour space with respect to galactocentric distance. The most concentrated areas of colour space are

	Radial bin 1	Radial bin 2	Radial bin 3
N_1	274	274	278
N_2	70	85	56
U-B	-0.64	-0.57	-0.38
α_V	2.09	2.15	2.04
β	1.79	1.96	2.00
M_c ($M_\odot$)	2×10^5	3×10^5	2×10^5
t_4 (Myr)	80	80	200

Table 2.5: Summary of data for the three radial bins used throughout this study. These are values as calculated using a mass cut of 5000 $M_\odot$ with full detections in the UV band. The bins were chosen to accommodate approximately equal numbers of clusters in each bin for our plots. However, this applies only to class 1 sources, as these were used for the analysis. N_1 and N_2 refer to the number of class 1 and class 2 sources respectively. U-B is the median value of the U-B colour of clusters in each bin, α_V is the fit to the V band luminosity function, while β is the fit to the mass function. M_c is the truncation mass and t_4 is the average disruption timescale of a 10^4 $M_\odot$ cluster.

slightly redder in the outer radial bins. This is likely due to small variations in the age of the clusters with distance, as age is the primary factor affecting colour distribution (extinction is expected to go in the opposite direction). Similar variations are also seen in other galaxies, such as NGC 4041 and M 83.

- The shape of the luminosity functions for all radial bins are as expected, with the power law section of the best fit with an index value of $\alpha \approx$ -2, as found in numerous other studies and galaxies. Negligible differences were found in the indices fitted for different radial bins, with the largest differences in the UV and U bands, though all are within errors on the fit. In agreement with the luminosity function, as they are potentially related, the mass distributions also show only small variations. There is a steepening of α for redder bands, which is predicted if the cluster mass function is truncated at the high mass end. This is due to the more rapid fading of clusters in bluer bands, as clusters with the same mass, but different ages, are more spread across a luminosity range in bluer bands, giving rise to a shallower function.

- The age distribution for NGC 1566 is best fit with a single power law within the age range where the data is not incomplete. There is no evidence of a three-component shape, or variation between successive radial bins. t_4, the average timescale for disruption of a 10^4 $M_\odot$ cluster, is twice as large in the outermost bin than the inner two. This would suggest that clusters disrupt twice as slowly in the outer environment of the galaxy than in the inner bins, in support of the effect of environment on disruption. NGC 1566 lies on the relation between M_* and Σ_{SFR} put forward by Johnson et al. (2017), which suggests that there is a relationship between disruption and evironment within the galaxy.

- The mass distributions show a slight steepening with increasing radial distance, but within error estimates. Additionally, the data suggest a truncation in the mass function. This finding is supported by the comparison of the observed luminosity function with models, which show that a Schechter function is a good fit. The index of the slopes are all ~ 2, as observed for other galaxies.

2.8.2 Galactic properties

$\mathrm{T_L(U)}$ and Γ were calculated for NGC 1566 and both values to lie within the correlations with Σ_{SFR}. An interesting result of the study was that we found Γ to be slightly lower than expected for a galaxy with a fairly high SFR. This is when compared to galaxies similar to NGC 1566. While the galaxy still fits into the current scaling relations for these properties, it indicates that the CFE is not strongly dependent on SFR.

Chapter 3

Young massive clusters in M 83

Summary

This chapter concerns early cluster evolution, investigating how long clusters remain embedded in the gas left over from star formation. To do this, I use the young massive cluster population of M 83 (a well-studied face-on spiral galaxy) and analyse their ages and masses to find when they first became free of gas. Through visual inspection of the clusters, and comparison of their SEDs and position in colour-colour space, I find that the clusters are all exposed (no longer embedded) by $\sim$ 2-4 Myr. I also present several other methods of constraining the ages of very young massive clusters. This can often be difficult using SED fitting due to a lack of information to disentangle age-extinction degeneracies, which is overcome well using UV when available. The individual morphology of the Hα around each cluster has a significant effect on the measured fluxes, which contributes to inaccuracies in the age estimates for clusters younger than 10 Myr using SED fitting. Methods used here help constrain ages of young clusters include using the near-infrared and spectral features, such as Wolf-Rayet stars.

3.1 Introduction

The work presented in this chapter addresses how long the clusters remain embedded in gas after star formation. The stars belonging to the cluster will form from a mass of cold gas, but how long after this initial stage does the cluster keep leftover gas from the formation process bound to it?

To investigate this question I studied the young massive cluster (YMC) population of M 83. M 83, is a nearby spiral at 4.5 Mpc (Thim et al., 2003), with a rich cluster population that has been widely studied, for example, Bastian et al. (2012), Chandar et al. (2010b), Whitmore et al. (2011), Adamo et al. (2015) and the paper this chapter is based on Hollyhead et al. (2015), are only a few recent papers on the topic. M 83 has been widely studied partly due to this rich population of clusters (7290 clusters and possible associations within the catalogue used in this paper from Silva-Villa et al., 2014), which means in depth studies can be carried out and population statistics are meaningful. The clusters also span a wide range of ages and masses making age or mass distributions highly representative of a fully sampled cluster IMF. Additionally, M 83 is thought to be very similar to our own Milky Way galaxy (in stellar mass, bar strength and galaxy type, though it has a higher star formation rate, e.g. Larsen & Richtler, 2000), and so any results regarding the cluster population of M 83 could potentially be used to infer results for the Milky Way, whose complete cluster population cannot be determined or studied due to the clusters' and our position in the disc (Larsen, 2008).

Other YMC studies both within and outside the Milky Way show the importance of feedback within star forming regions and clusters and give an indication of the timescales for clusters to become gas free. For example, the Arches cluster towards the centre of our galaxy has an age of 2.5-4 Myr (Blum et al., 2001), a mass of $\approx 2 \times 10^4$ $M_\odot$(Espinoza et al., 2009) and is observed to be free of gas. Other clusters of similar masses, such as NGC 3603 (aged $\sim$ 1-2 Myr, M $\sim 10^4$ $M_\odot$) or Westerlund 1 (aged $\sim$ 3-6 Myr, M $\approx 5 \times 10^4$ $M_\odot$) (Negueruela et al., 2010; Gennaro et al., 2011; Brandner et al., 2008; Harayama et al., 2008; Lim et al., 2013) also have no dense gas bound to them. It has been found that even for lower mass systems than those already mentioned, the clusters can potentially be gass free within $<$ 1 Myr (Seale et al., 2012). However this is not the case for all lower mass regions, as some seem to require more time to clear gas, such as W3-main (e.g. Bik et al., 2014) or NGC 346 in the SMC (e.g. Smith, 2008). It has also been found that feedback may prompt further star formation around

the central source, such as in the Ruby Ring region (Adamo et al., 2012) or Cluster 23 in ESO 338-IG04 (Östlin et al., 2007), though it is difficult to determine whether star formation in a region is triggered by feedback or coincidental (e.g. Dale et al., 2012).

This study focuses on the Hα morphology around the YMCs. Hα emission traces the ionised gas associated with the clusters, so through visual inspection of how the Hα is orientated, it is possible to determine whether gas is still contained within the cluster or is outside of it. By comparing the Hα morphology with the age of the clusters we can constrain the age by which the clusters have become gas free.

This technique was previously used by Whitmore et al. (2011), who investigated clusters in Field 1 of M 83, as illustrated by Fig. 3.1. They used Hα morphology as a potential age dating technique for clusters, rather than specifically studying the length of the embedded phase. This study provided an excellent starting point for Field 1, which was expanded into the other 6 fields by Hollyhead et al. (2015).

Investigating early cluster formation and the role of feedback can also provide information on globular cluster (GC) formation. It has been thought that YMCs are the current day precursors to GCs (e.g. Schweizer & Seitzer, 1998; Kruijssen, 2015), which were originally thought to only form in the early universe. Using YMCs, such as those in this study, one can infer how GCs formed and evolved to their current state. In particular, in this chapter we relate the findings from YMCs to constraints on the formation of multiple populations in GCs (see § 3.4.4, or Chapter 1 for more information on MPs.)

In § 3.2 I discuss the data used for the study and how this was used to identify and classify clusters. Additionally, I discuss issues with age dating young clusters and how this problem was mitigated. § 3.4 describes the results and other methods for constraining cluster ages. In § 3.5 I discuss the implications of the results for GC formation scenarios, in particular the Fast Rotating Massive Star scenario (FRMS) while in § 3.6 I summarise the conclusions of the study.

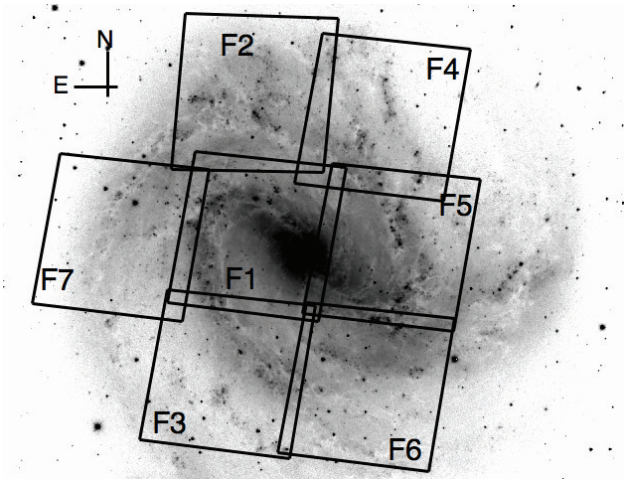

Figure 3.1: The orientation of the seven M 83 fields in HST WFC3. As can be seen, the majority of the galaxy is covered, with a few outer regions missed. Image taken from Adamo et al. (2015).

3.2 Observations and Techniques

3.2.1 Data

Studying the cluster population of M 83 requires sufficiently high quality data to resolve individual clusters. In addition, there is a further constraint as the detail of the Hα morphology needs to be visible around each cluster. In order to satisfy these requirements, HST WFC3 data was used, as it provides sufficient resolution at the distance of 4.5 Mpc. The images were obtained from the publicly available HST Legacy Archive for all seven fields of M 83 in the U (F336W), B (F438W), V (F547M) (F555W for Fields 1 and 2), Hα (F657N), I (F814W) and H (F160W) bands. The archive provides fully reduced and drizzled data. The orientation of the seven fields is shown in Fig. 3.1, taken from Adamo et al. (2015). No transformation was made in the data to the Cousins-Johnson filter system, however we adopt U, B, V, Hα, I and H for shorthand, as the WFC3 filters correspond approximately to these wavelengths.

Bastian et al. (2012) and Silva-Villa et al. (2014) used these images to identify an extensive catalogue of clusters within M 83 using a combination of automated and manual procedures, as described in more detail in Chapter 2. Photometry in the U, B, V, Hα and I bands was already available and we added H band magnitudes for this study. Photometry was performed for each of the existing clusters on WFC3 IR channel H band images, and added to the catalogue.

The coordinates were transposed to the H band images using the XYXY transform in the astronomy library for IDL, and DAOPHOT was used to find the magnitudes with a 1.5 pixel aperture

and 2.4 pixel background apertures with annuli of 0.9 pixels. The pixel size of the IR detector is 0.13", giving aperture sizes of $\sim$ 0.2", or $\sim$ 4.2 pc. We chose this small aperture size so that they were physically the same size as the 5 pixel aperture used for the other bands, ensuring that there would be no effect from spatial differences. Some of the sources were not bright enough in the H band to calculate magnitudes and the H band images covered a slightly smaller area of sky than the other filters. Despite this, $\sim$ 5600 of the 7290 clusters in the catalogue were updated with H band magnitudes.

An aperture correction of 0.62 (calculated from a sample of approximately 20 sources) was subtracted to correct for lost flux due to a small aperture. Furthermore, Fields 1 and 2 were dithered differently to the other 5 fields. Our very small apertures were highly susceptible to this difference, resulting in a fairly significant reduction to the magnitudes in Fields 3 to 7. We corrected for this by subtracting 0.6 from the magnitudes in those fields. This value was found from comparing magnitudes of the same sources in the overlapping regions between Fields 2 and 4. The H band photometry is used as a method for age dating clusters, as described in § 3.3.

3.2.2 Cluster selection

As part of the selection process Bastian et al. (2012) and Silva-Villa et al. (2014) used concentration indices (CIs) to refine the sample. A CI is a measurement of how centrally concentrated emission is for a source. This value helps distinguish between field stars and clusters; stars should be highly centrally concentrated as point sources, whereas clusters have extended profiles. Star contaminants can therefore be avoided by removing sources below an index selected from histogram plots. A histogram plot of the concentration index for each source demonstrates two defined sections: the first is a sharp peak consisting of individual stars followed by a lower peak with a smooth tail that illustrates the cluster population. Removing all sources with values in the first peak leaves the cluster candidates.

These candidates were then visually inspected to determine if the source was a likely cluster (class 1), an unlikely cluster or association (class 2) or an incorrectly identified as a cluster in the previous steps (class 3). The last of these populations were removed. Sources with errors greater than 0.1 magnitude were also removed and aperture corrections were applied to account for flux missed by the aperture. I used the most recent updated version of this catalogue from

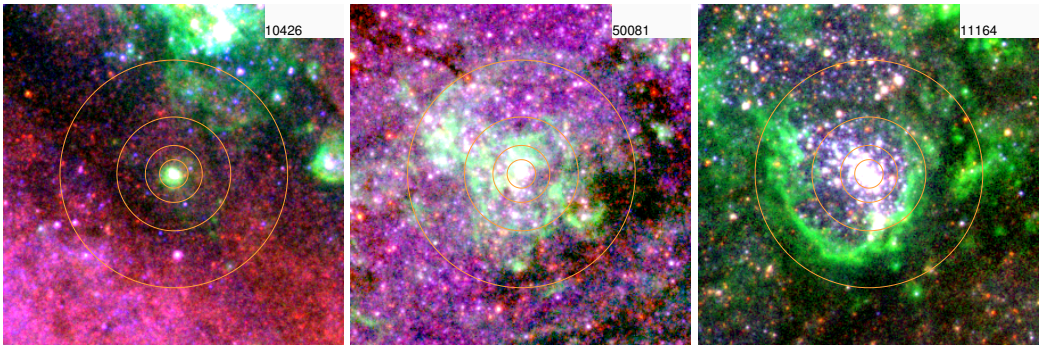

Figure 3.2: Examples of clusters in different categories. The number in the right hand corner gives the cluster's ID within the catalogue and the concentric circles indicate radial distances from the centre of the cluster to 10, 20, 40 and 80 pc respectively, to indicate how far the cluster has cleared gas. The left image is an embedded cluster, the middle cluster is partially embedded and the right cluster exposed, shown by the clear bubble. Blue colour traces B band emission, green traces Hα (and therefore ionised gas) and red I band.

Silva-Villa et al. (2014), which included photometry in the U, B, V, Hα and I bands as well as estimates of the age, mass and extinction (A_V) for each cluster. These properties were obtained by comparing each cluster's spectral energy distribution (SED) with models of simple stellar populations as per Adamo et al. (2010a,b).

YMCs were selected from the catalogue through age and mass cuts. No distinction was made between class 1 and 2; all were included in the selection. The final sample consisted of 91 clusters that were younger than 10 Myr and had a mass >5000 $M_\odot$. The lower mass cut was also applied to minimise the effect of stochastic sampling of the IMF.

3.2.3 Cluster categorisation

The clusters were then classified as embedded (no shells or areas where gas had been cleared), partially embedded (part of the cluster had cleared gas) or exposed (clear bubble around the cluster, possibly surrounded by a shell of ionised gas). Categorisation was carried out by visual inspection of the Hα morphology associated with each cluster. Images were created by cropping the original B, Hα and I fits files to a 12 x 12 arcsecond area with the cluster at the centre and stacking the three bands. Gas is traced by Hα and Hα continuum subtracted images (provided by William Blair, and as discussed in Blair et al., 2014) were used to confirm whether the cluster was embedded or not, if the colour image was unclear.

Examples of each category are shown in Fig. 3.2. The first cluster is classed as embedded, as it is enveloped by gas (shown as green), which is supported by a high A_V of 2.70, caused by

dust associated with the gas. SED fitting gives the cluster a very young age of $\sim$ 4 Myr, and therefore it is reasonable to expect that the cluster is still embedded, although I will return to issues of age fitting in § 3.3.

The second cluster is partially embedded, with a lower A_V of 0.39 and an age estimate of $\sim$ 7 Myr. These intermediate clusters provide a snapshot of how gas can be removed to progress to an exposed phase and can be used to provide an estimate of the age at which clusters start to become gas free, indicating that above this age clusters should be at least partially free of gas. For this reason, they could be considered as the most important clusters in the sample, however the classification between partially embedded and either embedded or exposed was sometimes difficult to discern, depending on how advanced the clearing is for the cluster.

The final cluster is exposed with an age of $\sim$ 6 Myr, as shown clearly by the bubble and shell of ionised gas, which has been cleared to a distance of $>$ 80 pc on the northern side, but only $\sim$ 30 pc on the southern side.

The poor quality of the photometry (offset location on the colour-colour diagram possibly caused by contamination from neighbouring sources) for some clusters produced incorrect estimates for their physical properties via SED fitting. These outlier sources could also be dominated by stochastic IMF sampling, which is known to produce extreme offsets with respect to traditional stellar evolutionary tracks (Fouesneau & Lançon, 2010). Therefore we excluded these sources. Several further clusters were removed due to poor quality images, possibly caused by the continuum that is also detected in the Hα band, meaning that the orientation of the Hα could not be accurately determined from visual inspection. After these clusters were removed, the final sample numbered at 35 exposed, 16 partially embedded and 15 embedded clusters.

Following classification, each of the partially embedded and exposed clusters were studied again to measure the extent of the gas cleared. Using tools in the GNU Gimp image processing program, the distance from the centre of the cluster to the closest point on the inner bubble edge was measured in pixels. The distance to the furthest point was then measured in the same way, unless it exceeded the largest circle on the image, in which case it was recorded as $>$ 80 pc, for simplicity. Pixel measurements were converted to parsecs to give the distances.

Finally, as an indication of the extent to which the bubbles had been cleared, the angular area of the circular region surrounding the cluster that had been cleared to these maximum and

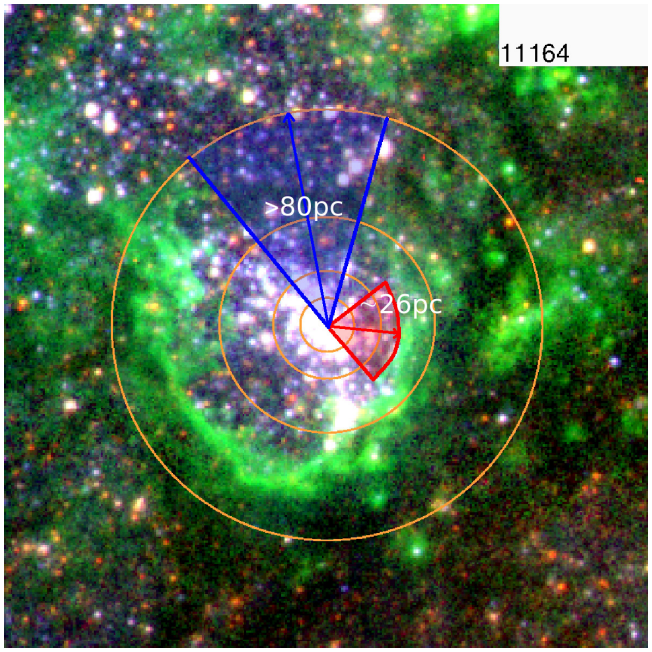

Figure 3.3: Illustration of the process used to obtain an indication of the extent of gas clearance from the clusters. The two shaded areas show the angles that were measured for the minimum and maximum distances cleared in red and blue respectively, labelled with the distance. Angles and pixel lengths were measured in GNU Gimp.

minimum distances were measured using tools in GNU Gimp, as shown in Fig. 3.3. These angular areas were converted into percentages of the area surrounding the cluster and included in Table 3.1. This information was used to compare with masses and determine whether a correlation exists between mass of the cluster and size of the bubbles, as discussed in § 3.4.3.

Two of the partially embedded clusters in Table 3.1, as indicated by *, actually have no maximum distance cleared. These two clusters initially look embedded and are surrounded by gas, however, after inspection of the clusters' SEDs and their position on the colour-colour plot (as discussed later in § 3.3 and § 3.3 respectively) it was clear that they were not completely obscured by gas, and had likely cleared an area in our line of sight. This caused them to appear bluer and could be re-classified as partially embedded.

Caveats and limitations

The analysis carried out for this project is subject to several limitations that weaken the results presented here. Firstly, the classification of clusters into embedded, partially embedded or exposed is very susceptible to changes in the viewing angle of the objects compared to the direction in which the clusters are gas free. This is mostly an issue for embedded and partially

embedded clusters, as mentioned in the previous section. For example, a cluster could appear embedded, however have cleared a line of sight towards us and have very little extinction. All useful cluster properties available were used to minimise the effect this had on classification, however without velocity information of the gas it cannot be certain whether the gas is associated with clusters that appear embedded, for example.

Another limitation is the data used for the study. Using only optical data limits the detection of clusters and produces a bias towards those clusters that are gas free. For example, a cluster that is still embedded at 10 Myr and not optically visible would be missed, therefore results linking the ages of clusters to gas could be biased. However, other studies do support near-completeness of optically selected cluster catalogues. Whitmore & Zhang (2002) studied clusters in the Antennae galaxies and found 85% overlap between compact radio sources (extremely young clusters) with optical clusters. This suggests that the study should not be missing too many embedded, obscured clusters. Additionally, H band images were analysed, (as well as ground-based JHK band images in Bastian et al., 2014a) and found no clear massive cluster progenitors that were not already included in our optical sample.

3.3 Refining age estimates of young clusters

The ages of clusters in this sample have originally been measured using SED fitting of U, B, V, Hα and I bands. The degeneracies associated with this method can give inaccurate estimates for clusters $\lesssim$ 10 Myr old. While using all five of the aforementioned bands provides the best age estimates for the majority of clusters, including Hα presents a problem with some of the partially embedded and exposed clusters. It is important to note that the SSP models used to fit the ages include nebular emission, which should improve accuracy, and an assumed covering fraction of 50% (50% of the ionising photons are absorbed within the aperture). Additionally these ages can be affected by an age/extinction degeneracy and model uncertainties due to factors such as covering fraction or metallicity, for example. This section explains potential methods of accounting for issues that can affect age-dating young clusters.

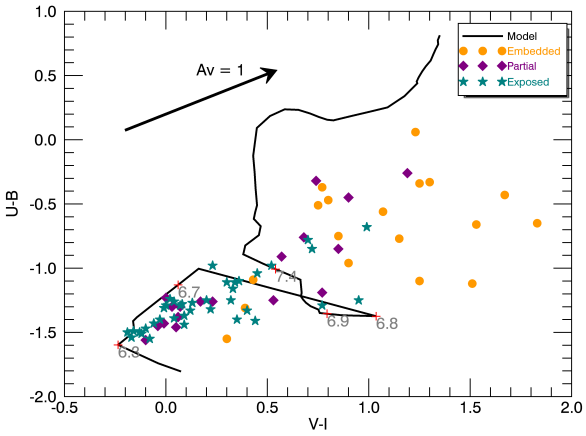

Figure 3.4: Colour-colour plot of U-B vs V-I for the final sample of clusters in M 83. The model track by Zackrisson et al. (2011) is overplotted to indicate where on the evolutionary track the clusters would lie. Orange circles indicate embedded clusters, purple diamonds are partially embedded and teal stars are exposed clusters. The extinction vector indicates the direction the clusters are moved due to extinction effects.

Colour-colour plot

An important tool in determining cluster ages that can also be used to improve age estimates is the colour-colour plot. Fig. 3.4 shows this plot for the final sample of clusters. The model plotted over the points is a cluster evolutionary model for M 83 at solar metallicity that includes nebular and continuum emission and uses a Kroupa IMF from Zackrisson et al. (2011), which was also used for SED fitting. The orange circles correspond to embedded clusters, the purple diamonds to partials and green stars to exposed clusters. Several of the logarithmic ages are shown along the model track. There are some key differences between these populations, which are evident in colour-colour space, and which can provide further information about the early evolution of these clusters.

The embedded clusters lie primarily towards the top right hand corner of the distribution. This is expected, as they all have young ages so should lie on the lower end of the model, but are highly extincted due to their surrounding gas and dust and are moved to the top right section. The exposed clusters also lie where we would expect, in the bottom left of the diagram. This indicates that they are still very young, however, unlike the embedded clusters, a lack of gas means they have much lower extinction and so are much closer to their position on the model. The partially embedded clusters lie scattered around the plot, with extinction varying due to the orientation of the exposed part of the cluster. If the cluster has cleared our line of sight from

gas, then the extinction will be lower than a cluster that has cleared in another direction. The position of points on the graph shows a positive result: the classifications of clusters using the colour-colour plot agree with those from the morphological analysis.

The colour-colour plot can also provide information about the age that clusters start to lose gas. In the region dominated by the exposed clusters, they appear to form a line which is approximately parallel to the extinction vector. This line could be showing the change in the amount of gas cleared over time. If the line is followed back along the extinction vector to the model track, it indicates that the clusters initially began their evolution to a gas free state at an age of ~ 2 Myr, depending on the model.

This plot also illustrates why SED fitting can experience issues when fitting ages for embedded and partially embedded clusters. The clusters are brought back along the extinction vector until they meet the model, giving estimates of the age and amount of extinction for the cluster. The shape of the model track introduces a potentially problematic degeneracy for embedded and partially embedded clusters in the top right of the distribution.

The plot indicates that clusters start becoming gas free at a few Myr, and it only takes this long to create a shell HII region. The embedded clusters have compact HII regions, indicating that they should be very young, and therefore be fitted ages on the earliest section of the model track, however they can be fitted to three different sections of the track due to the degeneracy, assigning them lower extinctions and older ages than they actually have. Partially embedded clusters can also be susceptible to this problem. This age-extinction degeneracy can only be resolved with UV model tracks and photometry, where there is minimal degeneracy (Calzetti et al., 2014).

The problem with Hα

Fig. 3.5 shows an approximation of the Hα excess for the three categories of clusters. The Hα excess is calculated using the following equation:

$$H\alpha_{excess} = (V + I)/2 - H\alpha \tag{3.1}$$

where V, I and Hα are magnitudes in each filter. This provides an indication of the contribution from gas emission to the Hα flux, by subtracting the contribution from the stars. $(\mathrm{V} + \mathrm{I})/2$

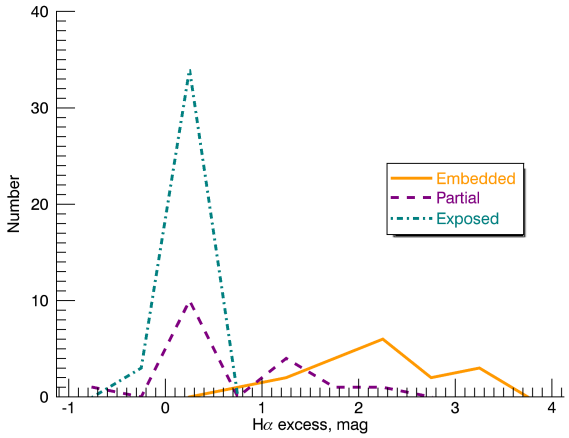

Figure 3.5: A histogram plot of Hα excess: the orange solid line is embedded clusters, the purple dashed line partially embedded clusters and the teal dot-dashed line is exposed clusters. They each peak at different levels of excess, with partially embedded clusters split into 2 peaks, indicating differences in the Hα morphology.

accounts for extinction and offers a close alternative to the actual continuum (as R band or similar bands close to Hα were not available).

When using SED fitting to estimate ages, young clusters would be expected to have a certain amount of Hα emission as they may still contain or be surrounded by ionised gas. As the figure shows, the exposed clusters peak at close to zero excess, so even for newly exposed clusters with gas still nearby, no contribution is made from the gas to the Hα. This would suggest that these clusters have cleared gas to a radius larger than the aperture used for the photometry at a young age. By using Hα in age fitting, these clusters appear older due to a lack of flux in this band, despite still being young enough to produce radiation that ionises the surrounding gas. If the clusters are exposed but there is still Hα emission within the aperture from the nearby gas, a fit using Hα may still be more accurate than without. Bastian et al. (2014a,b) found a similar effect in the nebular continuum in the near-infrared when studying YMCs.

The partially embedded clusters have 2 peaks in the histogram. This indicates 2 populations: those that have cleared gas in our line of sight and have close to zero Hα excess, and those that still have contribution from the gas. Each population would require different fits, sometimes including Hα and others not.

The embedded clusters all have Hα excess as the gas is still surrounding the clusters and therefore is always included in the measurement of Hα. It is unlikely that any embedded clusters would require a fit without Hα.

One of the main issues with Hα is the small apertures that are used to obtain photometry. They are ideal for capturing the continuum emission, but not emission from the entire region, so the Hα fluxes can be underestimated. This loss of flux cannot be accounted for in the aperture correction, as the morphology of the gas surrounding the clusters that may contribute to the Hα flux varies widely. This also means that the excesses displayed in Fig. 3.5 are heavily dependent on the size of the aperture used. Contamination from neighbouring Hα sources can also affect the flux in crowded regions.

Accounting for the problem

In order to minimise the effect a varying Hα morphology has on age determination, Angela Adamo provided ages based on SED fitting both including and excluding Hα flux. The fit that produced the minimum χ^2 was selected as the first optimal fit for the cluster. This way of selecting an appropriate fit proved to be inaccurate for the majority of clusters as most of the embedded clusters were also assigned non-Hα fits, clearly in contradiction with their morphology. These fits also put the embedded clusters at a much more advanced age than the exposed clusters, which is unphysical. Having found that this method was not entirely reliable, a more robust selection process was necessary.

The position of the cluster in the colour-colour plot, its SED and extinction were all used in determining the optimum fit for the cluster. Visual inspection was also used to confirm whether the fit seemed reasonable by inspecting potential nearby Hα sources. For example, an exposed cluster may be assigned a non-Hα fit due to the χ^2 value, however this fit does not account for nearby Hα emission (if the cluster is newly exposed and gas is still close), which can be evident from the strength of the Hα in the cluster's SED.

The SEDs proved the most valuable tool and could even possibly identify the progress of a partially embedded cluster. Later stage partials were identified from having very similar SEDs to exposed clusters (much brighter in blue bands) but with slightly higher Hα due to nearby gas. Earlier partials looked more akin to embedded clusters with high Hα and faint bluer bands, but could be distinguished by lower extinction. Several clusters were identified as partially embedded, despite appearing embedded, due to a lack of strong Hα and bright blue bands. These seemed to be the clusters that had cleared gas along our line of sight but not necessarily in all directions. By employing all of these methods, a new optimum fit was assigned to each

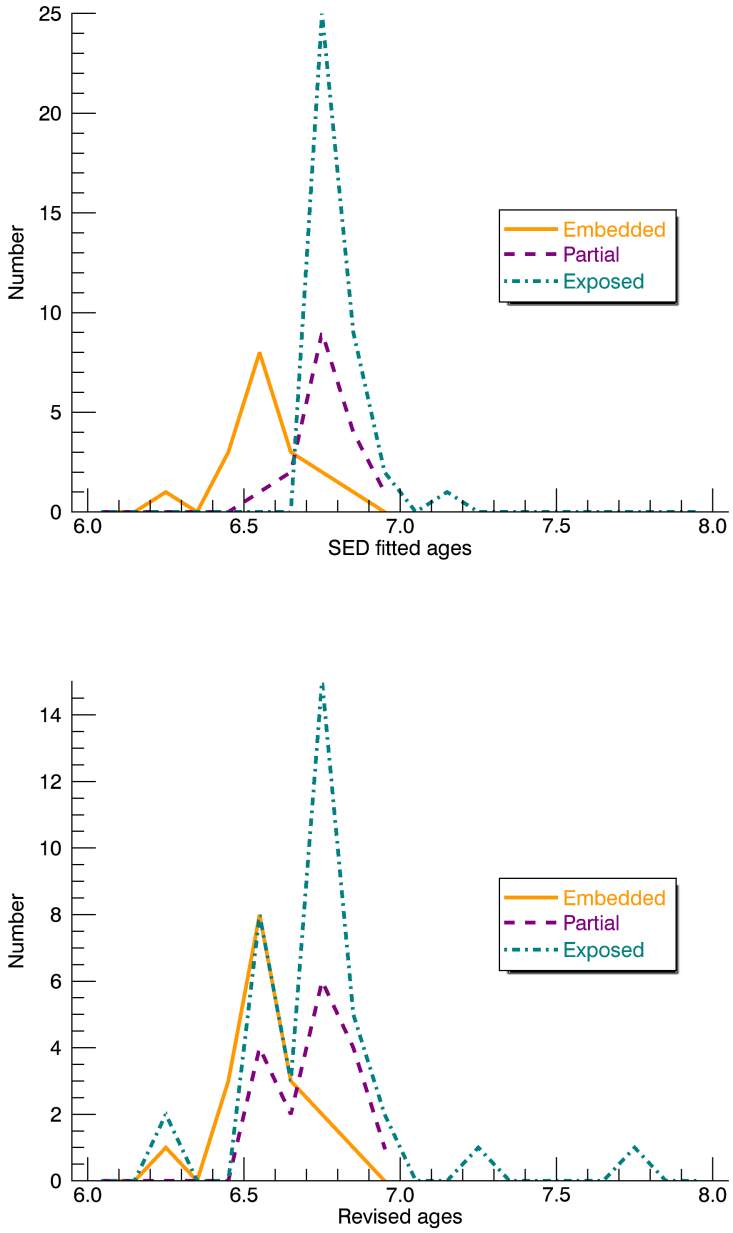

Figure 3.6: The top plot shows the distribution of ages using the original SED fitting with U, B, V, Hα and I bands. The orange solid line is embedded clusters, the purple dashed line is partially embedded clusters and the teal dot-dashed line are exposed clusters. The bottom plot shows the new age distribution for the cluster sample, after selecting the correct fit based on each cluster's SED, position on the colour-colour plot and Hα morphology.

cluster, as shown in Table 3.1.

Fig. 3.6 shows the distributions of SED fitted ages for embedded, partially embedded and exposed clusters. The top plot shows the original ages assigned by SED fitting, while the bottom plot shows the distribution after Hα morphology was taken into account. The large peaks in the data are caused by the quantised method of SED age fitting, where the outputted ages are not continuous and by the binning for the histogram. The new distributions peak a lot closer together and there is overlap between the different populations. The distribution for the embedded population of clusters has not changed, as they were consistently fitted with Hα. Their ages would not have improved without Hα, as they would have been assigned lower extinction and older ages due to the model degeneracy.

The partially embedded clusters now have two peaks, including a younger sub-population. The latter peak consists of those with an optimal fit including Hα, while the new younger peak are those without. The exposed clusters now also have several peaks. The oldest dominant peak are those still fitted with Hα. The two younger peaks align with the embedded cluster distribution, indicating a diverse range of interaction between the stellar component of the cluster with its gas. It could potentially indicate that some clusters become exposed at a faster rate than others. The overlap between different categories of clusters could also indicate that the transition from embedded to exposed phase is very short, and confirms that the partially embedded clusters represent an intermediate phase of cluster evolution to an exposed state. It also shows that this process is continuous and that a majority of the clusters have a compact bubble of ionised gas by ~ 3 Myr.

It is clear, however, that despite improvement for many clusters by tailoring the fit to their morphology, a problem still exists with the degeneracy within the colour-colour plot and fitting procedures for ages of the clusters. The youngest parts of the model track at ~ 2 Myr progress very rapidly. This means that, according to the model, clusters are unlikely to be found in this region, and these ages are less likely to be assigned to clusters. Additionally the degeneracy caused by clusters moving through several sections of the model track when corrected for extinction mean that ages can easily be assigned incorrectly. This most strongly affects ages of embedded and partially embedded clusters due to their higher extinction.

Using these techniques we identified 17 exposed clusters that were better fitted without Hα and were reassigned ages. Most of these ages were only marginally different from the cluster's

previous age, with only 7 clusters experiencing a fairly significant change in age. Several of the ages were older, in contrast with the apparent age of the cluster from the Hα morphology, though the majority were given younger ages. In addition to the exposed clusters, three partially embedded clusters were also assigned different ages. A youth indicator that is linked directly to the stars is therefore preferred over line emission. A potential indicator is the UV band, which will be explored further by Calzetti et al. (2015) and the HST Legacy Extragalactic UV Survey (LEGUS).

Final sample of young massive clusters in M83

Cluster ID	Cat	SED log(age) (Best fit)	Log(mass) (Best fit)	A_V	Max distance (pc)	Min distance (pc)	% max	% min	Best fit
10141*	1	6.60	4.03	0	n/a	n/a	n/a	n/a	No Hα
10165	2	6.70	4.00	0	> 80	23.1	46	10	No Hα
10426	0	6.60	4.00	2.7	n/a	n/a	n/a	n/a	Hα
10433	0	6.60	4.58	2.86	n/a	n/a	n/a	n/a	Hα
10438	1	6.85	4.79	1.52	28.0	7.8	4	18	Hα
10452	0	6.70	4.18	3.53	n/a	n/a	n/a	n/a	Hα
10594	2	6.30	4.46	0	48.9	14.9	9	19	No Hα
10597	2	6.60	4.72	0	54.9	10.0	5	22	No Hα
10645	2	6.60	3.97	0	> 80	10.0	28	31	No Hα
10732	2	6.60	4.03	0	> 80	20.0	21	28	No Hα
10915	1	6.75	3.73	2.78	10.0	0	16	83	Hα
10957	0	6.73	3.57	2.08	10.0	0	11	89	Hα
11164	2	6.60	4.01	0	> 80	26.5	16	28	No Hα
11174*	1	6.73	3.95	0.14	n/a	n/a	n/a	n/a	Hα
11266	1	6.88	3.82	0.83	30.9	0	17	21	Hα
11297	1	6.60	4.06	0	> 80	0	14	13	No Hα
11305	1	6.70	3.81	0.46	13.8	0	8	92	Hα

11312	0	6.60	3.92	2.7	n/a	n/a	n/a	n/a	Hα
11414	2	6.70	3.87	0	> 80	67.2	90	10	No Hα
20249	0	6.48	3.98	3.54	n/a	n/a	n/a	n/a	Hα
20281	2	6.60	4.08	0	23.1	10.0	8	17	No Hα
20288	2	6.78	4.08	0	> 80	40.0	45	14	No Hα
20314	1	6.73	3.81	0	30.2	0	5	15	No Hα
20417	2	6.60	4.26	0	> 80	40.0	20	38	No Hα
20866	2	6.88	3.75	0.02	> 80	15.6	33	35	Hα
20868	2	6.88	3.80	0.18	> 80	14.8	33	35	Hα
20953	1	6.73	3.70	0.75	> 80	53.2	63	13	Hα
30126	1	6.87	3.97	0.79	23.4	0	18	40	Hα
30701	0	6.60	3.82	2.19	n/a	n/a	n/a	n/a	Hα
30989	0	6.30	3.98	2.29	n/a	n/a	n/a	n/a	Hα
31015	2	6.60	3.93	0	> 80	15.0	13	18	No Hα
31016	2	6.70	4.00	0	> 80	20.0	9	5	No Hα
40027	0	6.48	4.19	3.77	n/a	n/a	n/a	n/a	Hα
40117	2	6.87	4.34	0.54	> 80	15.2	6	30	Hα
40358	2	6.88	3.89	1.22	> 80	24.0	32	7	Hα
40543	2	7.78	3.37	0	> 80	46.4	90	7	No Hα
40820	2	6.95	4.20	0.38	> 80	56.8	94	6	Hα

40840	2	7.30	3.23	0	> 80	44.9	78	7	No Hα
40915	2	6.78	3.70	0	23.7	10.0	27	11	Hα
40926	2	6.78	4.1	0	37.5	7.9	16	41	Hα
50015	2	6.78	3.88	0	40.0	5.5	3	20	Hα
50019	2	6.79	3.74	0	> 80	13.3	45	7	Hα
50035	2	6.60	2.50	0.78	> 80	10.0	12	43	No Hα
50081	1	6.88	3.77	0.39	35.3	0	14	52	Hα
50099	0	6.60	3.73	1.99	n/a	n/a	n/a	n/a	Hα
50140	2	6.30	4.21	0	> 80	43.1	60	11	No Hα
50160	1	6.70	3.70	0	n/a	n/a	n/a	n/a	Hα
50233	2	6.78	4.04	0	> 80	7.6	21	28	Hα
50256	2	6.87	3.81	0	> 80	28.4	24	10	Hα
50358	0	6.70	3.96	3.11	n/a	n/a	n/a	n/a	Hα
50377	1	6.78	3.94	0	> 80	0	11	22	Hα
50574	2	6.78	4.09	0	> 80	45.4	79	3	Hα
50611	2	6.78	3.70	0	> 80	14.8	5	13	Hα
50789	1	6.60	4.73	0	31.5	0	4	41	No Hα
50905	0	6.60	3.70	0.33	n/a	n/a	n/a	n/a	Hα
51080	2	6.78	4.11	0	48.3	10.0	3	31	Hα
51093	2	6.78	3.84	0	49.2	7.4	2	22	Hα

51095	2	6.78	3.96	0	40.0	10.0	16	5	Hα
60171	0	6.48	3.73	2.15	n/a	n/a	n/a	n/a	Hα
60558	2	6.78	3.90	0	> 80	8.3	20	23	Hα
60571	2	6.80	4.28	0	> 80	7.6	8	31	Hα
60582	0	6.60	4.06	3.48	n/a	n/a	n/a	n/a	Hα
60770	1	6.79	4.09	0	73.9	0	10	24	Hα
61053	0	6.70	3.87	3.08	n/a	n/a	n/a	n/a	Hα
61216	2	7.00	4.13	0.07	> 80	16.1	21	24	Hα
61310	1	6.92	3.81	0.32	> 80	4.5	5	11	Hα
61417	2	6.78	4.57	0	> 80	12.5	10	25	Hα

Table 3.1: Properties of the final clusters after removing poor sources. Cluster ID corresponds to the ID in the main Silva-Villa et al. (2014) catalogue, with the first digit indicating the field where the cluster is located. 'cat' indicates the category the cluster was sorted into: '0', '1' and '2' correspond to embedded, partially embedded and exposed respectively. Clusters indicated with a * are clusters that initially appear to be embedded from the Hα morphology, though are partially embedded when you consider their SEDs, position on the colour-colour plot and their extinction. 'Max distance' is the furthest radial distance cleared of gas by the cluster, 'Min distance' is the minimum. '% max' and '% min' relate to the percentage of the circular region surrounding each cluster cleared to the maximum and minimum distances. 'Best fit' is the optimum SED fit for the cluster after checking each cluster's individual SED, position on the colour-colour plot and Hα morphology. 'Hα' is a fit with U, B, V, Hα and I bands and 'No Hα' includes U, B, V and I.

Infrared age dating of clusters

Space-based resolution capabilities will soon be limited to near-IR data and the traditional extragalactic cluster population studies in optical and UV wavelengths will no longer be feasible with the retirement of HST. These clusters should be visible in the near-IR, however studies that attempted to use infrared data (e.g. Grosbøl & Dottori, 2013), using aperture photometry as with optical data, have proven unreliable due to spatial resolution effects (Bastian et al., 2014a). Despite this, space-based instruments with high spatial resolution (e.g. JWST) in the near-IR can still be relevant and useful to cluster studies.

As explained previously, current age dating methods for clusters, such as SED fitting, as used for this sample can be poor at providing accurate ages for clusters younger than $\sim$ 10 Myr, without a reliable band (such as Hα or UV) to overcome degeneracies.

A novel method for confirming age estimates has been developed by Gazak et al. (2013), which uses the presence of red supergiants (RSGs) in the cluster as an absolute age indicator. By plotting the J-H colour for each of the clusters against log(age) (obtained via SED fitting), a clear distinction between younger and older clusters exists in colour space. Younger clusters that are devoid of RSGs appear distinctly bluer, with values jumping to redder colours at older ages, immediately at the onset of RSGs. This is due to RSGs dominating the flux at red wavelengths, such as the near-IR (e.g. Davies et al., 2017). According to Gazak et al. (2013), any clusters with red J-H colours should be older than $\sim$ 6 Myr, the age of the jump in the plot. One caveat for this method is that extinction can also cause young clusters to have red J-H colours.

For this study, the log(age) (based on the best fit, as quoted in Table 3.1) was plotted against V-H colour (which was corrected for extinction) to find whether this jump is visible. The V band was chosen as no J band data was available for WFC3 in Fields 3, 4, 5, 6 and 7. The plot is shown in Fig. 3.7, and despite the difference in wavelength, the same feature is produced with the jump in colour at the same age, $\sim$ 6 Myr. Almost all of the YMCs lie where they are expected to be; older exposed clusters on average are redder in V-H, as they have RSGs and embedded younger clusters are the bluest. This indicated that the age estimates are fairly accurate, and at the expected values for these clusters. The model from Gazak et al. (2013) plotted over the data does not fit as cleanly as it does when using J-H colours. This is because RSGs are known to dominate J band flux, however in the V band they may not contribute as significantly, making the effect weaker.

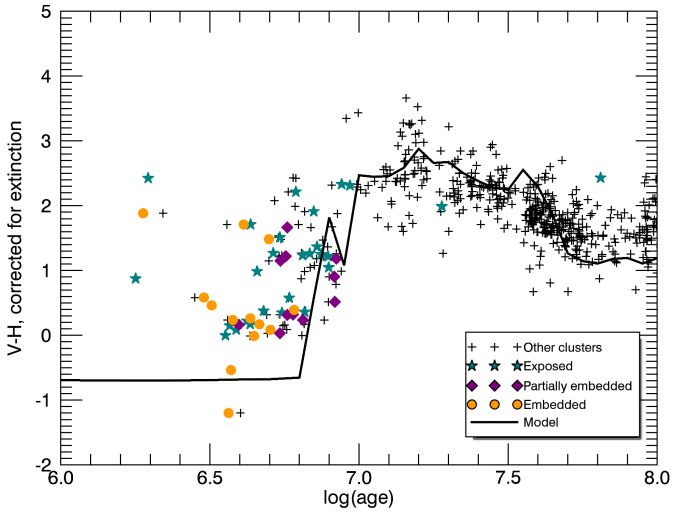

Figure 3.7: V-H colour for all clusters in the M 83 cluster sample, with the subsample of YMCs highlighted in colour with green stars, purple diamonds and orange circles corresponding to exposed clusters, partially exposed clusters and embedded clusters respectively. The jump from bluer, younger clusters to redder, older clusters due to the appearance of red supergiants is clear. On average, the population of embedded clusters is slightly redder than the embedded population, but this is not a significant difference. The model plotted over the data is calculated for the V-H band as per Gazak et al. (2013), and provided by Zach Gazak. The model does not fit that data as closely in V-H colour as it does for J-H, likely due to J band being the most affected by RSGs.

Wolf-Rayet features in clusters

Wolf-Rayet (WR) stars are the later evolutionary stages of massive stars (typically 10-25 $M_{\odot}$) and can be detected in clusters by broad emission lines in their spectra that are specific to these types of stars. The majority of WR stars are derived from O-type stars and so have total lifetimes of $\sim$ 5 Myr, 10 % of which is spent in a WR phase. Higher mass (25-30 $M_{\odot}$) RSGs can also become WR stars. The characteristic emission lines arise from fast stellar winds and heavy mass loss from the star (Crowther, 2007).

The presence of such high mass, short-lived stars in clusters within the sample indicates that the clusters should be young. In older clusters, any WR stars would have already evolved past supernovae, given their $\sim$ 5 Myr lifetimes, giving a refined age estimate of these clusters between 4-7 Myr. Bastian et al. (2006) previously used the same technique to age date clusters in the Antennae galaxies.

Hadfield et al. (2005) carried out a survey searching for WR stars in regions within M 83, discovering 132 sources. I cross-referenced the coordinates of the regions they identified as containing these objects with the coordinates of the cluster sample, examining images of the

Properties of clusters with WR features

Cluster ID	Cat	Log(Age)	Log(Mass)
10141	1	6.60	4.03
10438	1	6.85	4.79
10597	2	6.60	4.72
31015	2	6.60	3.93
50160	1	6.70	3.70
51080	2	6.78	4.11

Table 3.2: Clusters that coincide with identified WR regions in M 83. 'Cat' refers to classification of the cluster as embedded, partially embedded or exposed, as used throughout this thesis. The ages and masses are the revised figures as described in § 3.3.

position of the features to confirm that the features originated from the cluster. Five regions were found that coincided with the position of clusters in the YMC sample. In addition to these 5 clusters, I also had optical spectroscopy of one further cluster in the sample that showed WR features. These clusters and their properties are shown in Table 3.2.

The low number of sources corresponding to clusters in the sample is mostly due to the lack of coverage of the original study. Their spectra did not uniformly cover the entire galaxy and so many clusters will have been missed. Additionally, these stars will be harder to detect in clusters due to being "washed out" by the continuum of the cluster, so many WR sources will be required for a detection. There are many young massive clusters that do not align with the WR sources, although it is not guaranteed that all clusters should contain enough WR stars to make detection possible. So the clusters without corresponding WR features may not be older, they may have insufficient WR stars to be detected. Therefore the WR feature method can only be used to confirm young ages for some clusters but not decide on the correct age. The other methods discussed in this section should primarily be used for this purpose.

Using this method indicates that 5 of the clusters with WR features have been correctly assigned younger ages. It also suggests that cluster 10438 should be younger. This cluster is already thought to have been given too old an age due to degeneracy in the model track, and this test agrees with that conclusion. The sample of 6 clusters used here show that WR features can be used to constrain ages of young clusters.

3.4 Results

3.4.1 Statistical age results

After comparison of the categorisations of the clusters with their age estimates, the results indicate that clusters are no longer embedded, and are gas free by $\sim$ 4 Myr. The median ages for the embedded, partially embedded and exposed clusters were $\sim$ 4 Myr, $\sim$ 5 Myr and $\sim$ 6 Myr, respectively. Therefore, the age at which clusters become exposed should be between 4 and 5 Myr. The maximum age of the clusters in the embedded sample is $\sim$ 6 Myr, possibly indicating that the timescale for the clusters to progress from an embedded to exposed state is very short. Older ages for the embedded and partially embedded clusters could arise from model degeneracies in SED fitting. These incorrect ages may have skewed the median ages for embedded and partially embedded clusters, which should in fact be younger. This issue can be somewhat mitigated by determining the correct fit, taking into account that embedded clusters should be younger than exposed clusters (therefore younger than $\sim$ 6 Myr), as per the results of this chapter.

The majority of the clusters (53%) in the sample are exposed. If clusters that have removed any amount of gas from their surroundings i.e. partially embedded clusters are included as well, this means that 77% of the sample are no longer embedded. If we assume this sample is complete for M 83 for clusters younger than 10 Myr (a 10 Myr age cut was applied to the catalogue), and that the cluster formation rate is constant, this indicates that 7.7 Myr of the first 10 Myr of the life of young massive clusters are spent exposed to some extent. Alternatively, the first 2.3 Myr are spent in an embedded state, and clusters initially become exposed at this age, in agreement with the age indicated by the colour-colour plot discussed in § 3.3.

A key assumption of the calculation, however is that all clusters are optically visible and enter our catalogue when they form. It can be argued that far younger clusters may be completely obscured and not be included, however, as discussed in § 3.2.3, a study by Whitmore & Zhang (2002) of clusters in the Antennae indicates that by comparing compact radio sources (extremely young clusters) with optical clusters, there is $\sim$ 85% overlap. This indicates that very few of these sources would be missed. H band images also show no extra clusters than the optical catalogue. This is also an indication that the embedded phase of the clusters is very short.

3.4.2 Models of bubble expansion

Dale et al. (2014) carried out simulations of cluster formation and early evolution. Their simulations include the effects of both ionisation and stellar winds from OB stars, although no radiation pressure has been included, which is likely to be relevant for very dense star-forming regions, e.g. Fall et al. (2010). The simulations end 3 Myr after the formation of the first O-stars in each model cloud and some simulations already display bubbles formed by clusters with masses similar to the lower end of the range represented by the sample. This agrees with the results that these clusters will become gas free by 2-4 Myr. However, the bubbles created in Dale et al. (2014) are substantially smaller than those observed here.

Having measured the maximum distance cleared by each of the exposed clusters, 77% of clusters had cleared some extent of their gas to radii greater than 80 pc. In contrast, simulations of clusters with similar initial masses clear bubbles to a maximum possible distance of 40-50 pc in diameter. This indicates that the simulations do not reproduce the extremely efficient process that results in gas free clusters, as observed here. It could mean that the process is related to radiation pressure, as this was not included in the simulations. Only a few of the simulations in Dale et al. (2014) are likely to be dense enough for radiation pressure to be important, but that may not be true of the clusters studied here. Additionally the star formation rate used in the simulations may not be in agreement with current early cluster evolution studies. Cluster formation by gas exhaustion may be a possibility, in which case there should be a lower amount of gas to lose, as discussed in § 1.2).

An important note is that these simulations end 3 Myr after the birth of the first O-stars. Should they run until 6 Myr, the size of the bubbles in the simulations will increase and likely agree with measurements from M 83 clusters. Therefore, it can be concluded that some of the simulations of gas removal are in reasonable agreement with what is found in the young clusters in M 83.

3.4.3 Cluster mass and distance cleared

An interesting aspect of this study to take further, is whether or not there is a relationship between mass of the cluster and size of the bubble cleared. Using the measurements of the amount of space cleared by the cluster from Table 3.1, mass of the cluster was plotted against

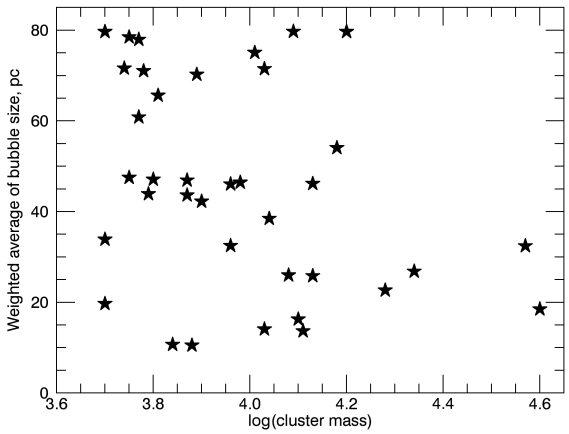

Figure 3.8: The plot of log(mass) of the cluster against the weighted average of the interior size of the bubble for exposed clusters. As shown, there appears to be no correlation between the two variables, and may require a third variable to constrain a relationship.

the weighted average of the distance cleared, as shown in Fig. 3.8. There was no clear correlation between the amount cleared and the mass of the cluster, for clusters in our mass range of $\sim$ 5000 - 6×10^4 $M_\odot$. A relationship would likely require a constraining third variable, and so position of the cluster in the galaxy (whether upstream or downstream of an arm, or in the inter-arm regions), and the cluster age were tested.

Including the cluster's age in the plot still did not constrain any relationship. To test galactic position, I visually classified the position of each cluster in the sample. This property was quantised into 6 possible categories: in the bulge/inner bar region, in the outer bar region, at the end of the bar (which has increased levels of star formation), in the upstream regions of the arm just after gas enters the arm region and is shocked (leading to star formation), in downstream regions at the arm's outer edge, after the expected star formation, or outside of the arm overdensities. We plotted cluster mass against the weighted average distance of the cleared bubble as a function of position in the galaxy and still no clear relationship could be determined.

Including the mass of the gas outside of the exposed clusters could help constrain a possible relationship. However, obtaining an accurate estimate of the amount of gas associated with the cluster would be very difficult using images that rely on photometric bands highly susceptible to the continuum. Furthermore, the physical size of the shell would be very hard to determine, especially in more crowded environments.

3.4.4 Implied constraints on age spreads within clusters

Phenomena observed in intermediate age (6-8 Gyr) clusters in the SMC and globular clusters, such as split main sequences or red giant branches and corresponding chemical spreads and anticorrelations (see Chapter 1) have previously been explained using age spreads, or multiple bursts of star formation (e.g. D'Ercole et al., 2010). The extent of the age spreads has been suggested to be up to a few hundred Myr (e.g. Milone et al., 2009), though this has been strongly contested by Bastian et al. (2013a) and Niederhofer et al. (2015b), who have found no evidence of age spreads in YMCs with resolved photometry or integrated spectroscopy. Additionally, stellar rotation has been shown to potentially exhibit the same effects seen in the main sequence turn offs (Bastian & de Mink, 2009). Cabrera-Ziri et al. (2014) also showed that the spectra of NGC 34 can only be reliably fit with a single stellar population, contesting the theory of multiple bursts of star formation.

The debate of the origin of multiple stellar populations continues, and these results can be used to apply some constraints to claims of age spreads. The clusters studied here are far younger than those with the proposed age spreads, and they have already become exposed and free of gas at $\sim 2-4$ Myr. The lack of ionised gas within the cluster at this time means that there can be no star formation until more gas has been accreted, although a feasible mechanism used to accrete this gas is still unclear.

Bastian et al. (2014b) explored clusters in the literature that are of greater masses than those in this study, with all clusters showing the same result as found for clusters in M 83. One cluster in particular (cluster 23 in galaxy ESO 338-IG04), which is very massive (5-20 $\times 10^6$ $M_\odot$) and metal-poor, so therefore highly comparable to GCs (Östlin et al., 2007), showed that gas was still moving away at a speed of ~ 40 km/s. After measuring the distance moved by the gas and using the speed, it can be determined that cluster 23 also first became free of gas by 2-3 Myr. This indicates that the timescale for gas removal seems to be uniform across cluster masses.

The pristine gas required to produce a second generation of stars would need to be accreted from other sources, as leftover gas is still moving away from the cluster. It is highly unlikely that these clusters would be able to accrete the amount of required material from elsewhere in the galaxy on necessary timescales to satisfy current theories of the origin of multiple populations with multiple epochs of star formation, especially considering the amount of gas would be on par with the existing cluster mass for a reasonable star formation efficiency.

3.5 Discussion

The results of this work have important consequences for one of the current globular cluster formation scenarios, the Fast Rotating Massive Star Scenario (FRMS; Krause et al., 2013). In this scenario, the first generation of stars form, which then become mass segregated leaving the high mass stars in the centre. Bubbles of gas surround each high mass star in narrow filaments. Decretion discs form around the high mass stars and ejected material mixes with the pristine gas from the filaments to form the second generation of stars within the disks. When the high mass stars have evolved to the supernova stage, the leftover pristine gas from the filamentary structures is arranged in a larger bubble surrounding all stars in the cluster, so that the cluster appears to be embedded in gas.

The young globular clusters must remain embedded in their natal gas for 25-30 Myr in the FRMS scenario, however the clusters in this study have shown that this is not the case, and they have in fact become gas free by $\lesssim 4$ Myr. This clearly indicates that the FRMS scenario, in its current form, is not feasible and clusters are far more efficient at removing gas than expected. One clear difference is the mass of the cluster that has formed. The FRMS scenario discusses clusters of mass $\gtrsim 10^6$ $M_\odot$, whereas the most massive cluster in this work is $\sim 5 \times 10^4$ $M_\odot$. However, the results of Bastian et al. (2014b) suggest that the effect of clusters clearing out gas is scalable between cluster masses. They present similar results for clusters of masses $\sim 10^6$ $M_\odot$, on par with those described in the FRMS scenario. The same effect is seen in these clusters; gas is cleared at the same age as for the lower mass clusters. One difference is the size of the bubble cleared; higher mass clusters appear to create larger bubbles on the same timescales. .

Supernovae have been considered as one of the main contributors to the removal of gas. It is feasible to include supernovae for systems at approximately solar metallicity, like M 83, however this only holds if the cluster contains very high mass stars. For the first supernovae to occur at 2-3 Myr after cluster formation (the age at which the clusters seem to start removing gas) the IMF must be well sampled. A reasonable estimate for the most massive star in clusters of ~ 5000 $M_\odot$ is ~ 40 $M_\odot$, which would not undergo a supernova phase until ~ 8 Myr, and so will not have made an impact on the removal of gas. Therefore for supernovae to be considered, stars much greater than this mass (likely at least one star of ~ 120 $M_\odot$) must exist in each of the clusters, which is unlikely to be the case for all clusters. At sub-solar metallicities, these

very high mass stars would collapse straight into a black hole phase, but supernovae could at least make a contribution to the gas removal at solar metallicity (Heger et al., 2003). However, it is now thought that massive, bound clusters such as these form by gas exhaustion, rather than expulsion, meaning that it is far easier to reach a gas-free state as observed here on short timescales due to the smaller amount of gas leftover. It may not be necessary to invoke any extra feedback or contribution from supernovae.

3.6 Summary

Here we summarise our main conclusions:

- The young massive clusters in our sample are all exposed and free of gas by $\sim$ 4 Myr. The age at which clusters seem to start becoming gas free is 2-3 Myr, as indicated by the position of exposed clusters in colour-colour space and statistical considerations of the relative population sizes of exposed or partially embedded clusters as opposed to embedded clusters.

- The mechanism for the removal of gas from clusters is far more efficient than previously thought. Supernovae could play a role but cannot be the sole contributors. Strong stellar winds from stars at advanced evolutionary stages, such as Wolf-Rayet stars, which have been identified in several of the YMCs in the sample could play a role, however gas exhaustion due to a higher star formation efficiency likely plays the main role.

- The lack of gas within these clusters provides constraints for the age spreads that have been proposed to exist in globular clusters. A spread of a few hundred Myr is required, however these clusters are gas free by $\sim$ 4 Myr, and so cannot form a new generation of stars, unless this gas is re-accreted and new pristine gas is obtained. The amount of gas that would need to be accreted over this short time frame is unlikely, especially considering the cluster's original gas is pushed away to large distances. It is also unlikely that gas from other sources could be accreted in the space of a few hundred Myr. This also has consequences for the FRMS scenario which currently requires clusters to remain embedded in natal gas for 25-30 Myr in order to form a second generation of stars is infeasible, as these clusters are gas free by $\sim$ 4 Myr.

- Age fitting using SEDs can be unreliable for young clusters due to degeneracies in the models and aperture effects. This degeneracy is best overcome by using UV magnitudes, however other methods can be used to constrain ages when this is not available. Constraints on age can be made by using the near-infrared bands, such as H (F160w), where the characteristic jump at $\sim$5-6 Myr from blue to red colours due to RSGs can provide an upper limit. The presence of Wolf-Rayet features also puts a constraint on age of the cluster of 4-7 Myr. Using Hα in the fit for the age of a young cluster and as an indicator of age can also be unreliable as it is not directly linked to the stars, but rather line emission and the continuum can have an effect.

Chapter 4

Constraining the origin of multiple populations in globular clusters

Summary

This chapter contains the results of a spectroscopic study of the intermediate age ($\approx 6-8$ Gyr) massive clusters Lindsay 1 and Kron 3 in the Small Magellanic Cloud. Analysis includes measuring CN and CH band strengths (at $\simeq$ 3839 and 4300 Å respectively), [C/Fe] and [N/Fe] measurement and membership determination using VLT FORS2 spectra. The clusters were found to have 17 and 18 cluster members respectively and contain sub-populations of potentially 6-7 stars enriched in nitrogen. This is strong evidence for the presence of multiple populations in both clusters, now two of the four intermediate age clusters to show such evidence, along with NGC 416 and NGC 339. This phenomenon was originally thought to be a unique characteristic of old globular clusters. The results presented here on clusters aged $\sim$ 6 Gyr old, this indicates that the mechanism responsible for their onset must operate until a redshift of 0.75, much later than the peak of globular cluster formation at redshift $\sim$ 3.

4.1 Introduction

The presence of multiple populations (MPs) in globular clusters (GCs) has destroyed the long held assumption that they were the quintessential single stellar population (all stars have the same age and abundances with negligible variation) by introducing star-to-star variations in light element abundances (see Chapter 1 for a detailed discussion). Now the question has turned to the cause of this phenomenon and producing a feasible GC formation theory.

Old GCs ($>$ 10 Gyr) in both the Milky Way and the LMC have been found to host MPs (e.g. Mucciarelli et al., 2009; Mateluna et al., 2012), while similarly aged, less massive open clusters have not. Therefore, it was traditionally thought that the main cluster property contributing to the presence, or lack thereof, of MPs is the cluster's mass. However, this has recently been called into question as younger ($\sim$ 1.5 Gyr) clusters of comparable mass to GCs do not appear to host them (e.g. NGC 1806, NGC 419; Mucciarelli et al., 2014a; Martocchia et al., 2017). This indicates that age could also be a contributing factor to whether massive clusters develop MPs, and is tested in the work in this chapter.

The gap between the single population 1-2 Gyr clusters and those $>$ 10 Gyr with MPs is therefore an important age range to study to provide insight into exactly when and how MPs originate. This is the aim of these studies into Lindsay 1 and Kron 3 (hereafter L1 and K3), intermediate age clusters in the SMC. At $\approx$ 8 and 6.5 Gyr respectively (Mighell et al., 1998; Glatt et al., 2008), L1 and K3 fit well into the unexplored age region for GCs. Additionally, they are low metallicity ([Fe/H] $\approx$ -1.35, -1.08; Mighell et al., 1998; Glatt et al., 2011) and massive ($\approx 1.7 - 2.6 \times 10^5$ and $3.9 - 5.84 \times 10^5$ $M_\odot$; Glatt et al., 2011), so are comparable with old GCs in properties other than age. In the study described in this chapter, CN and CH band strengths (Kayser et al., 2008; Pancino et al., 2010; Lardo et al., 2012) and C and N abundances are measured to look for MPs in both clusters.

In § 4.2 I discuss the data and its reduction, § 4.3 discusses determination of cluster members, § 4.4 the measurement of CN and CH band strengths and C and N abundances, and § 4.5 and § 4.6 the results and discussion respectively.

4.2 Observations and data reduction

Spectroscopic data for Lindsay 1 and Kron 3 were obtained in one observing run (program ID 096.B-0618(B)) at the ESO VLT telescope based in Paranal, Chile using the MXU mode on the FORS2 spectrograph. Five science exposures were obtained for Lindsay 1 and six for Kron 3 along with bias frames, flat fields and arc lamp spectra for wavelength calibration. The instrument configuration consisted of the GRIS 600B+22 grism with two 2kx4k E2V CCDs (15 μm pixel size), mosaic-ed. They are sensitive in the blue range below 600 nm, a requirement to accurately measure CN and CH bands at $\simeq$ 3883 and 4300 Å respectively. Each cluster was

centred on the master chip (hereafter chip 1), while the slave chip (chip 2) sampled the outer regions of the clusters. The resolution of the spectra is R $= \lambda/\delta\lambda \simeq 800$ and the spectral range covered for most stars was $\sim$ 3300 - 6600 Å, depending on their position in the instrument field of view.

Archival pre-imaging in the V and I bands was already available for these clusters (ESO-programme: 082.B-0505(A) P.I. D. Geisler), which was used to select targets, with an aim to sampling primarily the lower RGB to avoid abundance contamination due to stellar evolution and the first dredge-up. 34 targets were chosen for Lindsay 1 and 35 for Kron 3 spanning chips 1 and 2, though the 1" slit width prevented the selection of targets in the central regions of the clusters due to crowding. Where it was impossible to image a primary target due to slit positioning, a random star was chosen in its place.

The spectra were reduced using tools available in the IRAF software package (Tody, 1993)[1]. Bias frames were combined and subtracted from all images, followed by combining and normalising flat fields and applying this master flat to the science and arc lamp frames. Cosmic rays were removed using the L.A.Cosmic IRAF routine (van Dokkum, 2001). Having traced the apertures across the images, I found very little curvature and so opted not to use a correction routine but allow the *apall* task to account for this when extracting the spectra without applying an additional correction. I first combined the five science exposures and then extracted the spectra for all targets using the *apall* task. The *identify* and *dispcor* tasks were then used to wavelength calibrate the spectra using the arc lamp exposure.

Fig. 4.1 shows example spectra for stars in Lindsay 1 (4.1a) and Kron 3 (4.1b). Two stars with nearly identical T_{eff} and log(g) are shown in each, illustrating the CN and CH molecular absorption bands. Differences in the strength of the CN absorption can easily be seen, while the CH band is approximately the same.

4.3 Membership determination

An important step in ensuring C/N and CH/CN distributions and any implications are accurate is discerning the true cluster members from contaminants. Several different methods were used

[1]IRAF is distributed by the National Optical Astronomy Observatories, which are operated by the Association of Universities for Research in Astronomy, Inc., under cooperative agreement with the National Science Foundation.

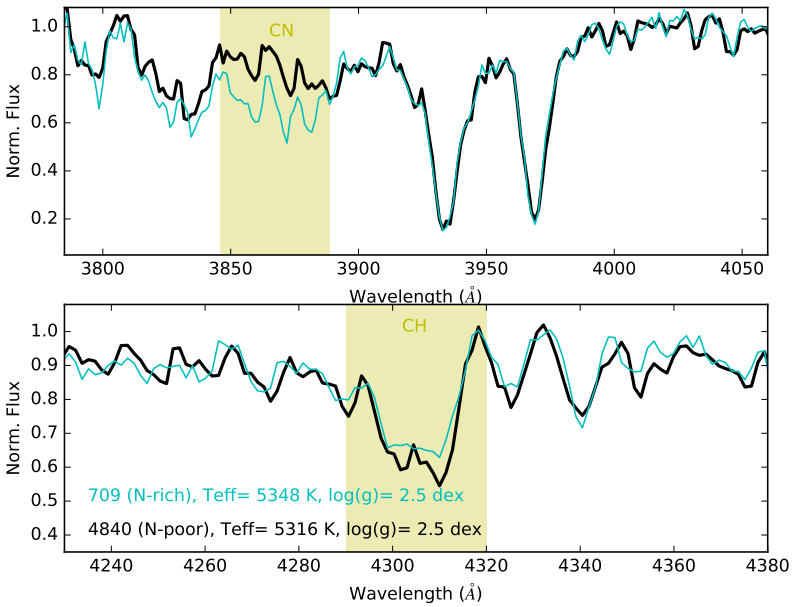

(a) Example spectra for Lindsay 1

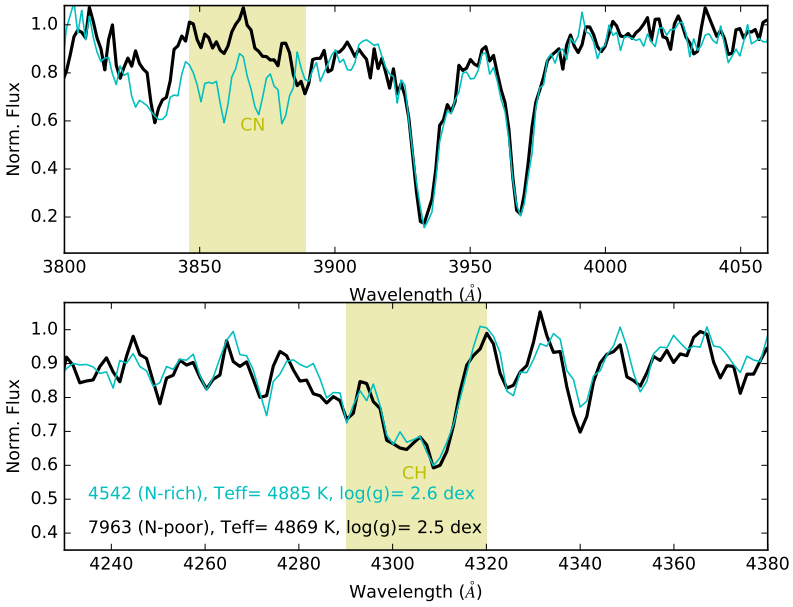

(b) Example spectra for Kron 3

Figure 4.1: Samples of the final extracted normalised spectra showing the CN and CH bands. Plot 4.1a shows two stars (one enriched and one normal) with very similar stellar properties for Lindsay 1 while plot 4.1b shows two stars for Kron 3. Large differences between the stars can be seen in the CN bands while very little difference is seen in the CH bands.

besides the traditional radial velocity (RV) measurements as there are fairly large errors associated with RVs for low resolution spectra. There is still a possibility of some field interlopers due to the potentially compatible field star RVs in the SMC (Carrera et al., 2008) however, compliance with all four membership criteria makes this very unlikely.

Fig. 4.2 shows the main criteria for cluster membership in the analysis. Firstly RVs were found with the *fxcor* utility in IRAF using a template spectrum of a likely member star, with a heliocentric-corrected velocity found independently from *rvidlines*. The RVs for each cluster are listed in Tables 4.1 and 4.2 and displayed in Fig. 4.2 against distance from the centre in arcminutes. The median velocity of all stars was measured as 141.21 km/s and 140.3 km/s for Lindsay 1 and Kron 3 respectively, in agreement with the expected velocities for L1 stars of 145.3 km/s and 135.1 km/s for K3 from FORS2 spectra by Parisi et al. (2015). There may also be a small offset due to slits being placed slightly off-centre from the star. A reasonable error on RV measurements at this resolution is $\approx$ 25 km/s, which was measured by comparing the difference in radial velocity measurements at the red end of spectra with the blue in *rvidlines*. This corresponds to $\approx 1\sigma$ for Kron 3 and $\approx 0.5\sigma$ for Lindsay 1. A deviation of this error from the median was the criteria for cluster membership. Red points in the plot are considered non-members and the blue shaded region corresponds to the acceptable RV range for membership.

The other two panels in Fig. 4.2 show CaII (H+K) and Fe5270 index measurements, which can be used as proxies for metallicity and iron abundance respectively. For Lindsay 1 a cut of 1σ from the median values of each was used as the membership criterion, however for Kron 3 this would have removed many potential cluster members and many more than those outside of the acceptable radial velocity range, therefore a 2σ range was used for K3.

Fig. 4.3 shows colour magnitude diagrams (CMDs) for each cluster, which were used to identify outliers that were unlikely to be cluster members. Target stars for spectroscopic observations were selected from photometry, however all of these targets were potentially not observable due to slit positioning on the mask and random stars were chosen in their place. Therefore this check was required to ensure all stars belonged to the red giant branch. Several outliers were removed from the Lindsay 1 sample while only one bright chip 2 star at V = 19.57 was removed from Kron 3, as its higher luminosity is an indication it may be more strongly affected by mixing. Non-member stars identified using all criteria are shown in the CMDs. Chip 1 stars are circles while chip 2 are triangles and non-members are shown in magenta while members

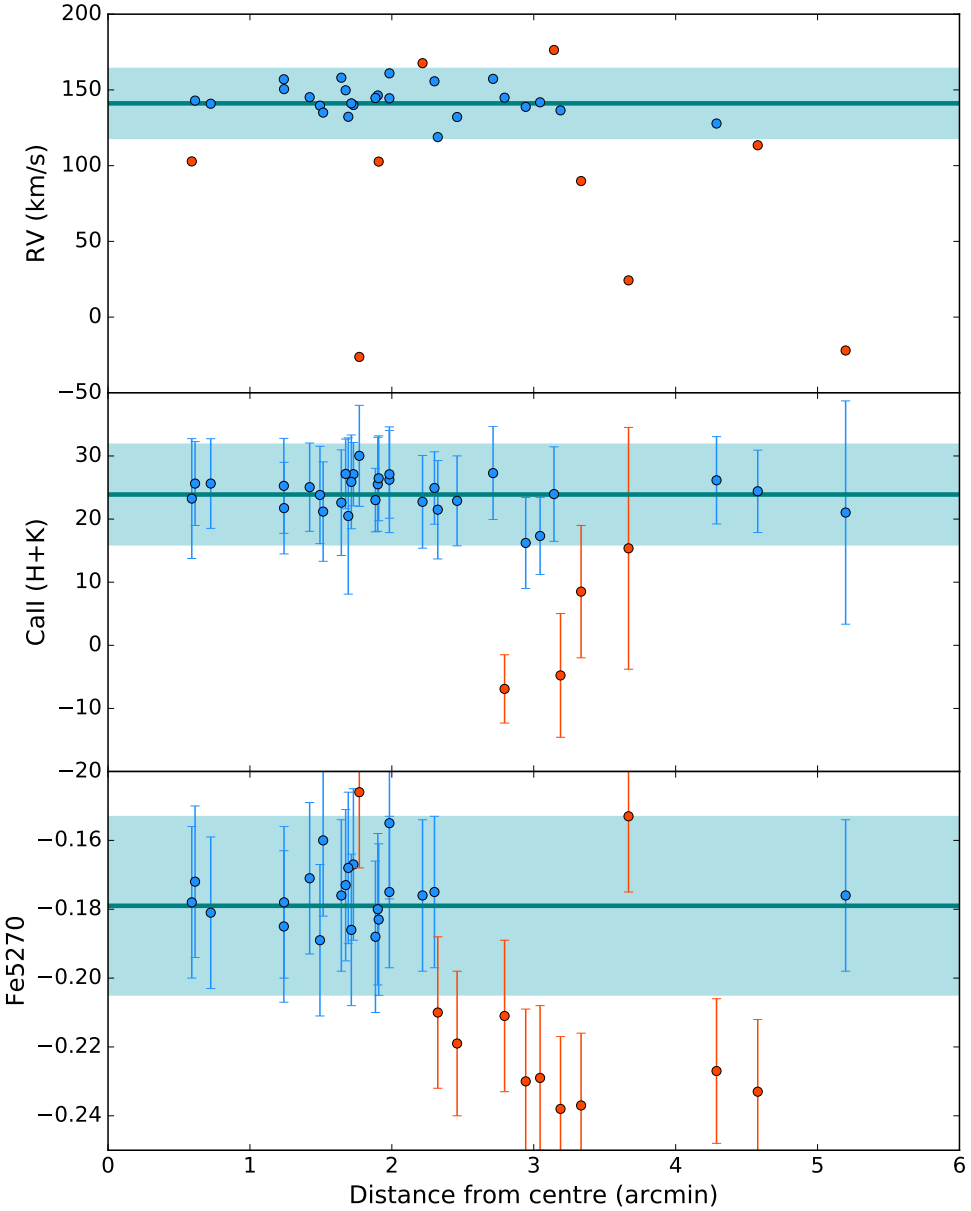

(a) Membership criteria for Lindsay 1

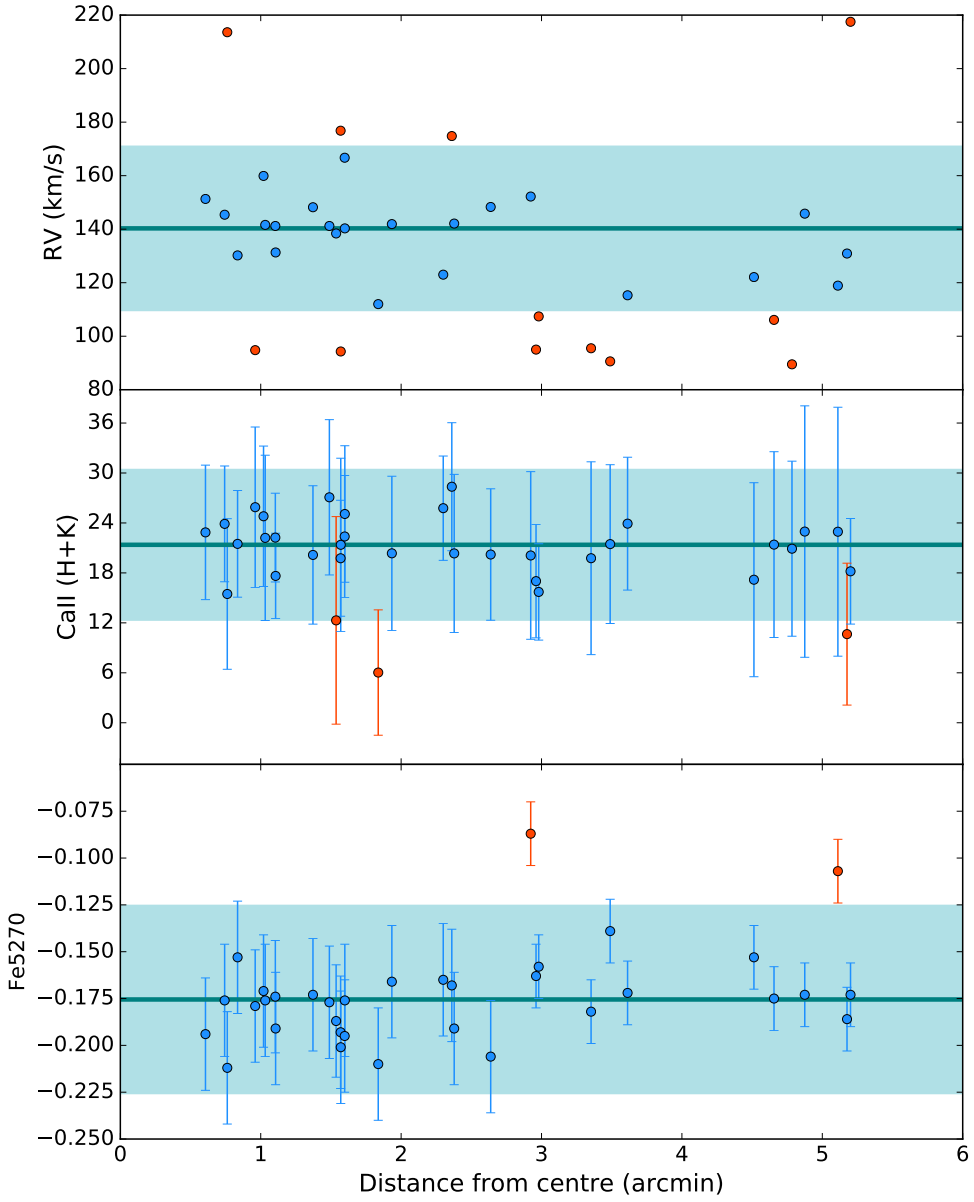

(b) Membership criteria for Kron 3

Figure 4.2: Criteria used to determine true cluster members: radial velocities (RVs) and CaII (H+K) and Fe5270 band strengths against distance from the centre in arcminutes. Top plots show the RVs with members in blue and non-members in red. The teal line is the median radial velocity of the cluster and the blue shaded regions show the allowed deviation from the median of 1 σ. CaII (H+K) and Fe5270 measurements are shown underneath, with an allowed deviation of 1 σ for Lindsay 1 and 2 σ for Kron 3.

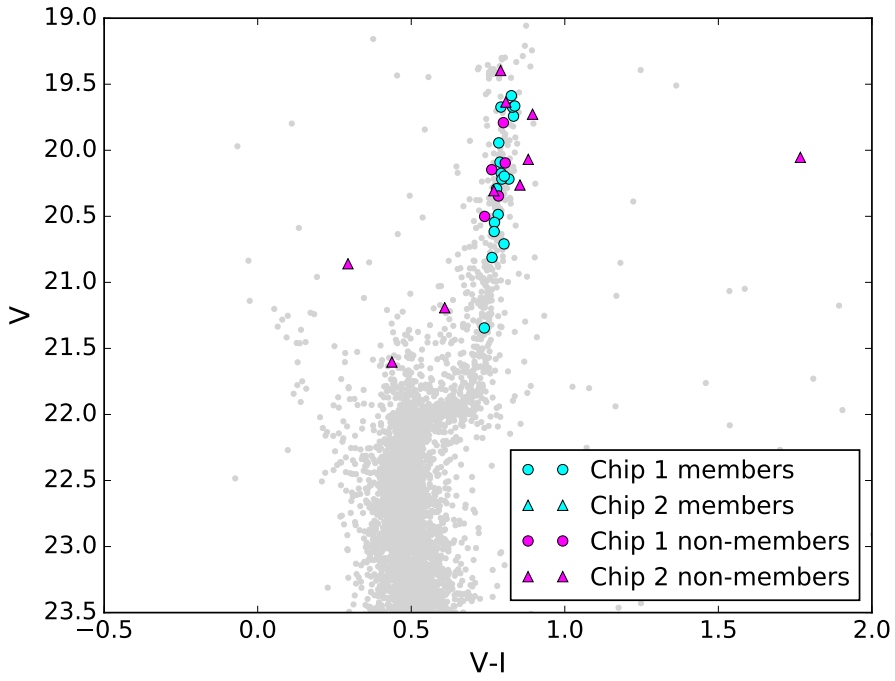

(a) Colour magnitude diagram for Lindsay 1

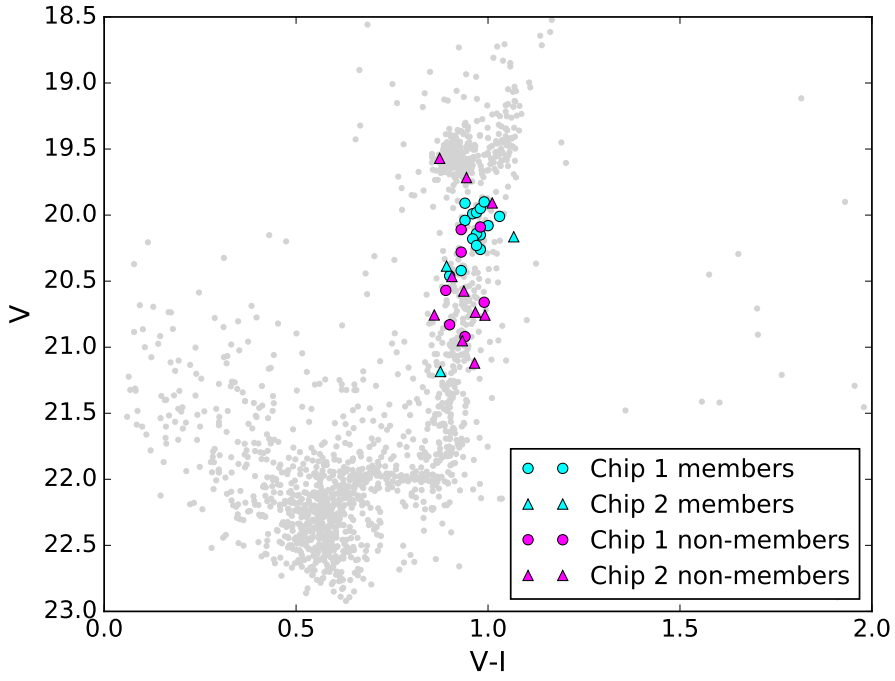

(b) Colour magnitude diagram for Kron 3

Figure 4.3: One of our criteria used to determine cluster membership. Plot 4.3a shows the CMD for all stars in the analysis of Lindsay 1 and plot 4.3b shows stars in Kron 3. Chip 1 stars are in cyan and chip 2 in magenta. The majority of stars in both cases appear to lie on the RGB, however the four stars in L1 far away from the RGB were removed in addition to the star at V = 19.57 for Kron 3. This was removed due to its high luminosity and the possibility of it being affected by mixing.

are in teal.

Finally, spectra were visually inspected to ensure that they were all reliably RGB stars. Stars 0008, 0101, 0140 and 0203 in Lindsay 1 were excluded on this basis, as two had strong absorption features in the red part of the spectrum, suggesting the stars were too cool and the other two had strong hydrogen absorption lines indicating that they are probably hotter, unevolved MS stars. Also star 5059 in Lindsay 1 displays a prominent Mg triplet (5177Å) feature in its spectra, indicating that this star is possibly more metal-rich than the rest of the cluster population. Also, spectral synthesis reveals that it has [C/Fe] abundance significantly higher ([C/Fe]=0.63$\pm$0.2 dex) than the bulk of L1 stars, for which [C/Fe]$\simeq$0.1 dex. 5059 was also excluded from the following analysis.

These criteria eliminated 17 stars in both Lindsay 1 and Kron 3, leaving 17 and 18 member stars respectively. Tables 4.1 and 4.2 list all stars for each cluster, including their reasons for exclusion from the analysis if not members.

4.4 Index measurement and abundance analysis

4.4.1 CN and CH band strengths

Indices quantifying the strength of the UV CN band (Sλ3883) and the G band of CH (CHλ4300), the CaII (H+K) and Fe5270 lines were measured. The same indices as defined in Norris et al. (1981); Worthey (1994), and Lardo et al. (2013) were adopted for this work. The uncertainties related to the index measurements were obtained with the expression derived by Vollmann & Eversberg (2006) as shown in equation (4.1) where $\sigma(\mathrm{W}_\lambda)$ is the error on the line width, $\Delta\lambda$ is the wavelength range measured over, W_λ is the measured width and S/N is the signal-to-noise. The indices, together with other useful information on the target stars, are listed in Tables 4.1 and 4.2. The measurement of the CaII (H+K) and Fe5270 lines were used to help determine cluster membership, as discussed in § 4.3. The typical S/N for the CN and CH bands used for calculations is $\sim$25 and $\sim$40 respectively.

$$\sigma(W_\lambda) = \sqrt{2} \cdot \frac{\Delta\lambda - W_\lambda}{S/N} \tag{4.1}$$

4.4.2 C and N abundances

To obtain a quantitative estimate of the detected enhancements in nitrogen of L1 stars, [C/Fe] and [N/Fe] abundance ratios were derived via spectral synthesis of the CH band at ≃4300 Å and the CN bands at ≃3883 Å, respectively.

The atomic and molecular line lists were taken from the latest Kurucz compilation downloaded from F. Castelli's website[2] both for atomic and molecular transitions. Model atmospheres were calculated with the ATLAS9 code starting from the grid of models available in F. Castelli's website using the appropriate values of [Fe/H], $T_{\rm eff}$, log(g), and $v_{\rm mic}$.

The effective temperature, $T_{\rm eff}$, was calculated using the Alonso et al. (1999) $T_{\rm eff}$-colour calibration. The (V-I) colour was used, adopting E(B-V) =0.06 and [Fe/H] =-1.35 from Mighell et al. (1998) for Lindsay 1 and [Fe/H] = -1.08 from Da Costa & Hatzidimitriou (1998) with E(V-I) = 0.008 from Glatt et al. (2008) for Kron 3. The surface gravity was determined using $T_{\rm eff}$, the distance modulus ((m-M)$_V$=18.8 for Lindsay 1 and $(m-M)_V$=18.9 for Kron 3 from Glatt et al., 2008), bolometric corrections BC(V) from Alonso et al. (1999) and assuming a mass of 0.95 $M_\odot$ from BaSTI isochrones. Each star was assigned a microturbulent velocity of v_t =2.0 km/s.

Model spectra have been computed by means of SYNTHE code developed by Kurucz. Abundances have been derived through a χ^2 minimisation between the observed spectrum and a grid of synthetic spectra calculated at different abundances. Abundances for C and N were determined together in an iterative way, assuming the measured C abundance to derive N from the synthesis of the molecular CN band. The adopted solar abundances are from Asplund et al. (2009).

The sensitivity of the derived [C/Fe] and [N/Fe] abundances to the adopted atmospheric parameters was determined in the same fashion as done in Lardo et al. (2013). Briefly, the abundance analysis was repeated changing only one parameter at each iteration for three stars that are representative of the temperature and gravity range explored. Typically for the temperature δ[C/Fe] / $\delta T_{\rm eff}$ $\simeq$ 0.12 dex and δ[N/Fe] / $\delta T_{\rm eff}$ $\simeq$ 0.15 dex. The errors in abundances are mostly due to uncertainties in gravity and those due to microturbulent velocity are negligible (on the order of 0.05 dex or less). In addition to the stellar parameters and oxygen abundance

[2] http://wwwuser.oats.inaf.it/castelli/linelists.html

errors, an uncertainty exists in the measurement of the individual abundances. This intrinsic error was estimated by means of Monte Carlo simulations by repeating the fitting procedure using a sample of 500 synthetic spectra where Poissonian noise has been injected in order to reproduce the noise conditions observed around the analysed bands. These uncertainties are of the order of $\simeq$0.15 and $\simeq$ 0.25 dex, respectively for C and N. All these sources of error were combined to give the final errors on [C/Fe] and [N/Fe] abundances ($\sim$0.2 and 0.3 dex, respectively).

4.5 Results

In Fig. 4.4 the C and N abundances are plotted against V band magnitude to check for effects of evolutionary mixing. The top panels in each plot show negligible spread in [C/Fe], while the lower panels show spreads of $\sim$ 1 dex and $\sim$ 0.8 dex in [N/Fe] for Lindsay 1 and Kron 3 respectively. The y axes for [C/Fe] and [N/Fe] are of equal width to demonstrate the magnitude of the spread. The red lines are the median abundances for each calculated with all sources for C and the lower group of stars for N abundances. There are no obvious trends of both [C/Fe] and [N/Fe] with luminosity, meaning that the observed spread in [N/Fe] is not due to internal evolution of the stars. Also, N-rich and N-poor stars are observed at the same magnitude, indicating that the observed stars-to-star variation in N must be intrinsic.

Fig. 4.5 shows [C/Fe] against [N/Fe] and the band strengths, CN Sλ3883 and CHλ4300 plotted for sources that were determined to be members of the cluster, with equally sized axes to emphasise the difference in spread. In both cases, the plots show negligible spread in carbon, within the error bars and therefore suggests that the sources all have a similar amount of carbon. Conversely, nitrogen shows a much larger spread that is significant compared to errors. Gold points on the plots indicate enriched stars, while silver are potentially enriched and black are normal composition. These categorisations were made using [N/Fe]. Enriched stars are $> 1\sigma$ away from the median [N/Fe], while potentially enriched stars are $\sim 1\sigma$ away and could belong to either population within errors.

Fig. 4.6 shows the same plots for Kron 3. The same patterns are seen, with nitrogen showing a larger spread than carbon, however this is less pronounced than for Lindsay 1. Defining an intermediate population of potentially enriched stars was not done for Kron 3 due to a much

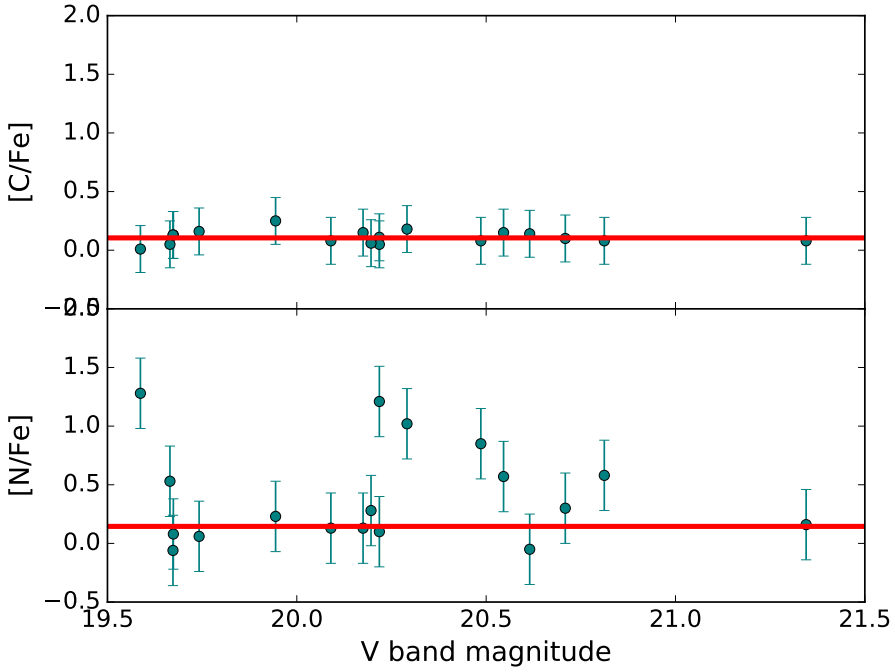

(a) [C/Fe] and [N/Fe] against V band magnitude for Lindsay 1

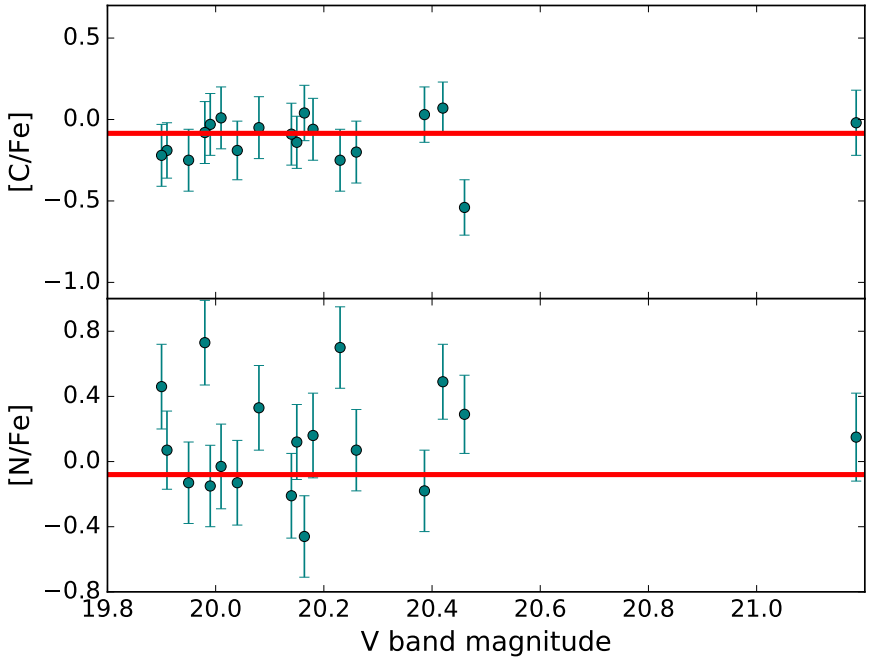

(b) [C/Fe] and [N/Fe] against V band magnitude for Kron 3

Figure 4.4: These two plots show carbon and nitrogen abundances ([C/Fe] and [N/Fe] respectively) for all true cluster members plotted against their apparent V band magnitude for each cluster, with the median value of the main population shown as a red line. [C/Fe] shows negligible spread around the median and nearly all sources are within errors, while [N/Fe] shows an enriched population by up to $\sim$ 1 dex for L1 and $\sim$ 0.8 dex for K3.

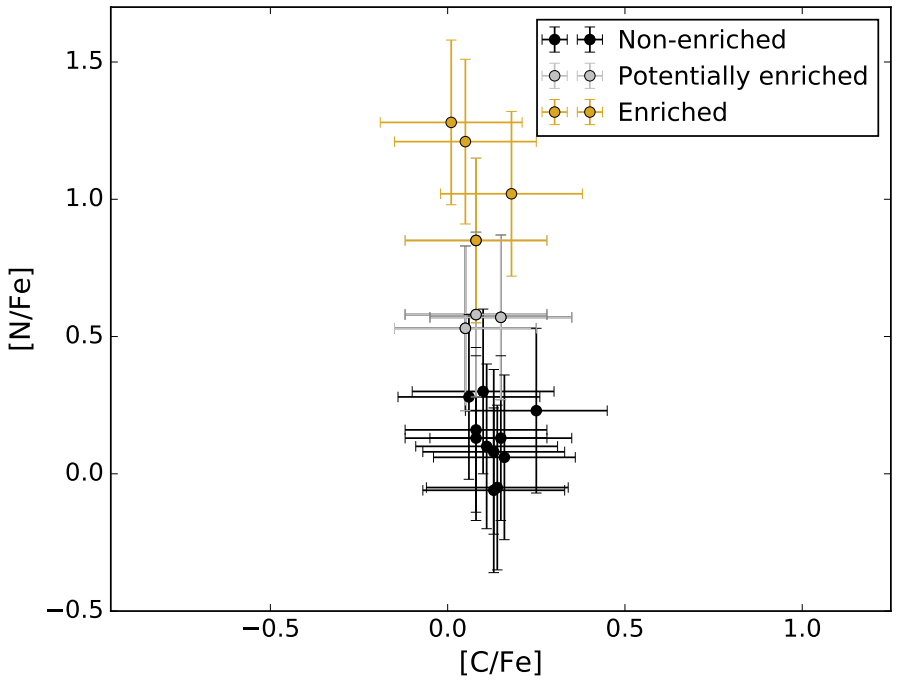

(a) [C/Fe] vs [N/Fe] for Lindsay 1

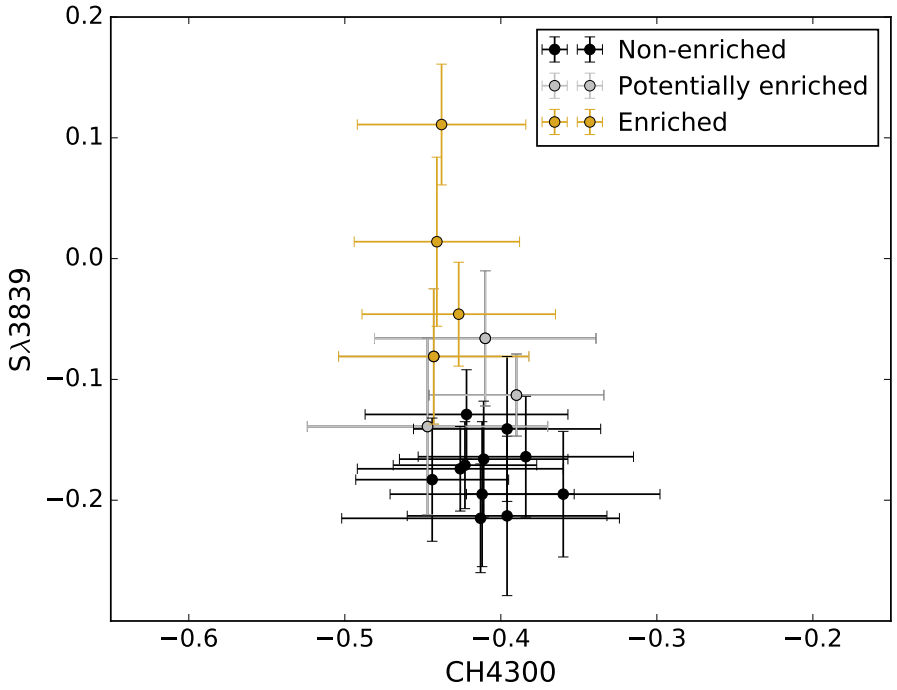

(b) CN Sλ3839 and CHλ4300 band strengths for Lindsay 1

Figure 4.5: The top plot shows carbon abundance plotted against nitrogen abundance for cluster members of Lindsay 1 and the lower plot shows CN Sλ3839 and CHλ4300 band strengths, which also trace nitrogen and carbon respectively. Black points are non-enriched stars, silver points are sources that may be enriched and gold points are nitrogen enriched stars. Enriched sources are chosen based on [N/Fe].

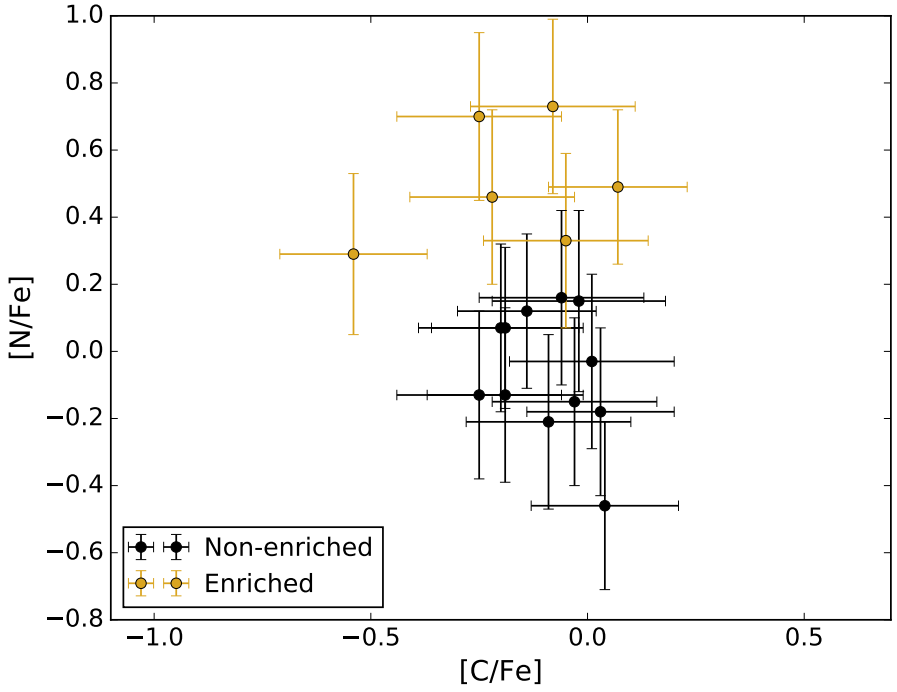

(a) [C/Fe] vs [N/Fe] for Kron 3

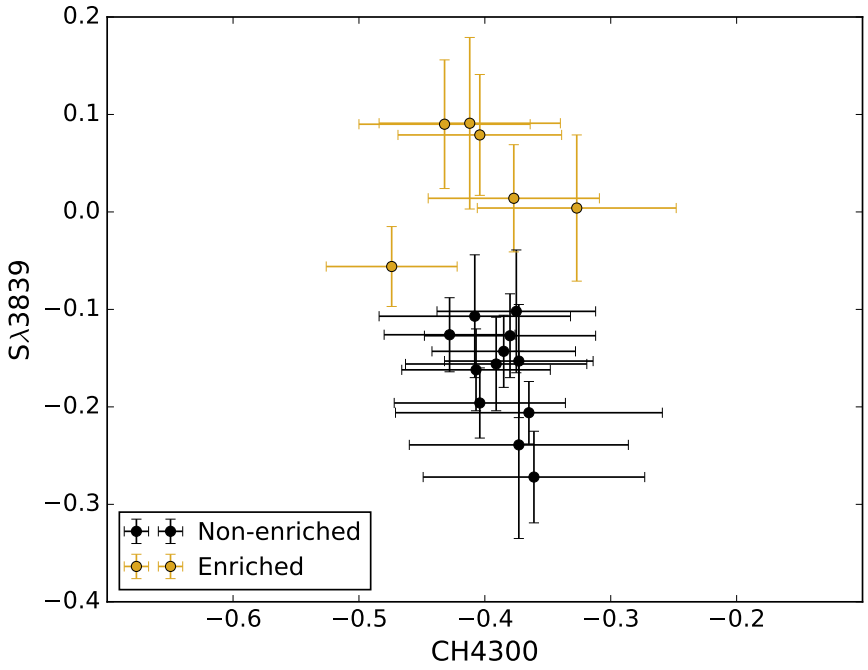

(b) CN Sλ3839 and CHλ4300 band strengths for Kron 3

Figure 4.6: The top plot shows carbon and nitrogen abundances for Kron 3 and the bottom plot shows CN and CH band strengths. Black points are non-enriched stars and gold points are nitrogen enriched stars. Enriched sources are chosen based on [N/Fe].

smaller difference between the medians of the enriched and non-enriched population ($\sim$ half the difference for Lindsay 1) and so the distinction would be less meaningful.

These plots indicate that there are nitrogen rich stars present in the sample of each cluster, and is strong evidence for the presence of MPs like those seen in the ancient GCs in the Milky Way, LMC and Fornax (e.g. Larsen et al., 2014). This can be further illustrated in plotting [N/Fe] against CN Sλ3839, as in Fig. 4.7.

4.6 Discussion and conclusions

Spectroscopy was obtained for 34 targets towards L1 and 35 towards K3, and through thorough membership criteria 17 and 18 stars have been determined to be true members for each cluster respectively. Out of these member stars, potentially 7 show enriched [N/Fe] compared to a fairly constant [C/Fe] in Lindsay 1 and 6 in Kron 3, which is evident in Fig. 4.5 and Fig. 4.6. This is strongly indicative of the presence of MPs in both clusters, two of the youngest clusters to show abundance variations, though not the least massive (NGC 6535 at $10^{3.31}$ $M_{\odot}$, Milone et al., 2017a). Niederhofer et al. (2017b) have also found evidence in support of MPs in L1 using HST photometry. In certain filter combinations the RGB splits into two sequences, in support of these findings using FORS2 spectroscopy. Stars in this study that overlap with their catalogue also lie on the correct RGB branch depending on whether they are N-enriched or not.

Evolutionary mixing can be disregarded as an explanation for elevated N abundances, as the C abundances show no variation. This indicates that abundance estimates for the main N-poor population should be similar to those of the stars' original gas cloud (apart from some small evolutionary effects due to internal stellar mixing). Additionally, as the sources are lower RGB stars, they are fainter than the bump in the LF ($V_{BUMP} = 19.30 \pm 0.05, 19.38 \pm 0.04$; Alcaino et al., 2003; Alves & Sarajedini, 1999, for Lindsay 1 and Kron 3, respectively) meaning that any evolutionary mixing should have had minimal impact on the C and N abundances (e.g. Gratton et al., 2000).

N enriched stars were also visually examined for Lindsay 1 using HST ACS F555W band images (proposal ID 10396, P.I Gallagher) taken from the Hubble Legacy Archive (HLA). Though the ACS image was smaller than the coverage with FORS2, 3 of the 6 enriched stars were within ACS field of view, including 0709, the most enriched star. All of these targets

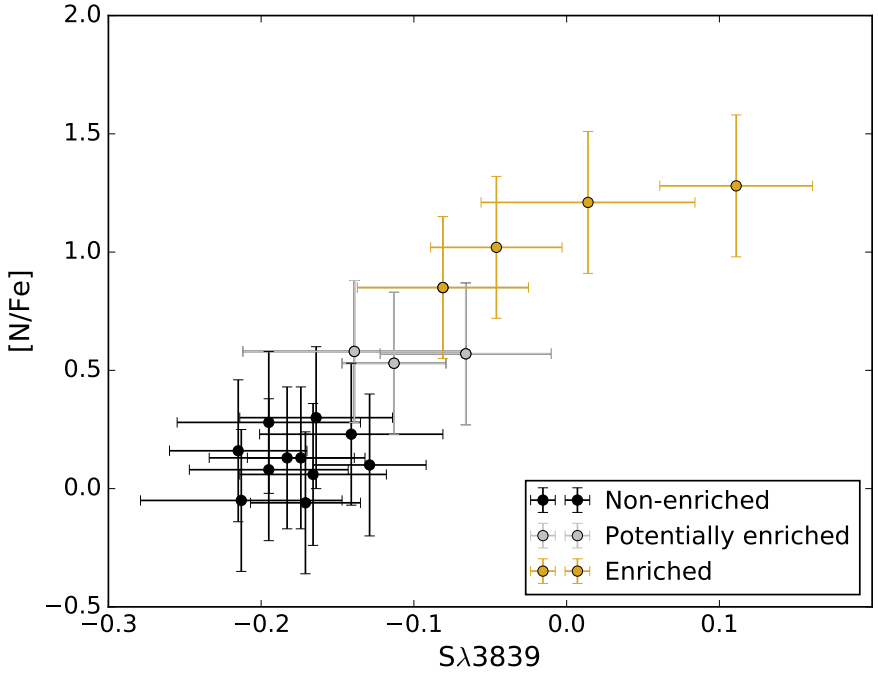

(a) [N/Fe] vs CN SλSλ3839 for Lindsay 1

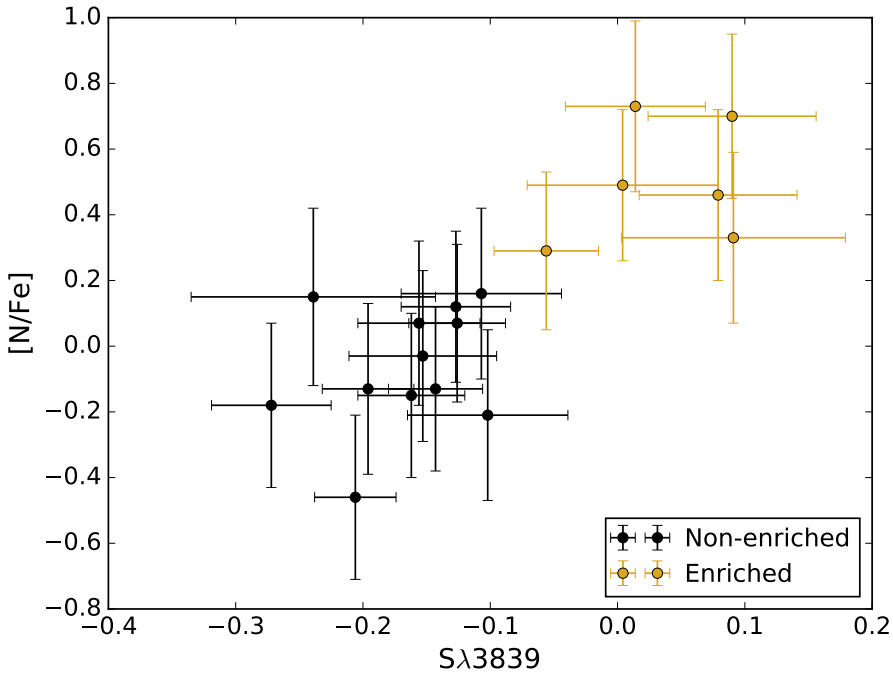

(b) [N/Fe] vs CN SλSλ3839 for Kron 3

Figure 4.7: Nitrogen abundance against CN band strength for both clusters. These plots more clearly illustrate the spread in nitrogen.

appeared to be reliable sources, isolated single stars without contamination from nearby objects. Based on evidence for a lack of evolutionary mixing, the quality of the sources and the stringent membership tests, the spread in [N/Fe] is very likely to be real and indicates that this method of studying MPs is valid.

It is important to note, however that this study is only sampling the outer regions of the clusters, as the centre of the cluster is too crowded to obtain spectra of single stars with the slits on FORS2. Therefore, the observed ratios (N-enriched/N-normal) cannot be used to derive $F_{\rm enriched}$. This may have affected previous studies of young and intermediate age LMC clusters (e.g. Mucciarelli et al., 2008, 2014b), hence, HST imaging of these clusters in filters sensitive to MPs should also be undertaken. In order to investigate other light elements, time-consuming, high resolution spectroscopy is necessary, however, this method can be regarded as a promising way to identify and study MPs on shorter timescales.

The sample of intermediate age clusters found with multiple populations is continuing to grow, with evidence also found in HST data of NGC 416 and NGC 339 (Niederhofer et al., 2017b). Therefore age appears to be a very important factor in the presence of MPs, especially as clusters of comparable mass and younger than $\approx$ 2 Gyr do not show MPs. Constraining the age where MPs are present, and therefore potentially discovering the exact mechanism causing their existence is an important task in the cluster field today. So far, all massive clusters in the range 6-8 Gyr show evidence for MPs indicating that this mechanism must operate until a redshift of at least 0.75, much later than the peak of globular cluster formation at a reshift of $\approx$ 3. This means the mechanism could still be working to create multiple populations in young massive clusters, so they potentially can be considered analogues to GCs and used to constrain GC formation theories.

Massive clusters at $\approx$ 1-2 Gyr generally display the peculiarity in their CMDs of an extended main sequence turn-off. This was originally thought to be due to age spreads and MPs, however this was shown to be unlikely in a number of clusters in the LMC (Niederhofer et al., 2015b) and is instead potentially due to rotation (e.g. Brandt & Huang, 2015; Niederhofer et al., 2015a; Bastian & de Mink, 2009). Recently, the 1.5 Gyr cluster in the SMC, NGC 419, has been found to show no evidence for MPs (Martocchia et al., 2017), indicating that the mechanism begins operating after this age, or that the signal for MPs at these younger ages is weaker and undetectible. The sample size of clusters with ages between 1 and 6 Gyr is currently small and

more targets need to be studied for MPs to further constrain their onset.

Stellar properties for Lindsay 1

ID	Chip	RA (Degrees, J2000)	Dec (Degrees, J2000)	V (Mag)	I (Mag)	Teff (K)
0098	1	0.989304	-73.502296	20.17 ± 0.01	19.38 ± 0.06	5448±97
0229	1	0.984237	-73.499611	19.74 ± 0.01	18.91 ± 0.06	5327±92
0384	1	1.003554	-73.496887	20.81 ± 0.02	20.05 ± 0.06	5544±101
0511	1	1.052596	-73.494812	20.29 ± 0.02	19.51 ± 0.06	5495±99
0709	1	0.907271	-73.491982	19.59 ± 0.01	18.76 ± 0.06	5348±93
0954	1	0.936742	-73.489082	20.49 ± 0.02	19.70 ± 0.06	5480±98
1203	1	0.822492	-73.486412	20.22 ± 0.01	19.40 ± 0.06	5372±94
1451	1	1.060442	-73.483788	21.34 ± 0.01	20.61 ± 0.06	5626±104
1831	1	0.841108	-73.480164	20.55 ± 0.01	19.77 ± 0.06	5518±100
2230	1	1.057479	-73.476318	20.61 ± 0.01	19.84 ± 0.06	5521±100
2564[b]	1	1.005662	-73.473251	20.35 ± 0.01	19.56 ± 0.06	5477±98
2789	1	1.007921	-73.471268	19.67 ± 0.01	18.84 ± 0.06	5336±92
3041	1	0.930142	-73.469093	20.22 ± 0.01	19.42 ± 0.06	5442±97
3393[b]	1	0.843433	-73.465889	20.50 ± 0.01	19.76 ± 0.06	5622±104
3712	1	0.887554	-73.463203	20.71 ± 0.01	19.91 ± 0.06	5421±96
4024	1	0.909817	-73.460358	19.94 ± 0.01	19.16 ± 0.06	5473±98
4478	1	0.886458	-73.456039	20.20 ± 0.01	19.39 ± 0.06	5417±95
4840	1	0.876167	-73.452339	19.67 ± 0.01	18.83 ± 0.06	5316±91
5059[bd]	1	0.899946	-73.449783	20.15 ± 0.01	19.39 ± 0.06	5547±101
5230	1	0.971921	-73.447319	20.09 ± 0.02	19.30 ± 0.07	5461±97
5376[b]	1	0.812771	-73.444771	20.10 ± 0.01	19.29 ± 0.06	5408±95
5499[b]	1	1.019025	-73.442169	19.79 ± 0.01	18.99 ± 0.06	5427±96
5589	1	0.992879	-73.440163	19.67 ± 0.01	18.88 ± 0.06	5451±97
0008[ab]	2	0.890948	-73.554520	20.05 ± 0.02	18.29 ± 0.02	3767±23
0048[bd]	2	1.069129	-73.542152	20.07 ± 0.03	19.19 ± 0.03	5190±86
0074[d]	2	0.882093	-73.537750	20.31 ± 0.03	19.54 ± 0.03	5524±100
0101[abd]	2	0.998957	-73.531647	20.69 ± 0.03	18.55 ± 0.02	3590±6
0124[abcd]	2	0.953859	-73.526321	21.19 ± 0.04	20.58 ± 0.05	6098±124
0140[acd]	2	1.008711	-73.523109	21.60 ± 0.06	21.17 ± 0.08	6873±158
0158[d]	2	0.936475	-73.520729	19.40 ± 0.02	18.60 ± 0.02	5455±97
0178[d]	2	0.923483	-73.518082	19.64 ± 0.02	18.83 ± 0.02	5402±95
0203[acd]	2	1.026435	-73.514931	20.86 ± 0.03	20.57 ± 0.07	7682±195
0225[d]	2	0.976222	-73.511978	19.73 ± 0.02	18.83 ± 0.02	5152±85
0249[d]	2	0.945876	-73.509010	20.26 ± 0.03	19.41 ± 0.02	5266±89

Lindsay 1 stellar properties continued...

ID	log(g)	[C/Fe] (Dex)	[N/Fe] (Dex)	Sλ3883	CHλ4300
0098	2.80± 0.04	0.15± 0.20	0.13± 0.30	-0.18± 0.05	-0.44± 0.05
0229	2.50± 0.04	0.16± 0.20	0.06± 0.30	-0.17± 0.05	-0.41± 0.05
0384	3.00± 0.04	0.08± 0.20	0.58± 0.30	-0.14± 0.07	-0.45± 0.08
0511	2.80± 0.04	0.18± 0.20	1.02± 0.30	-0.05± 0.04	-0.43± 0.06
0709	2.50± 0.04	0.01± 0.20	1.28± 0.30	0.11± 0.05	-0.44± 0.05
0954	2.90± 0.04	0.08± 0.20	0.85± 0.30	-0.08± 0.06	-0.44± 0.06
1203	2.70± 0.04	0.11± 0.20	0.10± 0.30	-0.13± 0.04	-0.42± 0.06
1451	3.30± 0.04	0.08± 0.20	0.16± 0.30	-0.22± 0.05	-0.41± 0.09
1831	2.90± 0.04	0.15± 0.20	0.57± 0.30	-0.07± 0.06	-0.41± 0.07
2230	3.00± 0.04	0.14± 0.20	-0.05± 0.30	-0.21± 0.07	-0.40± 0.06
2564[b]	2.80± 0.04	0.19± 0.20	0.13± 0.30	-0.18± 0.05	-0.40± 0.08
2789	2.50± 0.04	0.13± 0.20	0.08± 0.30	-0.19± 0.05	-0.36± 0.06
3041	2.80± 0.04	0.05± 0.20	1.21± 0.30	0.01± 0.07	-0.44± 0.05
3393[b]	2.90± 0.04	0.10± 0.20	0.44± 0.30	-0.17± 0.04	-0.45± 0.05
3712	3.00± 0.04	0.10± 0.20	0.30± 0.30	-0.16± 0.05	-0.38± 0.07
4024	2.70± 0.04	0.25± 0.20	0.23± 0.30	-0.14± 0.06	-0.40± 0.06
4478	2.80± 0.04	0.06± 0.20	0.28± 0.30	-0.19± 0.06	-0.41± 0.06
4840	2.50± 0.04	0.05± 0.20	0.53± 0.30	-0.11± 0.03	-0.39± 0.06
5059[bd]	2.80± 0.04	0.63± 0.20	0.81± 0.30	-0.02± 0.05	-0.38± 0.08
5230	2.70± 0.04	0.08± 0.20	0.13± 0.30	-0.17± 0.04	-0.43± 0.07
5376[b]	2.70± 0.04	0.09± 0.20	0.09± 0.30	-0.14± 0.03	-0.42± 0.09
5499[b]	2.60± 0.04	0.07± 0.20	0.04± 0.30	-0.17± 0.06	-0.44± 0.07
5589	2.60± 0.04	0.13± 0.20	-0.06± 0.30	-0.17± 0.04	-0.42± 0.05
0008[ab]	1.50± 0.05	-	-	-0.18± 0.12	-0.49± 0.12
0048[bd]	2.60± 0.04	-0.04± 0.20	0.03± 0.30	-0.11± 0.05	-0.40± 0.07
0074[d]	2.80± 0.04	0.23± 0.20	-0.31± 0.30	-0.14± 0.05	-0.44± 0.07
0101[abd]	1.20± 0.03	-	-	-0.04± 0.13	-0.51± 0.13
0124[abcd]	3.40± 0.04	0.04± 0.20	9.99± 0.30	-0.28± 0.06	-0.51± 0.06
0140[acd]	3.80± 0.04	-	-	-0.29± 0.05	-0.51± 0.08
0158[d]	2.40± 0.04	-0.40± 0.20	0.62± 0.30	-0.16± 0.03	-0.52± 0.05
0178[d]	2.50± 0.04	-0.32± 0.20	0.35± 0.30	-0.15± 0.04	-0.48± 0.04
0203[acd]	3.60± 0.04	-	-	-0.30± 0.03	-0.50± 0.04
0225[d]	2.50± 0.04	-0.13± 0.20	0.16± 0.30	-0.09± 0.04	-0.38± 0.06
0249[d]	2.70± 0.04	-0.04± 0.20	0.20± 0.30	-0.16± 0.04	-0.42± 0.06

Lindsay 1 stellar properties continued...

ID	CaII (H+K)	Fe5270	RV (km/s)
0098	25.51± 7.45	-0.18± 0.02	146.3
0229	27.11± 5.02	-0.17± 0.02	140.0
0384	22.60± 8.37	-0.18± 0.02	158.1
0511	26.23± 8.38	-0.17± 0.02	144.5
0709	27.16± 5.52	-0.17± 0.02	149.8
0954	21.74± 7.26	-0.18± 0.02	150.5
1203	27.28± 7.37	-	157.3
1451	20.49± 12.38	-0.17± 0.02	132.3
1831	24.92± 5.74	-0.17± 0.02	155.7
2230	23.82± 7.71	-0.19± 0.02	139.6
2564[b]	23.25± 9.49	-0.18± 0.02	102.8
2789	25.62± 6.65	-0.17± 0.02	142.9
3041	25.63± 7.10	-0.18± 0.02	140.9
3393[b]	22.74± 7.35	-0.18± 0.02	167.6
3712	21.19± 7.88	-0.16± 0.02	135.0
4024	25.26± 7.53	-0.19± 0.02	157.0
4478	25.89± 7.43	-0.19± 0.02	141.1
4840	27.10± 6.96	-0.16± 0.02	160.9
5059[bd]	30.02± 8.00	-0.15± 0.02	-26.3
5230	25.05± 6.99	-0.17± 0.02	145.2
5376[b]	23.96± 7.49	-	176.4
5499[b]	26.46± 6.73	-0.18± 0.02	102.7
5589	23.01± 5.03	-0.19± 0.02	144.7
0008[ab]	21.03± 17.69	-0.18± 0.02	-22.0
0048[bd]	24.41± 6.52	-0.23± 0.02	113.5
0074[d]	26.15± 6.92	-0.23± 0.02	127.8
0101[abd]	15.37± 19.16	-0.15± 0.02	24.3
0124[abcd]	8.50± 10.49	-0.24± 0.02	89.8
0140[acd]	-4.77± 9.80	-0.24± 0.02	136.5
0158[d]	17.32± 6.12	-0.23± 0.02	141.8
0178[d]	16.22± 7.21	-0.23± 0.02	138.8
0203[acd]	-6.91± 5.41	-0.21± 0.02	144.9
0225[d]	22.89± 7.12	-0.22± 0.02	132.1
0249[d]	21.49± 7.80	-0.21± 0.02	118.8

Table 4.1: Table of stellar properties for all 34 stars in L1. Stars that were found to be non-members using the criteria specified in § 4.3 are indicated with [a], [b], [c] or [d] depending on whether they were removed due to the CMD, their radial velocity, CaII (H+K) or Fe5270 band strengths respectively.

Stellar properties for Kron 3

ID	Chip	RA (Degrees)	Dec (Degrees)	V (mag)	I (mag)	Teff (K)
0225	1	6.13550	-72.82457	19.99 ± 0.01	19.03 ± 0.01	4820 ± 40
0514[a]	1	6.26053	-72.82125	20.09 ± 0.01	19.11 ± 0.01	4780 ± 39
0825[b]	1	6.21331	-72.81841	20.57 ± 0.01	19.68 ± 0.01	4997 ± 44
1201[a]	1	6.19462	-72.81501	20.83 ± 0.01	19.93 ± 0.02	4972 ± 43
1517	1	6.29201	-72.81255	20.42 ± 0.01	19.49 ± 0.01	4914 ± 42
1903	1	6.26787	-72.80966	20.46 ± 0.01	19.56 ± 0.01	4960 ± 43
2349	1	6.11590	-72.80645	20.15 ± 0.01	19.17 ± 0.01	4795 ± 39
2680	1	6.15693	-72.80423	20.14 ± 0.01	19.17 ± 0.02	4800 ± 39
3130	1	6.23144	-72.80103	19.91 ± 0.03	18.97 ± 0.04	4897 ± 41
3546	1	6.21991	-72.79807	20.08 ± 0.02	19.08 ± 0.02	4753 ± 38
3910	1	6.21948	-72.79566	19.98 ± 0.02	19.01 ± 0.03	4829 ± 40
4281[a]	1	6.23649	-72.79307	20.66 ± 0.02	19.67 ± 0.02	4764 ± 38
4542[a]	1	6.27232	-72.79085	20.11 ± 0.01	19.18 ± 0.01	4885 ± 41
4873[b]	1	6.27068	-72.78851	20.92 ± 0.01	19.98 ± 0.01	4885 ± 41
5174	1	6.24555	-72.78618	19.95 ± 0.03	18.97 ± 0.04	4788 ± 39
5697[a]	1	6.22082	-72.78246	20.28 ± 0.02	19.35 ± 0.02	4904 ± 41
6130	1	6.17525	-72.77927	20.18 ± 0.01	19.22 ± 0.02	4825 ± 40
6463	1	6.24893	-72.77658	20.26 ± 0.01	19.28 ± 0.01	4782 ± 39
6862	1	6.20662	-72.77340	19.90 ± 0.01	18.91 ± 0.02	4751 ± 38
7293	1	6.23680	-72.76972	20.01 ± 0.01	18.98 ± 0.01	4689 ± 36
7604	1	6.23182	-72.76646	20.23 ± 0.01	19.26 ± 0.01	4813 ± 39
7963	1	6.30215	-72.76238	20.04 ± 0.01	19.10 ± 0.01	4869 ± 41
0651[a]	2	6.22769	-72.84573	19.91 ± 0.02	18.90 ± 0.02	4723 ± 33
0599	2	6.22590	-72.84797	20.39 ± 0.03	19.49 ± 0.03	5000 ± 39
0715[a]	2	6.24757	-72.84168	21.12 ± 0.04	20.16 ± 0.04	4825 ± 36
0842[a]	2	6.24130	-72.83541	20.47 ± 0.03	19.56 ± 0.02	4965 ± 38
0419	2	6.29848	-72.85624	20.16 ± 0.03	19.10 ± 0.02	4607 ± 31
0329[a]	2	6.06679	-72.86083	20.76 ± 0.03	19.90 ± 0.03	5082 ± 41
0285[a]	2	6.26020	-72.86331	20.76 ± 0.04	19.77 ± 0.03	4765 ± 34
0220	2	6.27184	-72.86605	21.18 ± 0.04	20.31 ± 0.04	5041 ± 40
0176[b]	2	6.29390	-72.86897	20.58 ± 0.03	19.64 ± 0.03	4890 ± 37
0129[c]	2	6.11281	-72.87157	20.95 ± 0.05	20.02 ± 0.03	4900 ± 37
0791[a]	2	6.20798	-72.83820	19.72 ± 0.02	18.77 ± 0.02	4874 ± 37
0286[a]	2	6.14360	-72.87489	19.57 ± 0.01	18.70 ± 0.02	5046 ± 40
0905[c]	2	6.25722	-72.83270	20.74 ± 0.03	19.77 ± 0.02	4821 ± 35

Kron 3 stellar properties continued...

ID	log(g)	[C/Fe] (dex)	[N/Fe] (dex)	Sλ3883	CHλ4300
0225	2.48 ± 0.02	-0.03 ± 0.19	-0.15 ± 0.25	-0.162 ± 0.042	-0.407 ± 0.059
0514[a]	2.49 ± 0.02	-0.06 ± 0.19	-0.04 ± 0.26	-0.105 ± 0.047	-0.417 ± 0.079
0825[b]	2.79 ± 0.02	-0.83 ± 0.18	- ± -	-0.171 ± 0.032	-0.483 ± 0.048
1201[a]	2.89 ± 0.02	-0.10 ± 0.19	-0.03 ± 0.26	-0.187 ± 0.071	-0.424 ± 0.071
1517	2.69 ± 0.02	0.07 ± 0.16	0.49 ± 0.23	0.004 ± 0.075	-0.327 ± 0.079
1903	2.73 ± 0.02	-0.54 ± 0.17	0.29 ± 0.24	-0.056 ± 0.041	-0.474 ± 0.052
2349	2.52 ± 0.02	-0.14 ± 0.16	0.12 ± 0.23	-0.127 ± 0.043	-0.380 ± 0.068
2680	2.52 ± 0.02	-0.09 ± 0.19	-0.21 ± 0.26	-0.102 ± 0.063	-0.375 ± 0.063
3130	2.48 ± 0.02	-0.19 ± 0.17	0.07 ± 0.24	-0.126 ± 0.038	-0.428 ± 0.052
3546	2.48 ± 0.02	-0.05 ± 0.19	0.33 ± 0.26	0.091 ± 0.088	-0.412 ± 0.072
3910	2.47 ± 0.02	-0.08 ± 0.19	0.73 ± 0.26	0.014 ± 0.055	-0.377 ± 0.068
4281[a]	2.71 ± 0.02	0.13 ± 0.17	0.56 ± 0.24	0.006 ± 0.073	-0.405 ± 0.080
4542[a]	2.56 ± 0.02	-0.37 ± 0.16	0.45 ± 0.23	0.060 ± 0.057	-0.405 ± 0.062
4873[b]	2.88 ± 0.02	-0.20 ± 0.19	0.46 ± 0.26	-0.063 ± 0.059	-0.397 ± 0.081
5174	2.44 ± 0.02	-0.25 ± 0.19	-0.13 ± 0.25	-0.143 ± 0.037	-0.385 ± 0.057
5697[a]	2.63 ± 0.02	0.03 ± 0.17	-0.05 ± 0.24	-0.229 ± 0.068	-0.426 ± 0.070
6130	2.55 ± 0.02	-0.06 ± 0.19	0.16 ± 0.26	-0.107 ± 0.063	-0.408 ± 0.076
6463	2.56 ± 0.02	-0.20 ± 0.19	0.07 ± 0.25	-0.156 ± 0.048	-0.391 ± 0.072
6862	2.40 ± 0.02	-0.22 ± 0.19	0.46 ± 0.26	0.079 ± 0.062	-0.404 ± 0.065
7293	2.41 ± 0.02	0.01 ± 0.19	-0.03 ± 0.26	-0.153 ± 0.058	-0.373 ± 0.059
7604	2.57 ± 0.02	-0.25 ± 0.19	0.70 ± 0.25	0.090 ± 0.066	-0.432 ± 0.068
7963	2.52 ± 0.02	-0.19 ± 0.18	-0.13 ± 0.26	-0.196 ± 0.036	-0.404 ± 0.068
0651[a]	2.33 ± 0.02	0.12 ± 0.17	-0.31 ± 0.25	-0.136 ± 0.040	-0.385 ± 0.085
0599	2.66 ± 0.02	0.03 ± 0.17	-0.18 ± 0.25	-0.272 ± 0.047	-0.361 ± 0.088
0715[a]	2.86 ± 0.02	0.01 ± 0.19	-0.32 ± 0.26	-0.142 ± 0.076	-0.404 ± 0.126
0842[a]	2.67 ± 0.02	-0.06 ± 0.18	-0.15 ± 0.25	-0.250 ± 0.042	-0.422 ± 0.063
0419	2.36 ± 0.02	0.04 ± 0.17	-0.46 ± 0.25	-0.206 ± 0.032	-0.365 ± 0.106
0329[a]	2.84 ± 0.02	-0.02 ± 0.20	0.09 ± 0.27	-0.186 ± 0.058	-0.362 ± 0.100
0285[a]	2.69 ± 0.02	-0.05 ± 0.19	-0.12 ± 0.26	-0.130 ± 0.086	-0.411 ± 0.085
0220	2.99 ± 0.02	-0.02 ± 0.20	0.15 ± 0.27	-0.239 ± 0.096	-0.373 ± 0.087
0176[b]	2.68 ± 0.02	-0.14 ± 0.18	-	-0.251 ± 0.042	-0.433 ± 0.050
0129[c]	2.83 ± 0.02	-0.02 ± 0.20	-0.45 ± 0.27	-0.219 ± 0.098	-0.341 ± 0.128
0791[a]	2.33 ± 0.02	-0.44 ± 0.17	0.11 ± 0.24	-0.224 ± 0.034	-0.486 ± 0.057
0286[a]	2.35 ± 0.02	-0.41 ± 0.17	-0.03 ± 0.24	-0.227 ± 0.029	-0.436 ± 0.065
0905[c]	2.71 ± 0.02	0.08 ± 0.19	-0.12 ± 0.26	-0.215 ± 0.040	-0.373 ± 0.078

Kron 3 stellar properties continued...

ID	CaII (H+K)	Fe5270	RV (km/s)
0225	25.773 ± 6.265	-0.165 ± 0.030	123.0
0514[a]	28.352 ± 7.689	-0.168 ± 0.030	174.8
0825[b]	6.031 ± 7.529	-0.210 ± 0.030	112.0
1201[a]	21.375 ± 10.399	-0.201 ± 0.030	94.3
1517	20.342 ± 9.493	-0.191 ± 0.030	142.1
1903	20.352 ± 9.258	-0.166 ± 0.030	141.9
2349	25.076 ± 8.199	-0.176 ± 0.030	140.3
2680	22.207 ± 9.929	-0.176 ± 0.030	141.6
3130	17.637 ± 5.127	-0.191 ± 0.030	131.3
3546	21.487 ± 6.405	-0.153 ± 0.030	130.2
3910	23.889 ± 6.953	-0.176 ± 0.030	145.4
4281[a]	25.892 ± 9.632	-0.179 ± 0.030	94.8
4542[a]	19.759 ± 6.964	-0.193 ± 0.030	176.8
4873[b]	12.297 ± 12.465	-0.187 ± 0.030	138.4
5174	22.241 ± 5.330	-0.174 ± 0.030	141.2
5697[a]	15.468 ± 9.046	-0.212 ± 0.030	213.6
6130	22.867 ± 8.077	-0.194 ± 0.030	151.3
6463	20.158 ± 8.311	-0.173 ± 0.030	148.2
6862	24.803 ± 8.432	-0.171 ± 0.030	159.9
7293	27.081 ± 9.327	-0.177 ± 0.030	141.2
7604	22.376 ± 7.319	-0.195 ± 0.030	166.7
7963	20.208 ± 7.894	-0.206 ± 0.030	148.3
0651[a]	21.459 ± 9.536	-0.139 ± 0.017	90.6
0599	23.915 ± 7.979	-0.172 ± 0.017	115.3
0715[a]	19.764 ± 11.581	-0.182 ± 0.017	95.5
0842[a]	17.012 ± 6.814	-0.163 ± 0.017	95.0
0419	17.181 ± 11.652	-0.153 ± 0.017	122.1
0329[a]	20.907 ± 10.513	-	89.5
0285[a]	21.396 ± 11.161	-0.175 ± 0.017	106.1
0220	22.965 ± 15.101	-0.173 ± 0.017	145.8
0176[b]	10.645 ± 8.522	-0.186 ± 0.017	130.9
0129[c]	22.947 ± 14.951	-0.107 ± 0.017	118.9
0791[a]	15.715 ± 5.787	-0.158 ± 0.017	107.4
0286[a]	18.192 ± 6.340	-0.173 ± 0.017	217.5
0905[c]	20.094 ± 10.069	-0.087 ± 0.017	152.2

Table 4.2: Table of stellar properties for all 35 stars in K3. Stars that were found to be non-members using the criteria specified in § 4.3 are indicated with [a], [b] or [c] depending on whether they were removed due to their radial velocity, CaII (H+K) or Fe5270 band strengths respectively.

Chapter 5

Conclusions

The three projects composing this thesis have all contributed to the current understanding of the formation and evolution of massive clusters in different age regimes and environments. The study into NGC 1566 explored the properties of the cluster population of the galaxy and looked not only at the properties of the clusters themselves but also at their relationship with their host galaxy. Investigating the Hα morphology of young massive clusters in M 83 revealed information about early cluster evolution and spectroscopy of RGB stars in Lindsay 1 and Kron 3 showed that multiple populations were not exclusive to ancient globular clusters. The conclusions that can be taken from this body of work are as follows:

- **Clusters are gas free by 2-3 Myr -** The Hα morphology of YMCs in M 83 indicate agreement with other clusters in the Milky Way or nearby galaxies such as R136 or the Arches, where they are gas free by $\approx$ 2-3 Myr. The clusters are very efficient at removing gas on such short timescales, and while the amount of gas that should be lost is potentially reduced due to a higher SFE during the formation of bound clusters, the mechanisms responsible are still highly efficient. Simulations by Dale et al. (2014) indicate that gas could be removed entirely by processes other than supernovae, such as radiation pressure and stellar feedback from massive stars. Several clusters were coincident with Wolf-Rayet features, however, it is not conclusive that they are associated with the clusters themselves. The extent of the role played by each potential contributor to gas loss (gas exhaustion, massive stellar winds and radiation pressure) is still uncertain.

- **Hα can give inaccurate age estimates at young ages in SED fitting -** Age and mass fitting techniques for young clusters can encounter a variety of issues leading to inaccuracies in estimates, particularly when using Hα to break the age-extinction degeneracy. The morphology of ionised gas surrounding clusters in M 83 indicates that Hα magnitudes may be overestimated in models used for the SED fitting process leading to more advanced ages being assigned to younger clusters. This is due to the lack of gas within the photometric aperture because of the efficiency of the clusters' in evolving to a gas free state, leading to a lower Hα magnitude than expected. Fits can be tailored to specific clusters based on their Hα morphology, though this is difficult to achieve with large samples of clusters due to the necessary visual inspection of each cluster. Additionally, Hα is associated with line emission rather than the actual stellar component of the clusters, so may not be the optimum tool in age-dating young clusters. An alternative to Hα that was used in the fitting for NGC 1566 clusters is UV photometry. Knowledge of UV SED models can also disentangle the degeneracy and is directly related to the young stars in the clusters and is unlikely to be affected by emission from nearby sources.

- **Cluster disruption in NGC 1566 is environmentally and mass dependent -** NGC 1566 shows strong evidence in support of a theory of cluster disruption that is environmentally and mass dependent, in agreement with other studies such as those of M 83 (e.g. Bastian et al., 2012). The average timescale for disruption of a 10^4 $M_\odot$ cluster is twice as long in the outermost radial bin than the inner two bins. This indicates that clusters potentially survive twice as long in the less active outer regions of the galaxy, alluding to an environmental dependence. The shape of the age distribution supports a mass-dependent disruption mechanism as modelled in Lamers (2009) and displays a flat section from 10-100 Myr. This is indicative of a low rate of disruption in the galaxy, in between that of M 83 with high disruption and M 31 with lower disruption. An age variation between bins is supported by the radial colour-colour plots that indicate a difference in U-B colour that is redder with increasing bins. This suggests younger clusters reside towards the centre of NGC 1566, as older clusters have been destroyed.

- **NGC 1566 potentially has a radial dependence in mass and luminosity and is best fit with a Schechter mass function -** Radially, NGC 1566 shows a slight steepening in mass function, though this is within errors. If real, this suggests more massive clusters form preferentially towards the centre of the galaxy. A downturn is observed in all bins. The

luminosity functions in UV, U, B V and I bands show a slight increase in the steepness of the power law slope fit from inner to outer bins, though within errors. The largest in these differences was found in bluer bands. If this variation is real, it could indicate a decrease in the number of young clusters across successive radial bins and potentially that formation of massive clusters is concentrated towards the galaxy centre. Redder bands display a steeper fits than bluer bands across all bins, which is expected alongside a truncated mass function as clusters fade more rapidly in bluer bands so clusters of the same mass but varying ages are spread out in luminosity space. The luminosity function was modelled using an underlying Schechter mass function and measurements of the power law fits matched well with the observed data, in support of a mass distribution best fit with a Schechter function.

- **NGC 1566 shows that Γ depends more strongly on $\Sigma_{\rm SFR}$ than SFR -** Calculations of cluster formation efficiency (Γ) indicate that NGC 1566 is forming less stars in clusters than would be expected from the SFR alone. This could be related to the gas density across the galaxy. A lower $\Sigma_{\rm SFR}$ indicates a low density of cold gas and potentially a lower SFE because of this leading to less bound clusters. It also indicates SFR does not correlate with Γ as strongly as $\Sigma_{\rm SFR}$ does.

- **Intermediate age massive clusters display evidence for multiple populations -** Chemical analysis of CN and CH bands in Lindsay 1 and Kron 3 shows evidence for the presence of a N-enriched sub-population in both clusters. This indicates that the multiple population phenomenon is not limited to ancient GCs but extends to clusters formed much more recently than the peak of GC formation at z $\approx$ 3. This places strong constraints on GC formation theories and removes one doubt surrounding YMCs as GC analogues.

5.1 Final comments

It is thought that there is a common formation mechanism in operation between clusters of varying masses. A recent question has been whether GCs also fall into this category, as the discovery of multiple populations has suggested they follow their own formation process. Previously, YMCs have been used to constrain the current formation theories for multiple populations, all of which fall short of fully describing observations of GCs. However an issue with

this was the uncertainty as to whether YMCs could truly be young GCs. The biggest question raised was the lack of MPs found in YMCs, however the work presented in this thesis about intermediate age clusters suggests that this is no longer one of the issues in comparing YMCs to GCs.

The intermediate age massive cluster Lindsay 1 at 8 Gyr was the first non-GC to show evidence for multiple populations, as described in this work. Now further evidence has reduced this age limit to 2 Gyr (Martocchia et al., in prep), indicating that whatever the mechanism responsible, it must operate until at least a redshift of ≈ 0.17, which is far removed from the peak of GC formation at a redshift of 3. The ability to reliably use YMCs to constrain GC formation is invaluable for advancing current theories.

The work on M 83 also ties into these current open questions about GCs. The question still remains whether multiple populations are produced by multiple epochs of star formation in the cluster. Though there is already significant evidence to suggest this is not the case, as described in Chapter 1, providing further constraint on current theories helps to move toward a consistent working model and solve the question of multiple populations. The Hα morphology of clusters in M 83 indicates that clusters should be gas free by 2-3 Myr, which is supported by other more massive clusters such as cluster 23 in ESO 338-IG04 with a mass $\approx 10^7$ M$_\odot$. This places severe constraints on the age spreads that would be feasible. Currently, the age spreads required for multiple population formation scenarios are much larger than 2-3 Myr, meaning the cluster would have to accrete approximately its own mass in pristine gas with the same composition as the initial gas cloud before being able to form a second generation. Depending on the model used, this would need to be achieved over 25-300 Myr, which would be extremely difficult.

Chapter 6

Future work

There are still many unanswered questions and future work that needs to be carried out in order to gain a more complete picture of the process of cluster evolution. Here I suggest several projects that would be useful in contributing to cluster formation and evolution theories, some of which I will be actively involved in:

- Many individual galaxies, such as NGC 1566, have been studied for their cluster populations. A step forward in these studies could include consolidating all the current information on properties such as mass and age distributions, as well as Γ and $T_L(U)$ to easily compare measurements in different galaxies. There are also inconsistencies across cluster population studies, such as the criteria of objects to create the cluster catalogues and the age and mass cuts imposed on the populations used to determine property distributions. In addition to a lack of uniformity, not all galaxies studied have values for properties of interest, for example Γ (cluster formation efficiency). The Legacy Extra-Galactic UV Survey (LEGUS) aims to address many of these inconsistencies across an extensive sample of nearby spiral galaxies using HST data. Combining this dataset with the Hi-PEEC sample (PI A. Adamo) which is similar to LEGUS but samples the starburst (i.e., high SFR) end of the distribution will be invaluable to see how Γ (and $T_L(U)$) vary as a function of environment. In my future project I will be contributing to this project by improving the current Hi-PEEC pipeline for automated cluster population extraction at higher redshift in a more crowded environment and then analysing the populations for each galaxy. Combining these results for the age, mass and luminosity functions with

the LEGUS sample will provide a fuller picture of how the environment in a galaxy affects cluster formation in galaxies. In addition to this, I will examine the positions of clusters within their galaxies and look for further environmental dependencies on cluster properties, but at smaller scales.

- With the dawn of the James Webb Space Telescope (JWST), studies of cluster populations can delve into the near-infrared in unprecedented detail. It will be possible to study early phases of cluster evolution, particularly the embedded and emerging cluster phase at higher resolution than before, which can indicate more precisely the role feedback plays in the regulation of star formation. In addition to this, the evolution of HII regions, particularly those associated with clusters can be investigated as well as the star/cluster formation history using wavelengths that are not affected by dust. These cluster formation histories can then be compared to existing ones to form a more complete picture of cluster formation. I will hopefully be a part of an Early Release Science programme (PI Angela Adamo) to investigate the well studied cluster population of M 83 with the new tools provided by JWST, in particular the embedded population of young clusters and their emergence.

- To constrain massive cluster formation, in particular that of GCs, it would be useful to look to higher redshift. The same level of detail that is possible with nearby clusters would not be easily achievable, however any information that can be obtained from how clumps and cluster complexes form in the more distant universe could be useful. Gravitationally lensed distant galaxies offer to some hope in probing similar spatial scales as nearby galaxies (10s of parsecs; Vanzella et al., 2017). Comparing the mass distributions of such objects to those observed today on a larger scale would be useful in determining whether the formation of clusters at higher redshift did happen under the same mechanism as the present day. Also examining the clumps' relationship with their host galaxy may be interesting. A key aspect of GC studies that would benefit most from the ability to study GCs forming in situ is that of multiple populations, the origins of which are still highly uncertain. Formulating a working formation scenario for multiple populations is still an open question, and though YMCs are used as analogues to constrain theories, there is still debate on whether this is a valid method. Though it may be impossible to obtain any useful information on the chemistry of the young GCs, observing the structure of the proto-clusters (centrally concentrated bursts of star formation for example)

can provide constraints for current theories and provide insights into how MPs form.

- Constraining the onset of multiple populations is still the key open question in globular clusters studies. The age of clusters with MPs has been found to be as young as 2 Gyr, however this sample size is small. Observing more clusters at $\approx$ 2 Gyr without extended main sequence turn-offs would be useful in finding out exactly what causes the anomalies at this age. I will be continuing work on this topic with new low resolution spectroscopic data obtained for NGC 1978 and Hodge 6 in the LMC using FORS2 on the VLT. The analysis of these clusters will be the same as that described in Chapter 4 for Lindsay 1 and Kron 3. Despite this, further clusters would also be useful. In order to significantly expand the number of clusters available for study, work on deciphering integrated spectroscopy of clusters to be able to identify signatures of multiple populations also needs to advance. his would also open up new cluster environments to study, to identify if the galaxy, or location in the galaxy in which the cluster formed, has played a role in the onset of MPs and the precise properties of the populations (for example, the ratio of enriched to non-enriched stars that varies between clusters). In addition to further chemical studies of clusters, looking further into the role rotation plays in clusters' evolution would provide a large step forward in this field. The coincident age at which clusters lose their extended main sequence turn off (and stellar rotation, which is the likely cause, is significantly reduced) and begin to show evidence for multiple populations may be related. Investigating how these rapidly rotating stars are affected by their early evolution may provide insight into MP formation and why an age of 2 Gyr seems to be the cut-off for MPs.

I think that the future of cluster population studies has many exciting advancements that can be made on a fairly short timescale. In the short term, uncovering the precise effect that environment plays in producing the properties of cluster populations that we have investigated will be a large step forward. This can be achieved on a very short timescale, as LEGUS and Hi-PEEC data will be instrumental in this, and are being studied now.

In the longer term, I think JWST will provide a wealth of information to compliment the current primarily optical studies. Particularly looking at very young clusters, which can be missed at optical wavelengths, at high resolution and discovering their early evolution and relationship with feedback. If our proposal is successful, I will be directly working on the early release

science data products for M 83 with JWST.

Even longer term than JWST is ELT and the possibilities this offers the cluster community are widespread and very exciting. One of the main topics I would like to see addressed and would like to be involved in is the investigation into GCs at higher redshift, where we may be able to observe them forming in much higher detail than currently possible. Identifying differences between the cluster formation in the early universe and the observations of the local universe would be instrumental in saying whether or not YMCs are indeed young GCs, and could provide insights into the onset of MPs and the unknown early evolution of GCs.

Bibliography

Adamo, A., Zackrisson, E., Östlin, G., & Hayes, M. 2010a, ApJ, 725, 1620

Adamo, A., Östlin, G., Zackrisson, E., et al. 2010b, MNRAS, 407, 870

Adamo, A., Östlin, G., & Zackrisson, E. 2011, MNRAS, 417, 1904

Adamo, A., Smith, L. J., Gallagher, J. S., et al. 2012, MNRAS, 426, 1185

Adamo, A., & Bastian, N. 2015, arXiv:1511.08212

Adamo, A., Kruijssen, J. M. D., Bastian, N., Silva-Villa, E., & Ryon, J. 2015, MNRAS, 452, 246

Alcaino, G., Alvarado, F., & Kurtev, R. 2003, A&A, 407, 919

Allen, L., Megeath, S. T., Gutermuth, R., et al. 2007, Protostars and Planets V, 361

Allison, R. J., Goodwin, S. P., Parker, R. J., et al. 2009, ApJ, 700, L99

Alonso, A., Arribas, S., & Martínez-Roger, C. 1999, A&A Supplement, 140, 261

Alves, D. R., & Sarajedini, A. 1999, ApJ, 511, 225

Anders, P., & Fritze-v. Alvensleben, U. 2003, A&A, 401, 1063

Asplund, M., Grevesse, N., Sauval, A. J., & Scott, P. 2009, ARA&A, 47, 481

Bastian, N., Gieles, M., Efremov, Y. N., & Lamers, H. J. G. L. M. 2005, A&A, 443, 79

Bastian, N., Emsellem, E., Kissler-Patig, M., & Maraston, C. 2006, A&A, 445, 471

Bastian, N., & Goodwin, S. P. 2006, MNRAS, 369, L9

Bastian, N., Ercolano, B., Gieles, M., et al. 2007, MNRAS, 379, 1302

Bastian, N. 2008, MNRAS, 390, 759

Bastian, N., & de Mink, S. E. 2009, MNRAS, 398, L11

Bastian, N., Trancho, G., Konstantopoulos, I. S., & Miller, B. W. 2009, ApJ, 701, 607

Bastian, N., Covey, K. R., & Meyer, M. R. 2010, ARA&A, 48, 339

Bastian, N., Adamo, A., Gieles, M., et al. 2011, MNRAS, 417, L6

Bastian, N., Adamo, A., Gieles, M., et al. 2012, MNRAS, 419, 2606

Bastian, N., Cabrera-Ziri, I., Davies, B., & Larsen, S. S. 2013a, MNRAS, 436, 2852

Bastian, N., Lamers, H. J. G. L. M., de Mink, S. E., et al. 2013b, MNRAS, 436, 2398

Bastian, N., Adamo, A., Schirmer, M., et al. 2014a, MNRAS, 444, 3829

Bastian, N., Hollyhead, K., & Cabrera-Ziri, I. 2014b, MNRAS, 445, 378

Bastian, N., Cabrera-Ziri, I., & Salaris, M. 2015, MNRAS, 449, 3333

Bastian, N., & Lardo, C. 2015, MNRAS, 453, 357

Bastian, N., Niederhofer, F., Kozhurina-Platais, V., et al. 2016, MNRAS, 460, L20

Bastian, N., Cabrera-Ziri, I., Niederhofer, F., et al. 2017, MNRAS, 465, 4795

Baumgardt, H. 2001, MNRAS, 325, 1323

Baumgardt, H., & Makino, J. 2003, MNRAS, 340, 227

Baumgardt, H., & Kroupa, P. 2007, MNRAS, 380, 1589

Baumgardt, H., Parmentier, G., Anders, P., & Grebel, E. K. 2013, MNRAS, 430, 676

Bell, R. A., & Dickens, R. J. 1980, ApJ, 242, 657

Bellini, A., Piotto, G., Milone, A. P., et al. 2013, ApJ, 765, 32

Bertelli, G., Nasi, E., Girardi, L., et al. 2003, AJ, 125, 770

Bertin, E., & Arnouts, S. 1996, A&A Supplement, 117, 393

Bik, A., Lamers, H. J. G. L. M., Bastian, N., Panagia, N., & Romaniello, M. 2003, A&A, 397, 473

Bik, A., Stolte, A., Gennaro, M., et al. 2014, A&A, 561, A12

Blaauw, A. 1964, ARA&A, 2, 213

Blair, W. P., Chandar, R., Dopita, M. A., et al. 2014, ApJ, 788, 55

Blum, R. D., Schaerer, D., Pasquali, A., et al. 2001, AJ, 122, 1875

Boily, C. M., & Kroupa, P. 2003, MNRAS, 338, 665

Boutloukos, S. G., & Lamers, H. J. G. L. M. 2003, MNRAS, 338, 717

Bragaglia, A., Gratton, R. G., Carretta, E., et al. 2012, A&A, 548, A122

Bragaglia, A., Carretta, E., D'Orazi, V., et al. 2017, arXiv:1708.07705

Brandner, W., Clark, J. S., Stolte, A., et al. 2008, A&A, 478, 137

Brandt, T. D., & Huang, C. X. 2015, ApJ, 807, 25

Bresolin, F., & Kennicutt, R. C., Jr. 2002, ApJ, 572, 838

Bressert, E., Bastian, N., Gutermuth, R., et al. 2010, MNRAS, 409, L54

Briley, M. M., Cohen, J. G., & Stetson, P. B. 2004, AJ, 127, 1579

Bruzual, G., & Charlot, S. 2003, MNRAS, 344, 1000

Burkert, A., & Tremaine, S. 2010, ApJ, 720, 516

Cabrera-Ziri, I., Bastian, N., Davies, B., et al. 2014, MNRAS, 441, 2754

Cabrera-Ziri, I., Bastian, N., Longmore, S. N., et al. 2015, MNRAS, 448, 2224

Cabrera-Ziri, I., Lardo, C., Davies, B., et al. 2016, MNRAS, 460, 1869

Caldwell, N., Harding, P., Morrison, H., et al. 2009, AJ, 137, 94

Calzetti, D., Armus, L., Bohlin, R. C., et al. 2000, ApJ, 533, 682

Calzetti, D., Lee, J. C., Adamo, A., et al. 2014, American Astronomical Society Meeting Abstracts #223, 223, 254.08

Calzetti, D., Lee, J. C., Sabbi, E., et al. 2015, AJ, 149, 51

Carrera, R., Gallart, C., Aparicio, A., et al. 2008, AJ, 136, 1039

Carretta, E., Bragaglia, A., Gratton, R., D'Orazi, V., & Lucatello, S. 2009, A&A, 508, 695

Carretta, E., Bragaglia, A., Gratton, R., et al. 2010, ApJ, 712, L21

Carpenter, J. M., & Hodapp, K. W. 2008, Handbook of Star Forming Regions, Volume I, 4, 899

Cartwright, A., & Whitworth, A. P. 2004, MNRAS, 348, 589

Cassisi, S., Salaris, M., Pietrinferni, A., & Hyder, D. 2017, MNRAS, 464, 2341

Chandar, R., Fall, S. M., & Whitmore, B. C. 2010a, ApJ, 711, 1263

Chandar, R., Whitmore, B. C., Kim, H., et al. 2010b, ApJ, 719, 966

Chandar, R., Whitmore, B. C., Calzetti, D., et al. 2011, ApJ, 727, 88

Chandar, R., Whitmore, B. C., Calzetti, D., & O'Connell, R. 2014, ApJ, 787, 17

Chandar, R., Fall, S. M., & Whitmore, B. C. 2015, ApJ, 810, 1

Clarkson, W. I., Ghez, A. M., Morris, M. R., et al. 2012, ApJ, 751, 132

Conroy, C. 2013, ARA&A, 51, 393

Crowther, P. A. 2007, ARA&A, 45, 177

Crowther, P. A., Schnurr, O., Hirschi, R., et al. 2010, MNRAS, 408, 731

D'Antona, F., Di Criscienzo, M., Decressin, T., et al. 2015, MNRAS, 453, 2637

Da Costa, G. S., & Hatzidimitriou, D. 1998, AJ, 115, 1934

Dale, J. E., Ercolano, B., & Bonnell, I. A. 2012, MNRAS, 427, 2852

Dale, J. E., Ngoumou, J., Ercolano, B., & Bonnell, I. A. 2014, MNRAS, 442, 694

Dalessandro, E., Massari, D., Bellazzini, M., et al. 2014, ApJ, 791, L4

Davies, B., Kudritzki, R.-P., Lardo, C., et al. 2017, ApJ, 847, 112

de Grijs, R., Anders, P., Bastian, N., et al. 2003, MNRAS, 343, 1285

de Grijs, R., & Anders, P. 2006, MNRAS, 366, 295

de Grijs, R., & Goodwin, S. P. 2008, MNRAS, 383, 1000

de Mink, S. E., Pols, O. R., Langer, N., & Izzard, R. G. 2009, A&A, 507, L1

de Vaucouleurs, G. 1973, ApJ, 181, 31

Decressin, T., Meynet, G., Charbonnel, C., Prantzos, N., & Ekström, S. 2007, A&A, 464, 1029

D'Ercole, A., Vesperini, E., D'Antona, F., McMillan, S. L. W., & Recchi, S. 2008, MNRAS, 391, 825

D'Ercole, A., D'Antona, F., Ventura, P., Vesperini, E., & McMillan, S. L. W. 2010, MNRAS, 407, 854

D'Ercole, A., D'Antona, F., & Vesperini, E. 2016, MNRAS, 461, 4088

Draper, P. W., Gray, N., Berry, D. S., & Taylor, M. 2014, Astrophysics Source Code Library, ascl:1403.024

Elmegreen, B. G., & Efremov, Y. N. 1997, ApJ, 480, 235

Elmegreen, B. G. 2002, ApJ, 564, 773

Elmegreen, B. G. 2010a, ApJ, 712, L184

Elmegreen, B. G., & Hunter, D. A. 2010b, ApJ, 712, 604

Elmegreen, B. G. 2011, EAS Publications Series, 51, 31

Elson, R. A. W., & Fall, S. M. 1985, PASP, 97, 692

Espinoza, P., Selman, F. J., & Melnick, J. 2009, A&A, 501, 563

Fall, S. M., Chandar, R., & Whitmore, B. C. 2005, ApJ, 631, L133

Fall, S. M. 2006, ApJ, 652, 1129

Fall, S. M., Krumholz, M. R., & Matzner, C. D. 2010, ApJ, 710, L142

Fedotov, K., Gallagher, S. C., Konstantopoulos, I. S., et al. 2011, AJ, 142, 42

Ferland, G. J., Korista, K. T., Verner, D. A., et al. 1998, PASP, 110, 761

Ferraro, F. R., Dalessandro, E., Mucciarelli, A., et al. 2009, Nature, 462, 483

Fitzpatrick, E. L. 1986, AJ, 92, 1068

Fouesneau, M., & Lançon, A. 2010, A&A, 521, A22

Gazak, J. Z., Bastian, N., Kudritzki, R.-P., et al. 2013, MNRAS, 430, L35

Gennaro, M., Brandner, W., Stolte, A., & Henning, T. 2011, MNRAS, 412, 2469

Gieles, M., Baumgardt, H., Bastian, N., & Lamers, H. J. G. L. M. 2004, The Formation and Evolution of Massive Young Star Clusters, 322, 481

Gieles, M., Larsen, S. S., Bastian, N., & Stein, I. T. 2006a, A&A, 450, 129

Gieles, M., Larsen, S. S., Scheepmaker, R. A., et al. 2006b, A&A, 446, L9

Gieles, M., Portegies Zwart, S. F., Baumgardt, H., et al. 2006c, MNRAS, 371, 793

Gieles, M., Lamers, H. J. G. L. M., & Portegies Zwart, S. F. 2007a, ApJ, 668, 268

Gieles, M., Athanassoula, E., & Portegies Zwart, S. F. 2007b, MNRAS, 376, 809

Gieles, M. 2009, MNRAS, 394, 2113

Gieles, M. 2010, Galaxy Wars: Stellar Populations and Star Formation in Interacting Galaxies, 423, 123

Gieles, M., & Portegies Zwart, S. F. 2011, MNRAS, 410, L6

Ginsburg, A., Goss, W. M., Goddi, C., et al. 2016, A&A, 595, A27

Girardi, L., Bertelli, G., Bressan, A., et al. 2002, A&A, 391, 195

Glatt, K., Grebel, E. K., Sabbi, E., et al. 2008, AJ, 136, 1703-1727

Glatt, K., Grebel, E. K., Gallagher, J. S., III, et al. 2009, AJ, 138, 1403-1416

Glatt, K., Grebel, E. K., Jordi, K., et al. 2011, AJ, 142, 36

Gnedin, O. Y., & Ostriker, J. P. 1997, ApJ, 474, 223

Goddard, Q. E., Bastian, N., & Kennicutt, R. C. 2010, MNRAS, 405, 857

Goodwin, S. P., & Whitworth, A. P. 2004, A&A, 413, 929

Goudfrooij, P., Girardi, L., Kozhurina-Platais, V., et al. 2014, ApJ, 797, 35

Gratton, R. G., Sneden, C., Carretta, E., & Bragaglia, A. 2000, A&A, 354, 169

Gratton, R., Sneden, C., & Carretta, E. 2004, ARA&A, 42, 385

Gratton, R. G., Villanova, S., Lucatello, S., et al. 2012a, A&A, 544, A12

Gratton, R. G., Carretta, E., & Bragaglia, A. 2012b, A&ARv, 20, 50

Gratton, R. G., Lucatello, S., Carretta, E., et al. 2012c, A&A, 539, A19

Grosbøl, P., & Dottori, H. 2012, A&A, 542, A39

Grosbøl, P., & Dottori, H. 2013, A&A, 551, L13

Hadfield, L. J., Crowther, P. A., Schild, H., & Schmutz, W. 2005, A&A, 439, 265

Harayama, Y., Eisenhauer, F., & Martins, F. 2008, ApJ, 675, 1319-1342

Harbeck, D., Smith, G. H., & Grebel, E. K. 2003, AJ, 125, 197

Harris, G. L. H., & Harris, W. E. 2011, MNRAS, 410, 2347

Heger, A., Fryer, C. L., Woosley, S. E., Langer, N., & Hartmann, D. H. 2003, ApJ, 591, 288

Hénault-Brunet, V., Evans, C. J., Sana, H., et al. 2012, A&A, 546, A73

Henshaw, J. D., Caselli, P., Fontani, F., et al. 2016, MNRAS, 463, 146

Hollyhead, K., Bastian, N., Adamo, A., et al. 2015, MNRAS, 449, 1106

Hollyhead, K., Adamo, A., Bastian, N., Gieles, M., & Ryon, J. E. 2016, MNRAS, 460, 2087

Hollyhead, K., Kacharov, N., Lardo, C., et al. 2017, MNRAS, 465, L39

Hopkins, P. F. 2013, MNRAS, 428, 1950

Hunter, D. A., Elmegreen, B. G., Dupuy, T. J., & Mortonson, M. 2003, AJ, 126, 1836

Johnson, L. C., Seth, A. C., Dalcanton, J. J., et al. 2016, ApJ, 827, 33

Johnson, L. C., Seth, A. C., Dalcanton, J. J., et al. 2017, ApJ, 839, 78

Jordán, A., Côté, P., Blakeslee, J. P., et al. 2005, ApJ, 634, 1002

Karachentsev, I. D., & Makarov, D. A. 1996, AJ, 111, 794

Kayser, A., Hilker, M., Grebel, E. K., & Willemsen, P. G. 2008, A&A, 486, 437

Kilborn, V. A., Koribalski, B. S., Forbes, D. A., Barnes, D. G., & Musgrave, R. C. 2005, MNRAS, 356, 77

Kirk, H., Johnstone, D., & Tafalla, M. 2007, ApJ, 668, 1042

Kennicutt, R. C., Jr. 1998, ApJ, 498, 541

Kennicutt, R. C., & Evans, N. J. 2012, ARA&A, 50, 531

Konstantopoulos, I. S., Smith, L. J., Adamo, A., et al. 2013, AJ, 145, 137

Korchagin, V., Kikuchi, N., Miyama, S. M., Orlova, N., & Peterson, B. A. 2000, ApJ, 541, 565

Krause, M., Charbonnel, C., Decressin, T., Meynet, G., & Prantzos, N. 2013, A&A, 552, A121

Kroupa, P. 2001, MNRAS, 322, 231

Kroupa, P., & Boily, C. M. 2002, MNRAS, 336, 1188

Kruijssen, J. M. D., Pelupessy, F. I., Lamers, H. J. G. L. M., Portegies Zwart, S. F., & Icke, V. 2011, MNRAS, 414, 1339

Kruijssen, J. M. D. 2012, MNRAS, 426, 3008

Kruijssen, J. M. D. 2015, MNRAS, 454, 1658

Kruijssen, J. M. D., Dale, J. E., & Longmore, S. N. 2015, MNRAS, 447, 1059

Kruijssen, J. M. D., & Bastian, N. 2016, MNRAS, 457, L24

Lada, C. J., & Lada, E. A. 2003, ARA&A, 41, 57

Lamers, H. J. G. L. M., Gieles, M., Bastian, N., et al. 2005, A&A, 441, 117

Lamers, H. J. G. L. M., & Gieles, M. 2006, A&A, 455, L17

Lamers, H. J. G. L. M. 2009, Ap&SS, 324, 183

Lardo, C., Bellazzini, M., Pancino, E., et al. 2011, A&A, 525, A114

Lardo, C., Pancino, E., Mucciarelli, A., & Milone, A. P. 2012, A&A, 548, A107

Lardo, C., Pancino, E., Mucciarelli, A., et al. 2013, MNRAS, 433, 1941

Lardo, C., Cabrera-Ziri, I., Davies, B., & Bastian, N. 2017, MNRAS, 468, 2482

Larsen, S. S., & Richtler, T. 1999, A&A, 345, 59

Larsen, S. S., & Richtler, T. 2000, A&A, 354, 836

Larsen, S. S. 2002, AJ, 124, 1393

Larsen, S. S. 2004a, The Formation and Evolution of Massive Young Star Clusters, 322, 19

Larsen, S. S. 2004b, A&A, 416, 537

Larsen, S. S. 2008, Mass Loss from Stars and the Evolution of Stellar Clusters, 388, 279

Larsen, S. S. 2009, A&A, 494, 539

Larsen, S. S., Strader, J., & Brodie, J. P. 2012, A&A, 544, L14

Larsen, S. S., Brodie, J. P., Grundahl, F., & Strader, J. 2014, ApJ, 797, 15

Lejeune, T., Cuisinier, F., & Buser, R. 1998, A&A Supplement, 130, 65

Lejeune, T., & Schaerer, D. 2001, A&A, 366, 538

Lim, B., Chun, M.-Y., Sung, H., et al. 2013, AJ, 145, 46

Longmore, S. N., Kruijssen, J. M. D., Bally, J., et al. 2013, MNRAS, 433, L15

Longmore, S. N., Kruijssen, J. M. D., Bastian, N., et al. 2014, Protostars and Planets VI, 291

Longmore, S. N. 2015, MNRAS, 448, L62

Mackey, A. D., & Gilmore, G. F. 2003, MNRAS, 338, 85

Mackey, A. D., Broby Nielsen, P., Ferguson, A. M. N., & Richardson, J. C. 2008, ApJ, 681, L17

Marino, A. F., Milone, A. P., Piotto, G., et al. 2011, ApJ, 731, 64

Martell, S. L., Smolinski, J. P., Beers, T. C., & Grebel, E. K. 2011, A&A, 534, A136

Martocchia, S., Bastian, N., Usher, C., et al. 2017, arXiv:1703.04631

Maschberger, T., & Kroupa, P. 2009, MNRAS, 395, 931

Massey, P., & Hunter, D. A. 1998, ApJ, 493, 180

Mateluna, R., Geisler, D., Villanova, S., et al. 2012, A&A, 548, A82

Mészáros, S., Martell, S. L., Shetrone, M., et al. 2015, AJ, 149, 153

de Meulenaer, P., Narbutis, D., Mineikis, T., & Vansevičius, V. 2014, A&A, 569, A4

Mighell, K. J., Sarajedini, A., & French, R. S. 1998, AJ, 116, 2395

Milone, A. P., Bedin, L. R., Piotto, G., & Anderson, J. 2009, A&A, 497, 755

Milone, A. P., Bedin, L. R., Piotto, G., et al. 2015, MNRAS, 450, 3750

Milone, A. P., Piotto, G., Renzini, A., et al. 2017a, MNRAS, 464, 3636

Milone, A. P., Marino, A. F., D'Antona, F., et al. 2017b, MNRAS, 465, 4363

Misselt, K. A., Clayton, G. C., & Gordon, K. D. 1999, ApJ, 515, 128

Monelli, M., Milone, A. P., Stetson, P. B., et al. 2013, MNRAS, 431, 2126

Mucciarelli, A., Carretta, E., Origlia, L., & Ferraro, F. R. 2008, AJ, 136, 375

Mucciarelli, A., Origlia, L., Ferraro, F. R., & Pancino, E. 2009, ApJ, 695, L134

Mucciarelli, A., Dalessandro, E., Ferraro, F. R., Origlia, L., & Lanzoni, B. 2014a, ApJ, 793, L6

Mucciarelli, A., Lovisi, L., Lanzoni, B., & Ferraro, F. R. 2014b, ApJ, 786, 14

Mucciarelli, A., & Cosmic-Lab Team 2016, MmSAI, 87, 658

Narbutis, D., Vansevičius, V., Kodaira, K., Bridžius, A., & Stonkutė, R. 2008, ApJS, 177, 174-180

Negueruela, I., Clark, J. S., & Ritchie, B. W. 2010, A&A, 516, A78

Niederhofer, F., Georgy, C., Bastian, N., & Ekström, S. 2015a, MNRAS, 453, 2070

Niederhofer, F., Hilker, M., Bastian, N., & Silva-Villa, E. 2015b, A&A, 575, A62

Niederhofer, F., Bastian, N., Kozhurina-Platais, V., et al. 2017a, MNRAS, 464, 94

Niederhofer, F., Bastian, N., Kozhurina-Platais, V., et al. 2017b, MNRAS, 465, 4159

Norris, J., Cottrell, P. L., Freeman, K. C., & Da Costa, G. S. 1981, ApJ, 244, 205

Origlia, L., Massari, D., Rich, R. M., et al. 2013, ApJ, 779, L5

Östlin, G., Cumming, R. J., & Bergvall, N. 2007, A&A, 461, 471

Ostriker, J. P., Spitzer, L., Jr., & Chevalier, R. A. 1972, ApJ, 176, L51

Pacifici, C., da Cunha, E., Charlot, S., et al. 2015, MNRAS, 447, 786

Pancino, E., Rejkuba, M., Zoccali, M., & Carrera, R. 2010, A&A, 524, A44

Pancino, E., & the GES collaboration 2017, arXiv:1702.06083

Parisi, M. C., Geisler, D., Clariá, J. J., et al. 2015, AJ, 149, 154

Parker, R. J., Wright, N. J., Goodwin, S. P., & Meyer, M. R. 2014, MNRAS, 438, 620

Parmentier, G., Goodwin, S. P., Kroupa, P., & Baumgardt, H. 2008, ApJ, 678, 347-352

Patrick, L. R., Evans, C. J., Davies, B., et al. 2016, MNRAS, 458, 3968

Peacock, M. B., Maccarone, T. J., Knigge, C., et al. 2010, MNRAS, 402, 803

Pellegrini, E. W., Oey, M. S., Winkler, P. F., et al. 2012, ApJ, 755, 40

Piatti, A. E., Keller, S. C., Mackey, A. D., & Da Costa, G. S. 2014, MNRAS, 444, 1425

Piotto, G., Milone, A. P., Anderson, J., et al. 2012, ApJ, 760, 39

Piotto, G., Milone, A. P., Bedin, L. R., et al. 2015, AJ, 149, 91

Portegies Zwart, S. F., McMillan, S. L. W., & Gieles, M. 2010, ARA&A, 48, 431

Prantzos, N., Charbonnel, C., & Iliadis, C. 2007, A&A, 470, 179

Rafelski, M., & Zaritsky, D. 2005, AJ, 129, 2701

Riello, M., Cassisi, S., Piotto, G., et al. 2003, A&A, 410, 553

Ryon, J. E., Adamo, A., Bastian, N., et al. 2014, AJ, 148, 33

Salaris, M., Weiss, A., Ferguson, J. W., & Fusilier, D. J. 2006, ApJ, 645, 1131

Salinas, R., & Strader, J. 2015, ApJ, 809, 169

Salpeter, E. E. 1955, ApJ, 121, 161

Schaerer, D., & Charbonnel, C. 2011, MNRAS, 413, 2297

Scheepmaker, R. A., Haas, M. R., Gieles, M., et al. 2007, A&A, 469, 925

Schiavon, R. P., Zamora, O., Carrera, R., et al. 2017, MNRAS, 465, 501

Schneider, F. R. N., Izzard, R. G., de Mink, S. E., et al. 2014, ApJ, 780, 117

Schweizer, F., & Seitzer, P. 1998, AJ, 116, 2206

Seale, J. P., Looney, L. W., Wong, T., et al. 2012, ApJ, 751, 42

Selman, F. J., & Melnick, J. 2008, ApJ, 689, 816-824

Silva-Villa, E., & Larsen, S. S. 2011, A&A, 529, A25

Silva-Villa, E., Adamo, A., & Bastian, N. 2013, MNRAS, 436, L69

Silva-Villa, E., Adamo, A., Bastian, N., Fouesneau, M., & Zackrisson, E. 2014, MNRAS, 440, L116

Smith, L. J. 2008, Dynamical Evolution of Dense Stellar Systems, 246, 55

Sneden, C., Kraft, R. P., Prosser, C. F., & Langer, G. E. 1992, AJ, 104, 2121

Sollima, A., Pancino, E., Ferraro, F. R., et al. 2005, ApJ, 634, 332

Thilker, D. A., Bianchi, L., Meurer, G., et al. 2007, ApJS, 173, 538

Thim, F., Tammann, G. A., Saha, A., et al. 2003, ApJ, 590, 256

Tody, D. 1993, Astronomical Data Analysis Software and Systems II, 52, 173

van Dokkum, P. G. 2001, PASP, 113, 1420

Vanzella, E., Calura, F., Meneghetti, M., et al. 2017, MNRAS, 467, 4304

Vázquez, G. A., & Leitherer, C. 2005, ApJ, 621, 695

Villanova, S., Piotto, G., & Gratton, R. G. 2009, A&A, 499, 755

Vollmann, K., & Eversberg, T. 2006, Astronomische Nachrichten, 327, 862

Walker, D. L., Longmore, S. N., Bastian, N., et al. 2015, MNRAS, 449, 715

Walker, D. L., Longmore, S. N., Bastian, N., et al. 2016, MNRAS, 457, 4536

Weidner, C., Kroupa, P., & Larsen, S. S. 2004, MNRAS, 350, 1503

Whitmore, B. C., Zhang, Q., Leitherer, C., et al. 1999, AJ, 118, 1551

Whitmore, B. C., & Zhang, Q. 2002, AJ, 124, 1418

Whitmore, B. C. 2003, A Decade of Hubble Space Telescope Science, 14, 153

Whitmore, B. C., Chandar, R., & Fall, S. M. 2007, AJ, 133, 1067

Whitmore, B. C., Chandar, R., Schweizer, F., et al. 2010, AJ, 140, 75

Whitmore, B. C., Chandar, R., Kim, H., et al. 2011, ApJ, 729, 78

Worthey, G. 1994, ApJS, 95, 107

Whitmore, B. C., Chandar, R., Bowers, A. S., et al. 2014, AJ, 147, 78

Zackrisson, E., Bergvall, N., & Leitet, E. 2008, ApJ, 676, L9

Zackrisson, E., Rydberg, C.-E., Schaerer, D., Östlin, G., & Tuli, M. 2011, ApJ, 740, 13

Zepf, S. E., Ashman, K. M., English, J., Freeman, K. C., & Sharples, R. M. 1999, AJ, 118, 752

Zhang, Q., & Fall, S. M. 1999, ApJ, 527, L81